

U.S. DEPARTMENT OF COMMERCE
National Technical Information Service

AD-A027 467

A LABORATORY STUDY OF WIND-WAVE-CURRENT INTERACTION
PART II

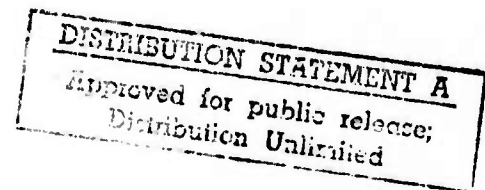
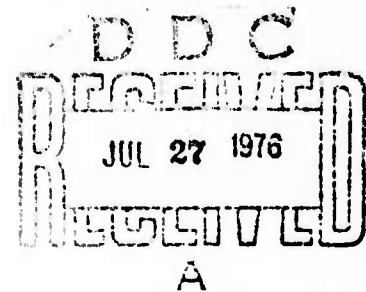
HYDRONAUTICS, INCORPORATED

PREPARED FOR
OFFICE OF NAVAL RESEARCH

JUNE 1976

215196

ADA 027467



HYDRONAUTICS, incorporated research in hydrodynamics

REPRODUCED BY
NATIONAL TECHNICAL
INFORMATION SERVICE
U. S. DEPARTMENT OF COMMERCE
SPRINGFIELD, VA. 22161

Research, consulting, and advanced engineering in the fields of NAVAL and INDUSTRIAL HYDRODYNAMICS. Offices and Laboratory in the Washington, D. C. area: Pindell School Road, Howard County, Laurel, Md.

**BEST
AVAILABLE COPY**

HYDRONAUTICS, INCORPORATED

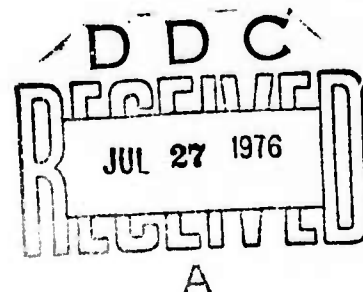
TECHNICAL REPORT 7619-1

A LABORATORY STUDY OF
WIND-WAVE-CURRENT INTERACTION
PART II

by

Richard S. Scotti,
Garry W. Elliott,
and Mark S. Rice

June 1976



Sponsored by

Advanced Research Projects Agency
ARPA Order No. 1910, Amendment No. 21

Under

ONR Contract No. N00014-76-C-0593, NR062-472

DISTRIBUTION STATEMENT A

Approved for public release;
Distribution Unlimited

UNCLASSIFIED

SECURITY CLASSIFICATION OF THIS PAGE (When Data Entered)

REPORT DOCUMENTATION PAGE		READ INSTRUCTIONS BEFORE COMPLETING FORM
1. REPORT NUMBER Technical Report 7619-1	2. GOVT ACCESSION NO.	3. RECIPIENT'S CATALOG NUMBER
4. TITLE (and Subtitle) A Laboratory Study of Wind-Wave-Current Interactions Part II		5. TYPE OF REPORT & PERIOD COVERED Technical Report
7. AUTHOR(s) Richard S. Scotti, Garry W. Elliott and Mark S. Rice		6. PERFORMING ORG. REPORT NUMBER TR 7619-1
9. PERFORMING ORGANIZATION NAME AND ADDRESS HYDRONAUTICS, Incorporated 7210 Pindell School Road Laurel, Maryland 20810		6. CONTRACT OR GRANT NUMBER(s) N00014-76-C-0593
11. CONTROLLING OFFICE NAME AND ADDRESS Advanced Research Projects Agency Arlington, Virginia 22209		10. PROGRAM ELEMENT, PROJECT, TASK AREA & WORK UNIT NUMBERS NR062 472
14. MONITORING AGENCY NAME & ADDRESS (if different from Controlling Office) Office of Naval Research Department of the Navy Arlington, Virginia 22209		12. REPORT DATE June 1976
		13. NUMBER OF PAGES
		15. SECURITY CLASS. (of this report) Unclassified
		15a. DECLASSIFICATION/DOWNGRADING SCHEDULE
16. DISTRIBUTION STATEMENT (of this Report)		
<div style="border: 1px solid black; padding: 5px; text-align: center;"> DISTRIBUTION STATEMENT A Approved for public release; Distribution Unlimited </div>		
17. DISTRIBUTION STATEMENT (of the abstract entered in Block 20, if different from Report)		
18. SUPPLEMENTARY NOTES		
19. KEY WORDS (Continue on reverse side if necessary and identify by block number) Wind Waves Wind Drift Layer Wave-Wave Interaction Wave Wave Spectral Analysis		
20. ABSTRACT (Continue on reverse side if necessary and identify by block number) This report addresses the second part of a HYDRONAUTICS, Incorporated study, which was performed to determine the effect of wind and a spatially varying subsurface current field on both the wind-induced drift layer and the surface-wave spectrum. Steady state wind-wave-current interactions were established over a region of uniform current gradients which simulated an internal-wave-fixed measuring system. Wave-height spectra were recorded by HYDRONAUTICS while wave-slope spectra were simultaneously made with a Digital Video System by Riverside Research Institute. The resulting data are ex-		

DD FORM 1473
1 JAN 73EDITION OF 1 NOV 68 IS OBSOLETE
S/N 0102-014-6601

UNCLASSIFIED

SECURITY CLASSIFICATION OF THIS PAGE (When Data Entered)

UNCLASSIFIED

SECURITY CLASSIFICATION OF THIS PAGE(When Data Entered)

pected to provide a firm foundation for theoretical arguments concerning the question of relaxation phenomena in the wind-drift layer.

i (u)

UNCLASSIFIED

SECURITY CLASSIFICATION OF THIS PAGE(When Data Entered)

HYDRONAUTICS, INCORPORATED

-i-

TABLE OF CONTENTS

	Page
ABSTRACT	iv
I. INTRODUCTION	1
II. EXPERIMENTAL FACILITIES AND MEASUREMENTS	3
II.1 Wind-Wave-Current Facility	3
II.2 Measurements	4
II.2.1 Wind Profiles.	4
II.2.2 Surface Wave Characteristics	6
II.2.3 Surface Drift Currents	8
II.2.4 Subsurface Currents.	10
III. THE EXPERIMENTS.	12
III.1 Preliminary Considerations.	12
III.1.1 Experimental Accuracy.	12
III.1.2 Selection of Test Conditions	13
III.1.3 Matrix of Flow Conditions Tested.	14
III.2 Experimental Results.	15
IV. RESULTS DISCUSSED AND SUMMARIZED	17
V. CONCLUDING REMARKS	23
REFERENCES	24

i (4-)

FILED
JUN 10 1964
FBI - NEW YORK
Hittor on file
A

HYDRONAUTICS, INCORPORATED

-ii-

LIST OF FIGURES

- Figure 1 - Schematic of Wind-Wave-Current Facility Showing Submerged Beach and Current System; 1975 Tests
- Figure 2 - Neyrpic Velocimeter
- Figure 3 - Calibration of Neyrpic Velocimeter No. 6272
- Figure 4 - Current Profile - Favorable Flow
- Figure 5 - Current Profile - Adverse Flow
- Figures 6, 8, 10 and 13 - Near Surface Drift Current - Semi-log Plots
- Figures 7, 9, 11 and 12 - Near Surface Drift Current - Linear Plots
- Figure 14 - Friction Velocity (U_x) vs Wind Speed (U_w)
- Figure 15 - Wind Speed (U_w) vs Drift Layer Thickness (δ) for Two Beach Angles (θ)
- Figure 16 - Fetch Effects
- Figures 17, 18, 19 and 20 - Shift in Dominant Wind-Wave Frequency Due to Spatially Varying Subsurface Current
- Figure 21 - Spectral Plot - Effect of Current on Dominant Wave Frequency and Amplitude
- Figure 22 - Power Spectra - Repeatability Test
- Figures 24, 25, 26, 27, 28, 29, 30, 31, 32, 33, 34, 35, 36, 37, 38, 39, 40, 42, 43, 45, 47, 49, and 50. - } Power Spectra - Wind Waves
- Figures 41, 43, 44, 46 and 48 - Cross Spectra - Wind Waves
- Figures 51, 52 and 53 - Power Spectra - Wind and Mechanical Waves

HYDRONAUTICS, INCORPORATED

-iii-

LIST OF TABLES

Table 1. Data Presentation Outline.

Table 2. Test Matrix (1975).

Table 3. Summary of Results - Wave-Height Measurements.

HYDRONAUTICS, INCORPORATED

-iv-

ABSTRACT

This report addresses the second part of a HYDRONAUTICS, Incorporated study, which was performed to determine the effect of wind and a spatially varying subsurface current field on both the wind-induced drift layer and the surface-wave spectrum. Steady state wind-wave-current interactions were established over a region of uniform current gradients which simulated an internal-wave-fixed measuring system. Wave-height spectra were recorded by HYDRONAUTICS while wave-slope spectra were simultaneously made with a Digital Video System by Riverside Research Institute. The resulting data are expected to provide a firm foundation for theoretical arguments concerning the question of relaxation phenomena in the wind-drift layer.

HYDRONAUTICS, INCORPORATED

I. INTRODUCTION

The present series of tests are part of a larger effort aimed at quantitatively delineating the physical processes involved in the interactions of internal waves and surface waves. HYDRONAUTICS, Incorporated has been involved in different theoretical and experimental aspects of this program since 1972, and has submitted nine reports on the subject to date. The present report addresses an experimental test series on resonant wind-wave-current interactions, the second joint effort of HYDRONAUTICS, Incorporated and Riverside Research Institute. The work was done in the HYDRONAUTICS Wind-Wave Facility during the fall of 1975.

The purpose of this report is to present the hydrodynamic measurements and preliminary findings of HYDRONAUTICS' 1975 test series. The complementary work conducted in the Wind-Wave Facility will be reported by Riverside Research Institute under their separate cover. In particular, the spatial wind-wave spectra taken with the Digital Video System (DVS) will be presented. It is anticipated that another report aimed at collaborating the flow field and surface wave spectra measurements with existing theoretical predictions will be prepared by HYDRONAUTICS in the near future.

The first laboratory study performed jointly by HYDRONAUTICS, Incorporated and Riverside Research Institute was conducted during the early fall of 1974 (References 1 and 2). The results of these tests were valuable in designing the present study and in making the necessary facility changes for the refined 1975 test series.

The objective of the second experimental study was to improve upon and complete the effort of the previous year. In addition further refinements in the RRI-DVS demonstrated a greater

HYDRONAUTICS, INCORPORATED

-2-

level of confidence in this system. For the purpose of the present report, it is sufficient to point out that both the experimental findings of 1974 and the theoretical predictions indicate that a TV system accuracy of better than 1/2 Db (or 5% in wave energy) would be necessary for measurement significance. This 1/2 Db accuracy is directly related to the small magnitude of nonresonant interactions between wind-generated-surface waves and subsurface current fields. Other improvements in the present experiments over last year's include increased accuracy in flow field measurement, better reproducibility of a given flow field condition, and a more uniform wind velocity profile above the water surface. Care was taken to insure that an accuracy of $\pm 5\%$ (or better) was maintained throughout the measurements. The largest improvements over 1974 test conditions are a result of the new current system. The earlier testing had been plagued with large scale vorticity which was transmitted to the test section after its inception at the current generating impeller. As a result of new diffusing devices, dye injections no longer indicated significant vorticity.

Existing theoretical models have been briefly reviewed in Reference 1. The driving force behind the present experimental work has been the urgent need for data to refine ongoing theoretical efforts. The question of how to draw correspondence between the conditions in the laboratory and those found in the oceanic environment is an important one which is being addressed in a companion study at HYDRONAUTICS.

Section II contains a description of the modified Wind-Wave Facility, its operational characteristics, and the physical measurements taken in it. Section III describes the experimental procedures and results. In Section IV the results are summarized and discussed, with concluding remarks and suggestions for further research to be found in Section V.

II. EXPERIMENTAL FACILITIES AND MEASUREMENTS

II.1 Wind-Wave-Current Facility

The HYDRONAUTICS wind-wave-current facility, shown schematically in Figure 1, is basically a 1.5 m-wide, 1.55 m-deep, and 22 m-long water tank. An axial flow fan, which is driven at an adjustable speed by an electric motor, is located at the upstream end. To avoid the problem of wave reflections that would occur in any tank of finite length, a permeable wave absorber has been installed at the downstream end. A removable, sectional cover has been placed on the tank to create a wind tunnel 31 cms-high (nominal) over a water depth of 124 cms (nominal). The cross sectional area of the air stream may be varied by changing the water level. Wind speeds up to 13 m/sec may be generated over the water surface at the nominal wind tunnel height.

Surface waves may be generated mechanically by a wave paddle located at the upwind end of the tank. The paddle consists of a stiff plate hinged at the tank bottom and driven by an electric motor through a variable speed reducer and an adjustable linkage. The frequency and amplitude of the paddle's motion are independently adjustable.

The facility is equipped with a variable current generation system also shown in Figure 1. The present system is an improved version of that used in the 1974 wind-wave-current tests. It consists of a false bottom or submerged beach and a recirculating pump system, including a reversible impeller, appropriate ducting, turning vanes and flow straighteners. The submerged beach is supported from below on adjustable screw threads which are conveniently accessible from above. The beach may be positioned at any inclination over the range from 0 to 2.65 degrees by cranking on the support screws. The turning vanes and flow diffusing and straightening sections were designed

and finely adjusted to provide two-dimensional current flow over the beach in either the upwind (adverse) or the downwind (favorable) directions. In the favorable direction the current is uniform across the flow to within $\pm 5\%$. In the adverse direction, however, owing to geometric and space limitations in the adverse flow diffuser section, the current flow nonuniformity increases to about $\pm 10\%$ over a given cross section. Extensive calibrations have been carried out on the current system and are presented in the next section.

The primary flow variables in the wind-wave-current facility are the wind speed and the artificial current direction, speed and streamwise gradient. The wind speed is controlled by the RPM of the fan motor. The current direction is determined by the sense of rotation of the impeller. The current gradient is controlled by the inclination of the beach, while the local current magnitude is directly related to the impeller RPM and the inclination of the beach. It is the current gradient that enables the simulation of certain key aspects of an internal wave using a stationary current system, in that an equivalent internal wavelength or time-scale for a propagating current can be defined. It should be noted, however, that all measurements are made relative to a coordinate system that effectively "rides" on a stationary internal wave. This point must be considered carefully before comparing the experimental laboratory data to other data or to theoretical predictions.

II.2 Measurements

II.2.1 Wind Profiles

Two methods were tried to determine the wind velocity profile above the water; hot wire anemometry and pitot-static manometer measurements. Simultaneous use of both devices within the wind-wave facility gave reasonable results with one stringent

limitation. When water droplets or spray contacted the hot wire device, thermal stresses led to wire failures. Though wire temperature was reduced to its lowest practical value, failures remained numerous. As a result, hot wire anemometry was discarded as a useful tool because of its frailty under near surface test conditions.

The wind profiles included in the present report were taken with a pitot-static probe and an alcohol micromanometer. The pitot-static probe was mounted on a motorized "A" frame for vertical and transverse profiles of the test section. Measurements, however, were taken at discreet intervals with the probe held fixed rather than with the probe continuously traversing the test section. In this way, wave-generated fluctuations in the air stream could be time-averaged. The output from the micromanometer was converted to an electrical signal by installing a simple wire capacitance probe within the glass tubing of the manometer. A parallel glass tube provided visual confirmation of the reading. The electrical signal was displayed on a strip chart recorder so that fluctuations in near-surface air-stream velocities could be averaged. This signal was also used to check for gross distortions in fixed-point velocities which might be due to relatively slow seiche-like motions within the tank.

As has been our previous experience, the wind velocity profile was found to follow the logarithmic law over with some interval above the water surface.

$$U = \frac{U_*}{k} \ln (z/z_0) \quad [1]$$

Friction velocities (U_*) and equivalent roughness lengths (z_0) were inferred from Equation [1] by means of a semi-log plot of the measured wind velocity profiles. This technique

while easily and commonly employed, suffers from limited accuracy inherent in fitting a straight line through experimental data. (Throughout the present test set, irregularities in the wind velocity profile were corrected by a fine mesh wire screen. A series of detailed wind velocity profiles showed that the characteristics of the air flow were improved by the presence of this screen.

Tests were also undertaken to determine the effect of small adverse or favorable (with respect to the wind direction) currents on the friction velocity (for a constant wind speed). Over the range

$$- 1.25 \leq \frac{U_c}{U_s} \leq 1.25$$

where U_c is the current speed and U_s is the surface drift under the action of wind, no measurable changes in U_x could be discerned. Repeated measurements for the same flow conditions suggest that our accuracy in determining U_x was on the order of $\pm 5\%$. Thus, it appears that the effects of current (over the range of values tested) on the shear velocity are small and negligible compared to the accuracies attained in the present experiments.

II.2.2. Surface Wave Characteristics

The principle diagnostic tool for the present tests was the RRI-TV camera system which is capable of measuring the two-dimensional surface wave slope spectrum over a given spatial view patch. To supplement and provide an independent check on the RRI data, an alternate means of simultaneously measuring surface wave characteristics was considered to be of value. Consequently, surface wave data were also taken by means of capacitance wire probes. Repeated calibrations demonstrated that these teflon-coated probes have a flat frequency response over the range of 0-30 Hz and an

output voltage that varied linearly with probe submergence. Two probes were positioned along the longitudinal axis of the wind-wave tank at a variable separation (L). Their output voltages were stored on separate channels of an FM tape recorder for later processing.

The output signal from a calibrated capacitance wave-height probe gives the position of the water surface at a fixed point in space as a function of time. The output of the two wave-height probes was reduced to yield power spectra. The utility of this presentation for the present study lies primarily in the reference point it provides for reduction of the RRI data. Specifically, the temporal frequencies of surface waves generated in the wind-wave facility, which can be measured directly from a power spectrum of the wind-height probe signal, are recoverable from a dynamic analysis of the RRI slope spectral data (Reference 4). The accuracy of this dynamic analysis is poor at the lower wave frequencies, particularly at the frequency of the dominant wave, but improves considerably for the high frequencies. A power spectrum of the wave-height probe signal, on the other hand, provides a very accurate measure of the frequency of the dominant wave. It has been found that reduction and analysis of the RRI-TV data was expedited and improved by the wave-height probe data. This point will be discussed more fully in forthcoming RRI and HYDRONAUTICS, Incorporated reports on the present tests.

The simultaneous use of two wave-height probes enables the computation of two-point (spatial) cross correlations and cross spectra. From cross correlations, the phase speed C_p of the dominant surface wave may be estimated by the relationship (Reference 3)

$$C_p = \frac{\tau}{L} \quad [2]$$

where τ is the time by which one signal must be delayed relative to the other for maximum correlation, and L is the probe longitudinal separation (generally set at less than one-half the dominant wavelength, λ_D). The cross spectrum, which is the Fourier transform of the cross correlation, gives, in principle, the phase speed for each wave component present in the surface wave spectrum. In practice, problems of aliasing wavelengths shorter than the wave-height probe separation, and of low signal-to-noise ratio limit the useful frequency range of the cross spectrum technique (Reference 3). In the present case, L was selected to avoid spatial aliasing and attention was focused in the vicinity of the dominant wave. The phase speed for each frequency component is estimated as

$$C_p(w) = \frac{2\pi w L}{\Phi(w)} \quad , \quad [3]$$

where w is the wave frequency in Hertz and Φ is the phase angle computed from the ratio of the imaginary to the real parts of the cross spectrum as

$$\Phi(w) = \tan^{-1} \left(- \frac{\text{Im}(w)}{\text{Re}(w)} \right) \quad [4]$$

The data from the wave-height probes were processed on a Unigon Fast Fourier Transform Analyzer—which is basically a hard-wired, special purpose mini(digital) computer—and plotted on an X-Y plotter. Such wind-wave spectra are included in later data sections of this report. Based upon Phillips' theory (References 4 and 5) and fetch limited laboratory conditions, one would expect an overdriven peak, shallow mid-range, and an asymptotic approach to a -5 slope only at the higher frequencies (Reference 6).

11.2.3 Surface Drift Currents

The drift current immediate to the water surface was measured by repeatedly timing floats of various sizes between

two stations in the wind direction and then averaging the results. Spherical particles with dimensions of 1.90, 3.18, 6.35 and 12.70 mm and a specific gravity of 0.95 were used as floats. The velocity of each float was taken as the drift current at the depth of the centroid of the longitudinally projected area of the submerged portion of the float. For the floats used in the present experiment, the corresponding centroid depths have been estimated (geometrically) to be 0.71, 1.19, 2.37 and 4.72 mm, respectively. For many of the wind-current setups tested, use of the two larger floats was impractical if not altogether impossible. For a few cases no float data could be taken because of the effects of strong velocity gradients on the motion of the floats. In particular, for cases with strong adverse subsurface currents, the drift-layer profile connecting the downwind surface drift to the upwind subsurface current has a zero velocity crossing (typically in the centimeter below the mean surface). For such cases the floats were observed to meander, stall, reverse directions and, generally, to behave erratically over the timed-travel interval. All data from erratic floats was considered to be unacceptable. All trials with a particular float which executed erratic motion under a flow setup were discontinued and disregarded.

This procedure of disregarding float data when the float motion was erratic over a large percentage (60% or more) of the timing runs represents a policy change from last year's experiments (Reference 1). At that time, owing to the known three-dimensionalities in the mean current flow, some meandering of the floats was expected. A "presmoothing" or "filtering" was built into that data by arbitrarily defining as acceptable only those floats which remained within a ± 15 cm wide band from the drop point along the longitudinal direction over the float travel distance. The number of trials was increased until the required number of successful runs (10) was obtained. In the present

experiments, no gross three-dimensionalities were present in the mean current flow. Consequently, erratic float behavior could only be attributed to the response of the floats to the above-mentioned drift layer characteristics, i.e., velocity gradient and zero velocity crossings. This point will be taken up again later when the present data is compared to last year's.

The efficiency of the timed-float technique has been demonstrated in many studies of the drift layer, including both the present and last year's study. Albeit cumbersome, time consuming, open to a number of unanswerable questions, and unesthetic, no better technique has been discovered as yet. The important questions of accuracy and reproducibility of results obtained with the time-float technique have been taken up in considerable detail in Reference 1. There it is estimated that an accuracy on the order of 5% (or better) is attained by taking the average of the middle light of ten float trials (ten, throw out the high and the low) over a one-meter travel distance.

II.2.4 Subsurface Currents

There are several devices available for measuring the speed of the subsurface current flows encountered in the present study. These include:

1. Hot film anemometers
2. Timed-neutrally buoyant floats
3. Time-dye streaks
4. Pitot-static probes
5. Neyrpic velocimeters

The first four have been used in the wind-wave facility in the past with some degree of success. The last, a French-made propeller-anemometer shown in Figure 2 was introduced just prior to the present experiments. In-house calibrations of the Neyrpic performed in an 80-ft long tow channel have demonstrated its superiority over the other devices for reasons of accuracy, and ease of

HYDRONAUTICS, INCORPORATED

-11-

use. A calibration curve is presented in Figure 3 which demonstrates remarkable linearity and an accuracy of 1% or better over the velocity range 3-150 cm/sec.

Utilizing Neyrpic velocimeters, detailed calibrations of the current system were performed; the independent variables are impeller rpm, inclination of beach (from the horizontal) and location-fetch (x), lateral position (y) and depth (z). Figure 4 presents current profiles for the case of favorable currents (with the wind), along the beach inclined at 2.65 degrees. The current depth, excluding the lower boundary layer along the beach, is seen to be uniform to within $\pm 1\%$. Figure 5 presents current profiles for the case of adverse currents along the same inclined beach. The deviation from uniformity here is $\pm 10\%$.

As discussed at some length in Reference 1, last year's experiments were overshadowed by ambiguity which arose due to the nonuniformity of the mean current flow produced by the previous current system. It was often impossible to separate those distortions of the wind-drift layer caused by interactions between surface waves and subsurface-spatially-varying currents from those caused by strong three-dimensionality of the current field itself. This subject will be taken up again later on in the present report. The point to be made here is that the current field, provided by the current system in the present study, was uniform to a fine measure, which suggests elimination of this ambiguity. The uniformity of the present flow was demonstrated both by velocity measurements and by flow visualization using concentrated vegetable dyes. This brief description of the wind-wave current facility, of its operating characteristics, and of

HYDRONAUTICS, INCORPORATED

-12-

the hydrodynamic measurements taken in the present study, should provide a foundation for the following discussion of the experiments themselves.

III. THE EXPERIMENTS

III.1 Preliminary Considerations

Prior to the design of the present experimental program, the results of the 1974 joint tests and the most recent theoretical developments were reviewed in a meeting with M. King, F. Lizzi and F. Nawar of RRI, A. Rubel of Advanced Technology Labs (ATL), J. Lewis of Techmate, and G. Elliott and R. Scotti of HYDRONAUTICS (Reference 7).

The intent was to bring modifications and improvements into this year's tests to insure that the overall objectives of the study were met. The most stringent requirements for this year's experiments was for greater accuracy both in the RRI-TV camera measurements and in HYDRONAUTICS flow measurements. The selection of the matrix of flow conditions to be tested was also important in the interest of producing discernable interaction effects within a reasonable number of experimental flow setups.

III.1.1 Experimental Accuracy

Existing theoretical predictions (References 9 and 10) suggest that spatial modulations, which may occur in the wind-wave current facility under appropriate flow conditions, are expected to be on the order of 20-25% or less. Moreover, the effects

are anticipated to be narrow-banded. The implications of these predictions are clearly that a high level of experimental accuracy must be maintained throughout each phase of the experimental program to insure that such small effects can be discerned. The stringent accuracy requirements imposed on the RRI-TV camera system will be discussed in a RRI technical report covering their activities in the present experiments. For hydrodynamic measurements, as well as for reproducibility of flow setup, an accuracy of $\pm 5\%$ was taken as the outer bound of acceptability.

Hydrodynamic measurements included:

1. mean wind speed
2. shear velocity (inferred from the mean wind profile)
3. near surface drift (measured with floats)
4. subsurface current speed
5. subsurface current gradient
6. relative surface wave height of the dominant wave.
7. surface wave frequency of the dominant wave.

An accuracy of $\pm 5\%$ (or better) was attained for all of the above measurements in the present tests. In addition, the following measurements were available from cross spectral plots with an accuracy of $\pm 10\%$ or better:

1. Phase speed of the dominant wave.
2. Wavelength of the dominant wave.
3. Phase angle (between probes) of the dominant wave.

III.1.2 Selection of Test Conditions

The following guidelines on the choice of test-flow conditions were arrived at by collaboration between ATL, Techmate and HYDRONAUTICS. Some independent thinking along these lines is given in a pretest report, dated May 1975, by J. Lewis of Techmate (Reference 8).

A. Wind speed, $U_w = 3.8$, and 6.2 (m/sec)

The lower value was selected to maximize the interaction phenomena. Below (approximately) 3m/sec the surface activity is small and difficult to measure quantitatively. The higher value was selected to include the effects of a significant change in shear velocity.

B. Subsurface current, U_c , both adverse and favorable.

$$-\frac{3}{4} \leq \frac{U_c}{U_s} \leq \frac{3}{4}$$

where U_s is the wind induced surface drift.

An avoidable and undesirable characteristics of the wind-wave-current facility was that changes in subsurface currents produced an effective change of fetch at a fixed station. Favorable currents decreased the fetch and adverse currents increased the fetch (at a fixed measuring station) relative to the wind-only case. This important point will be discussed in greater detail in Section IV. The larger values of current speed were selected to maximize the interaction effects. Smaller values were selected in accordance with what was practically possible in the facility to minimize the current-fetch effect.

C. Current gradient, $|\frac{\partial U_c}{\partial x}| \leq 10^{-2} (\frac{1}{\text{sec}})$

III.1.3 Matrix of Flow Conditions Tested

The twenty-eight different flow conditions which were tested in the present experiments are described in Tables 2 and 3, the test matrix for the 1975 joint tests. Details of the wind and subsurface current flows are given in Table 3, arranged according to data-run number. The following description explains the rationale behind the present data-run numbering system:

B refers to the beach; the number following B indicates its orientation:

1 = 0 degree inclination

4 = 2.65 degree inclination.

- C refers to the subsurface current; the numbers following C indicate the current generating impeller speed in RPM (minus mean adverse flow).
- W refers to the wind; the number following W indicates the blower speed in RPM.
- F refers to the fetch; the numbers following F indicate the fetch, measured from the point where the air stream first touches the water, in centimeters.
- M refers to the mechanical wave generator (when in use); the numbers following M indicate the speed of the motor-driven shaft in RPM.

The last four digits give the month and day on which the test was run.

In this year's experiments all tests were performed at the same measuring station, namely at 12.25 m from the point where the air stream first contacts the water. Last year's measurements were taken at an upstream station as well as to enable discernment of strongly fetch dependent effects. This aspect of the experiments was left out of the present tests in order to more fully span the ranges of the parameters in the available time.

III.2 Experimental Results

As discussed in Section III.1, the test matrix variables include: wind speed, current velocity, beach angle, and mechanical wave presence. The data taken under the present test matrix is organized as shown in the Data Presentation Outline (Table 1). As is indicated, the data has been divided into three basic groups: flat beach results, inclined beach results, and mechanical/wind-wave results.

During the flat beach experimentation, two wind conditions were considered. At 3.8 meter/second, run numbers 1 through 11 were recorded, while run numbers 12 through 15 were recorded at 6.2 m/sec. Since the objective of this aspect of the experimentation was to determine the interactive efforts of a spatially varying subsurface currents with the wind drift layer, a means of directly comparing wind drift layers is necessary. This is accomplished by subtracting the surface current with no wind (U_c) from the "overall local drift current", U_d , in a laboratory-fixed-reference frame.

$$q = U_d - U_c \quad [5]$$

The resulting value is referred to as the "relative wind drift velocity" (q). Among the data recorded at each wind speed, are conditions which have adverse (against the wind) currents and favorable (with the wind) currents of approximately equal magnitude. The drift layer profiles are thus presented in subgroups where any shift in the matrix variables would be apparent. These plots of q vs. Z (depth from surface) for various current combinations are presented as both a linear and semi-logarithmic plot. The information from the linear plot allows one to better fit a line through the semi-log representation, thus giving the best value of the friction velocity (U_x) (see Figures 6 through 13). For each of the data runs, the power spectra and wave-height cross spectra were taken as described earlier in this report. The spectra are to be found in Figures 23-53.

During the inclined-beach experimentation, the same two wind conditions were considered with various favorable and adverse currents. The data presentation is completely analogous to the flat beach condition as again shown in Table 1.

For several flat-beach conditions, mechanical waves were generated in the presence of known wind conditions. The mechanical

wave experimentation was limited to the lower wind speed of 3.8 meters/second. The measurements taken were restricted to wave-height power and cross spectra.

IV. RESULTS DISCUSSED AND SUMMARIZED

Improvement of the mean-current⁺ flow field for the 1975 test series has filled an important gap in the 1974 experimental approach. As a result, the confidence placed in the present test series is greater than that placed on earlier results. The repeatability, both over the short (several minutes) and long (several weeks) time periods, was consistently below $\pm 5\%$ and generally below $\pm 2\%$ for water velocity measurements (see Figures 4 and 5). In addition, corrections in cross-tank-wind-velocity profiles have hopefully resulted in more representative two-dimensional-wind-wave spectra. Thus the emphases placed on the two sets of data should reflect, to some extent, the change in confidence since the 1974 experimentation.

Figures 6, 8, 10 and 13 show the water velocity vs the logarithm of depth over the range from 0.07 to 25 cm. A logarithmic depth scale enables all of the data to be plotted conveniently on the same graph and, more importantly, is useful in determining the mean local value of the shear stress supported by the water itself. The law of the wall may be written as

$$\frac{U}{U_*} = \frac{1}{\kappa} \ln Z/Z_0 \quad [6]$$

where

$U_* = \left(\frac{\tau}{\rho} \right)^{\frac{1}{2}}$ is the friction velocity,
 κ is the Von Karman constant, and
 Z_0 is the equivalent roughness height
of the boundary surface or wall.

Wu, Reference 11, has shown that in the case of the wind-drift layer, Equation 6 may be rewritten as

$$\frac{U_s - U_D}{W_x} = \frac{1}{K} \ln Z/Z_0 \quad [7]$$

where

U_s is the surface drift velocity,

U_D is the local drift velocity, and

W_x is the shear velocity on the water side of the free surface.

In terms of the relative wind drift velocity (q), Equation [7] may be rewritten as

$$q = U_0 - U_c = \frac{W_x}{K} \ln Z + \text{constant} . \quad [8]$$

Thus, if the law of the wall is appropriate, the value of W_x can be deduced from the slope of a log-linear plot of q vs Z . Similarly, the values of U_x may be inferred from a plot of wind velocity vs distance above the free surface through

$$U_x = U \kappa \frac{1}{\ln Z/Z_0} = \left(\frac{\tau}{\rho} \right)^{\frac{1}{2}} . \quad [9]$$

A generally accepted approximation of the air/water interface requires the shear stress in the air to match that in the water; the following equation may be written:

$$\frac{\rho_{\text{air}}}{\rho_{\text{water}}} \approx \frac{W_x^2}{U_x^2} \quad [10]$$

where the exact equation would include a term relating the momentum transfer to the surface waves. The resulting ratio $\frac{W_x}{U_x}$ is generally considered to be of the order 1/30. As shown in Table 2, this approximate relation is valid for the present experimentation.

During the 1974 test series, it was found that the relative-wind-drift-velocity-profile (q) was shifted in velocity but maintained the same shape in the presence of spatially varying current gradients. A relaxation time was associated with this shift and its character assumed to be exponential. The relaxation time (τ') was found from the relation,

$$(q - q_0)_{\text{downstream}} = (q - q_0)_{\text{upstream}} e^{-T/\tau'} \quad [11]$$

where

$$T = \Delta x / \bar{U}_{\text{average}}$$

Δx was the distance between upstream and downstream measurement stations,

\bar{U}_{average} was the average of the mean velocities at the given station and depth

q_0 was the "no current" wind drift velocity.

The experimental curves which demonstrate this phenomena are given in Reference 1.

Although only one station was considered during the 1975 experimentation, when subsurface current was varied, a shift in the relative-wind-drift velocity profile was not observed. This would suggest that:

1. The boundary layer has relaxed completely at a fetch of 12.25 meters, (7.91 meters from the beach edge), or
2. The relaxation phenomena observed during the 1974 test series was a manifestation of the three-dimensional structure of the flow field.

The values of τ' found in 1974 were ranged from 21 to 227 seconds (Reference 1). These measurements were taken with a different beach configuration, where the fetch was 8.3 meters with the beach edge 2.56 meters from the test station. Thus, the 1974 and 1975 test results are taken at stations which are nearly 4

meters apart physically with an effective separation of 5.35 meters if the respective current-gradient-lengths are considered. If the relaxation phenomena exists and is describable through the exponential relation given in Equation [10], then one can predict the degree to which a drift layer should relax in moving from the 1974 test location to the present location. The typical numbers chosen from Reference 2 for this prediction are given below:

effective relaxation length: 5.35 m

mean depth: 0.71 mm

favorable flow

\bar{U}_{average} : 25.10 cm/sec

τ : 21 seconds.

Thus one would expect a relaxation length of 5.27 meters, while the actual effective separation was 5.35 meters. It would, therefore, seem reasonable that no relaxation related shift in the relative-drift-layer plots was observed at the present fetch.

In contrast, it may be that flow field distortions caused or accentuated the relaxation phenomena. In this case, the absence of shifts in the relative-wind-drift-layer profiles would indicate an almost immediate response of the wind-drift layer to spatially varying-subsurface current perturbations.

In addition to the considerations of current-related shifts in the drift-layer profile, it is interesting to note the drift-layer depths for various conditions as shown in Figures 6, 8, 10, and 13. These drift-layer depths appear to be a function of wind speed, beach angle, and to some extent current direction. Figure 15 illustrates a tenuously defined relation between beach angle, wind speed and drift-layer depth. The error bars indicated include both favorable and adverse currents within their limits.

However, it is generally observed that adverse currents are associated with shallower wind-drift layers. This is surprising since adverse currents increase the effective fetch and thus allow more momentum transfer to the water. It is also noted that the energy contained within the drift layer is a function of the wind speed and beach angle. This is reflected in the values of W_* and drift-layer depth (δ). The energy contained in the wind-drift layer does not appear to be a function of current magnitude/direction which is again surprising given fetch considerations. No attempt is made to explain the causes of these observations at this time; however, future attempts should consider physical constraints such as the ratio of wavelength to in situ depth, Reynolds wave stress within the drift layer, and the vertical velocity component which may add to turbulent mixing.

The surface wave spectra modifications recorded by the RRI Digital-Video-System (DVS) will be presented under their cover. The temporal wave spectra recorded by HYDRONAUTICS, Incorporated during the present test series represent a significant improvement over the 1974 data. Figures 21 and 22 are presented as typical power spectra as recorded during 1975. A line drawn on the power spectrum of a slope of -5 provides for comparison of the high frequency portion of the spectrum in the wind-wave facility to that predicted by Phillips (References 4 and 5) for the case of infinite fetch. The agreement is quite good, reflecting the solution of probe-frequency-response problems. The dominant frequency and relative amplitude measurements inferred from the power spectra slope are self-consistent with respect to current direction and magnitude. That is, as the current changes from strong adverse to strong favorable, the dominant wave frequencies are increasing while the dominant wave amplitudes are decreasing. This effect is due to many intimately-related phenomena. As briefly described in earlier sections, a change in current (magnitude and

direction) effectively changes the fetch for a given volume of water as it moves down the tank. In addition, a fixed probe will measure a different frequency since the laboratory-fixed reference frame is only "valid" for the zero current case. This so-called reference frame is difficult to generalize for the widely different roles which it must fill. For instance, the effective roughness length (k) seen by the wind is a function of wavelength and frequency in the wind-fixed reference frame. In this aspect, the roughness length is intimately related to the rate of energy transfer from the air to the water and thus affects the energy contained in wave motion and wind-drift boundary layer motion. The important point which this raises is that each aspect of wind-wave-current interactions has a specific reference frame which applies and this need not be the laboratory reference frame. Since wave height probes are fixed in space, the information (C_p , λ , f) which is obtained from such probe is not directly applicable to the dynamics of wind-wave-current interactions. Figures 17 through 20 describe the relationship between the frequency of the dominant wave and the subsurface current, as observed in the laboratory reference frame. A detailed discussion of the physics which would be expected to play a role in determining the shape of the aforementioned plots is not addressed in this study. However, it is important to note that the current related shifts in spectral plots may be a result of dynamic interactions rather than strict fetch considerations. The power spectra are presented for all test conditions in Figures 23 through 53, while representative cross spectra are given in Figures 41, 44, 46 and 48. The phase angle, phase speed and dominant wavelength are inferred from the cost spectra. The data obtained from these plots are also self-consistent. Phase speeds and phase angles generally increase with favorable currents while wavelength grows shorter. The spectral results are summarized in Table 3.

V. CONCLUDING REMARKS

A number of wind-wave-current phenomena have been documented during the present test program. The combined effects of wind speed and direction, current-streamwise gradient, fetch, and current direction and magnitude on surface wave modulations are complicated. To develop an experimental test plan, which would fully explore all experimental aspects of this problem, would involve a very extensive effort. However, the two experimental test series which have been conducted to date have certainly provided a strong base for theoretical work.

The question of a relaxation phenomena occurring within the wind-drift layer remains open to interpretation by theorists. A final anticipated report should correlate the data from both HYDRONAUTICS, Incorporated and Riverside Research Institute with theoretical predictions by Phillips and Vaglio-Laurin. Experimental work to date suggests that surface modulations in the laboratory are very small; however, the appropriate scaling laws for the open ocean conditions are only presently being worked out.

HYDRONAUTICS, INCORPORATED

-24-

REFERENCES

1. Scotti, R. S., "A Laboratory Study of Wind-Wave-Current Interactions, Joint Laboratory Tests with Riverside Research Institute, Part I," HYDRONAUTICS, Incorporated Technical Report 7211-8, January 1975.
2. "Wave Tank Experiments made at the HYDRONAUTICS Facility in the Fall of 1974," Riverside Research Institute, New York, N. Y., January 28, 1975.
3. Bendak, J. S. and Piersol, A. G., "Random Data: Analysis and Measurement Procedures," Wiley and Sons, 1971.
4. Phillips, O. M., "The Equilibrium Range in the Spectrum of Wind Generated Waves," JFM, Vol. 4, pp. 426-434, 1958.
5. Phillips, O. M., "The Dynamics of the Upper Ocean," Cambridge Press, 1965.
6. See for example: Mitsuyasn, H. and Honda, T., "The High Frequency Spectrum of Wind-Generated Waves," J. Ocean. Soc. of Japan, Vol. 30, No. 4, August 1974.
7. See letter to Dr. Richard F. Hoglund from Dr. Richard S. Scotti dated April 18, 1975.
8. Lewis, J. E., "Wind Waves - Energy Spectra, Statistical Stability and Current Interactions, A Pretest Report," Techmate, Inc., May 1975.
9. Private Communications, Dr. B. West of Physical Dynamics, Inc., September 6, 1974 and
10. Private Communications, Drs. R. Vaglio-Laurin and A. Rubel of Advanced Technology Labs, October 22, 1975.
11. Wu, J., "Wind-Induced Drift Currents," HYDRONAUTICS, Incorporated Technical Report 7303-3, August 1973.

Table 1
Data Presentation Outline

Facility and Instrumentation Description	Figures 1 - 5
Drift Layer Measurements	Figures 6 - 13
Test Matrix and Flow Summary Description	Table 2
Wind Friction Velocity (U_*) vs Wind Speed (U_w)	Figure 14
Wind Speed (U_w) vs Drift Layer Thickness (δ)	Figure 15
Wind Friction Velocity and Wind Velocity vs Fetch	Figure 16
Current Velocity (U_c) vs Dominant Wave Frequency	Figures 17 - 20
Spectral Data Summary	Table 3
Power Spectra vs Current Velocity (U_c)	Figure 21
Power Spectral Repeatability	Figure 22
Flat Beach Power Spectra - $U_w = 3.8$ m/sec	Figures 23 - 35
Flat Beach Power Spectra - $U_w = 6.2$ m/sec	Figures 36 - 39
Inclined Beach Power Spectra - $U_w = 3.8$ m/sec	Figures 40, 42, 43, 45, 47
Inclined Beach Cross Spectra - $U_w = 3.8$ m/sec	Figures 41, 44, 46, 48
Inclined Beach Power Spectra - $U_w = 6.2$ m/sec	Figures 49 and 50
Flat Beach Mechanical Wave Power Spectra - 3.8 m/sec	Figures 41 - 53

HYDRONAUTICS, INCORPORATED

Table 2
HYDRONAUTICS, INCORPORATED - RIVERSIDE RESEARCH INSTITUTE
TEST MATRIX (1975)
Fetch = 12.25 m

No.	Data Run No.	WIND		WATER		
		U_w (m/sec)	U_{*a} (cm/sec)	U_c (cm/sec)	$\frac{\partial U_c}{\partial x} \left(\frac{1}{\text{sec}} \right)$	W_* (cm/sec)
1	B1 C-424 W450F1225 1209	3.80	26.0	-13.10	0	-
2	B1 C-315 W450F1225 1113			- 9.80		-
3	B1 C-284 W450F1225 1209			- 8.70		-
4	B1 C-219 W450F1225 1205			- 6.80		1.35
5	B1 C-145 W450F1225 1204			- 4.60		0.74
6	B1 C-088 W450F1225 1204			- 2.30		-
7	B1 C 000 W450F1225 1113			0		0.64
8	B1 C 081 W450F1225 1204			2.90		0.79
9	B1 C 117 W450F1225 1205			4.50		0.87
10	B1 C 216 W450F1225 1113			8.40		0.93
11	B1 C 324 W450F1225 1209			12.80		0.82
12	B1 C-550 W750F1225 1210	6.20	37.0	-17.20		≈1.30
13	B1 C-353 W750F1225 1210			-10.95		≈1.30
14	B1 C 000 W750F1225 1210			0		1.41
15	B1 C 324 W750F1225 1210			13.50		1.32

(continued)

Table 2 - Continued

No.	Data Run No.	WIND		WATER		
		U_W (m/sec)	U^*_a (cm/sec)	U_c (cm/sec)	$\frac{\partial U_c}{\partial x} \left(\frac{1}{\text{sec}} \right)$	W^* (cm/sec)
16	†† B4 C-262 W450F1225 1211	3.80	26.0	-12.10	-11.3×10^{-3}	0.71
17	B4 C-220 W450F1225 1112			-10.30	-9.4×10^{-3}	-
18	B4 C-174 W450F1225 1211			-8.00	-7.5×10^{-3}	0.85
19	B4 C 000 W450F1225 1112			0	0	0.72
20	B4 C 190 W450F1225 1112			10.00	9.4×10^{-3}	0.78
21	B4 C 203 W450F1225 1211			10.80	10.1×10^{-3}	0.77
22	B4 C 294 W450F1225 1211			16.20	15.5×10^{-3}	0.71
23	B4 C-324 W750F1225 1212	6.20	37.0	-15.40	-14.4×10^{-3}	-
24	B4 C 000 W750F1225 1210			0	0	1.41
25	B4 C 294 W750F1225 1211			16.70	15.6×10^{-3}	1.42
26	B1 C 000 W450M75** F1225 1203	3.80	26.0	0	0	≈ 0.64
27	B1 C-145 W450 M75 F1225 1204			-4.40		≈ 0.74
28	B1 C 117 W450 M75 F1225 1205			4.34		≈ 0.87

$$* \quad \frac{\partial U_c}{\partial x} = \frac{U_c}{h} \tan \alpha, \quad \alpha = 2.62^\circ, \quad h(\text{Test}) = 48.83 \text{ cm.}$$

** Mechanical Wave: Period ≈ 0.8 sec, amplitude ≈ 4 cm.

† B1-Beach Inclination $\alpha = 0^\circ$.

†† B4-Beach Inclination $\alpha = 2.62^\circ$.

HYDRONAUTICS, INCORPORATED

Table 3
Summary of Results
Wave Height Measurements
(Dominant Wave Only)

No.	Data Run Number	Dominant Frequency (Hz)	λ (cm)	C_p (cm/sec)	Phase Angle ϕ (deg)
1	B1 C-424 W450F1225 1209	2.19	24.71	54.11	71.62
2	B1 C-315 W450F1225 1113	2.27	-	-	-
3	B1 C-284 W450F1225 1209	2.42	25.31	61.25	70.05
4	B1 C-219 W450F1225 1205	2.656	23.22	61.66	76.31
5	B1 C-145 W450F1225 1204	2.813	22.94	64.52	77.25
6	B1 C-088 W450F1225 1204	3.125	18.17	56.79	97.49
7	B1 C 000 W450F1225 1203	3.52	16.20	57.01	109.25
8	B1 C 081 W450F1225 1208	3.91	14.57	56.97	121.48
9	B1 C 117 W450F1225 1205	3.91	12.97	50.72	136.44
10	B1 C 216 W450F1225 1201	3.52	-	-	-
11	B1 C 324 W450F1225 1209	4.92	12.34	60.71	143.62
12	B1 C-550 W750F1225 1210	1.76	38.42	67.62	46.03
13	B1 C-353 W750F1225 1210	1.95	34.68	67.62	51.17
14	B1 C 000 W750F1225 1210	2.54	26.29	66.77	67.37
15	B1 C 324 W750F1225 1210	3.52	21.76	76.59	81.33
16	B4 C-262 W450F1225 1211	2.34	22.26	52.09	79.72
17	B4 C-226 W450F1225 1112	2.34	19.72	46.14	98.53
18	B4 C-174 W450F1225 1211	2.66	20.79	55.06	85.46
19	B1 C 000 W450F1225 1112	3.52	16.20	57.01	109.25
20	B4 C 190 W450F1225 1112	4.30	15.21	65.82	126.95
21	B4 C 203 W450F1225 1211	4.70	13.45	58.86	141.64
22	B4 C 294 W450F1225 1211	5.08	14.64	74.40	141.26
23	B4 C-324 W750F1225 1212	1.88	38.73	72.80	45.63
24	B4 C 000 W750F1225 1210	2.54	26.28	66.77	67.37
25	B4 C 294 W750F1225 1217	3.52	10.81	38.05	163.73
26	B1 C-145 W450 M75 F1225 1204	1.25	79.44	99.31	22.30
27	B1 C 000 W450 M75 F1225 1203	1.25	126.80	171.00	12.95
28	B1 C 117 W450 M75 F1225 1205	1.25	183.60	228.70	9.68

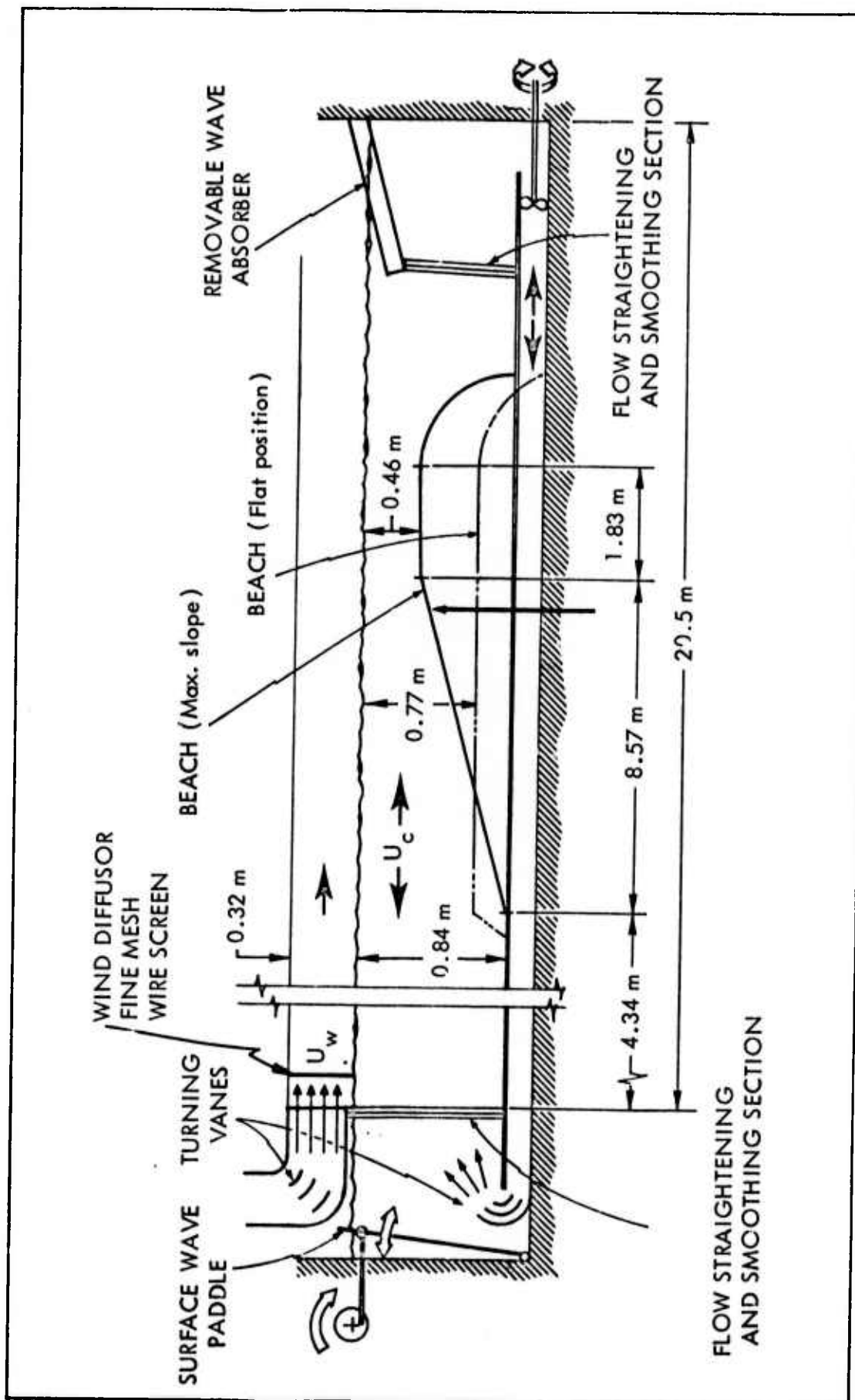


FIGURE 1 - SCHEMATIC OF WIND-WAVE-CURRENT FACILITY SHOWING SUBMERGED BEACH AND CURRENT SYSTEM; 1975 TESTS

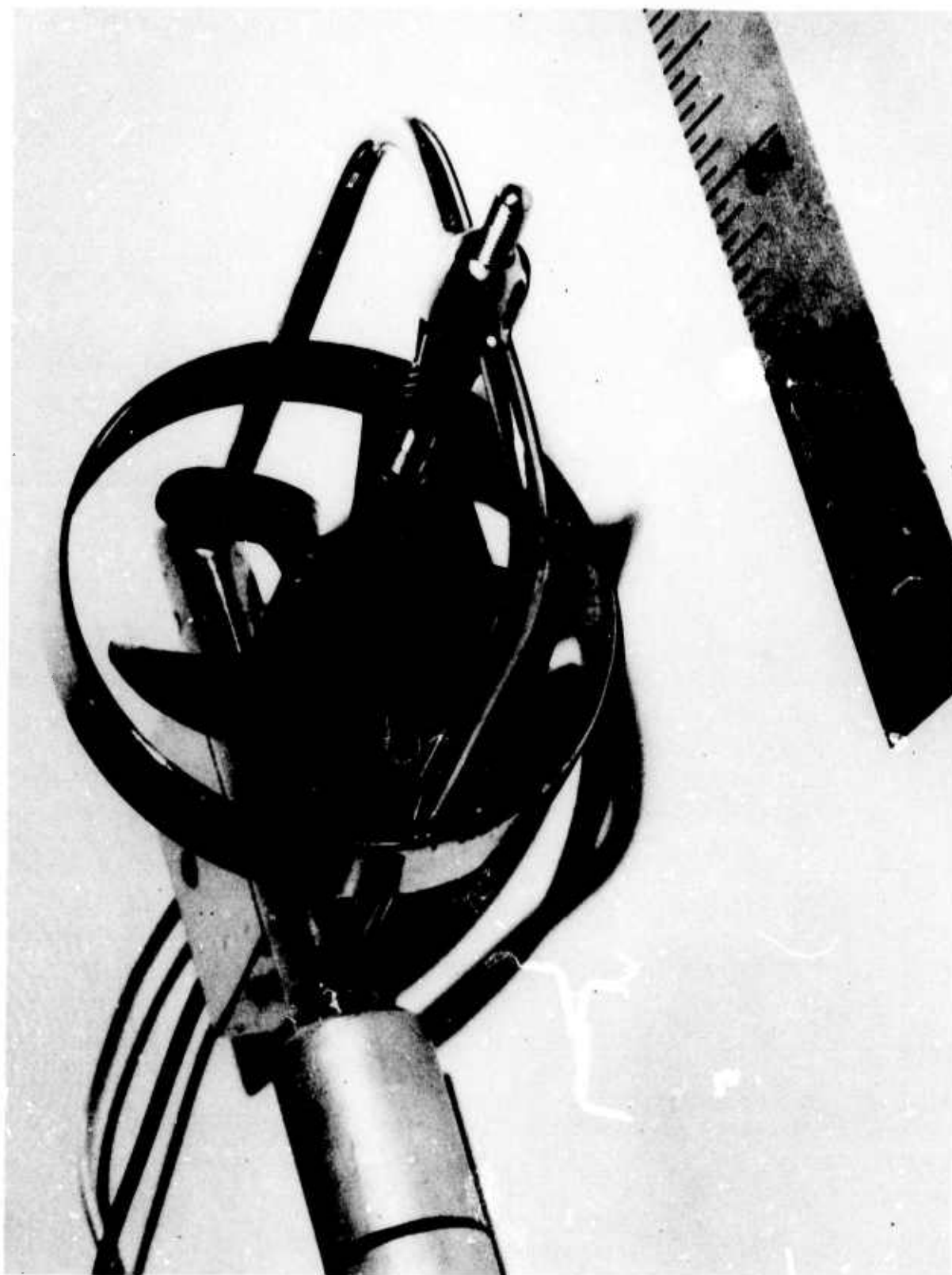


FIGURE 2 - NYREPIC VELOCIMETER

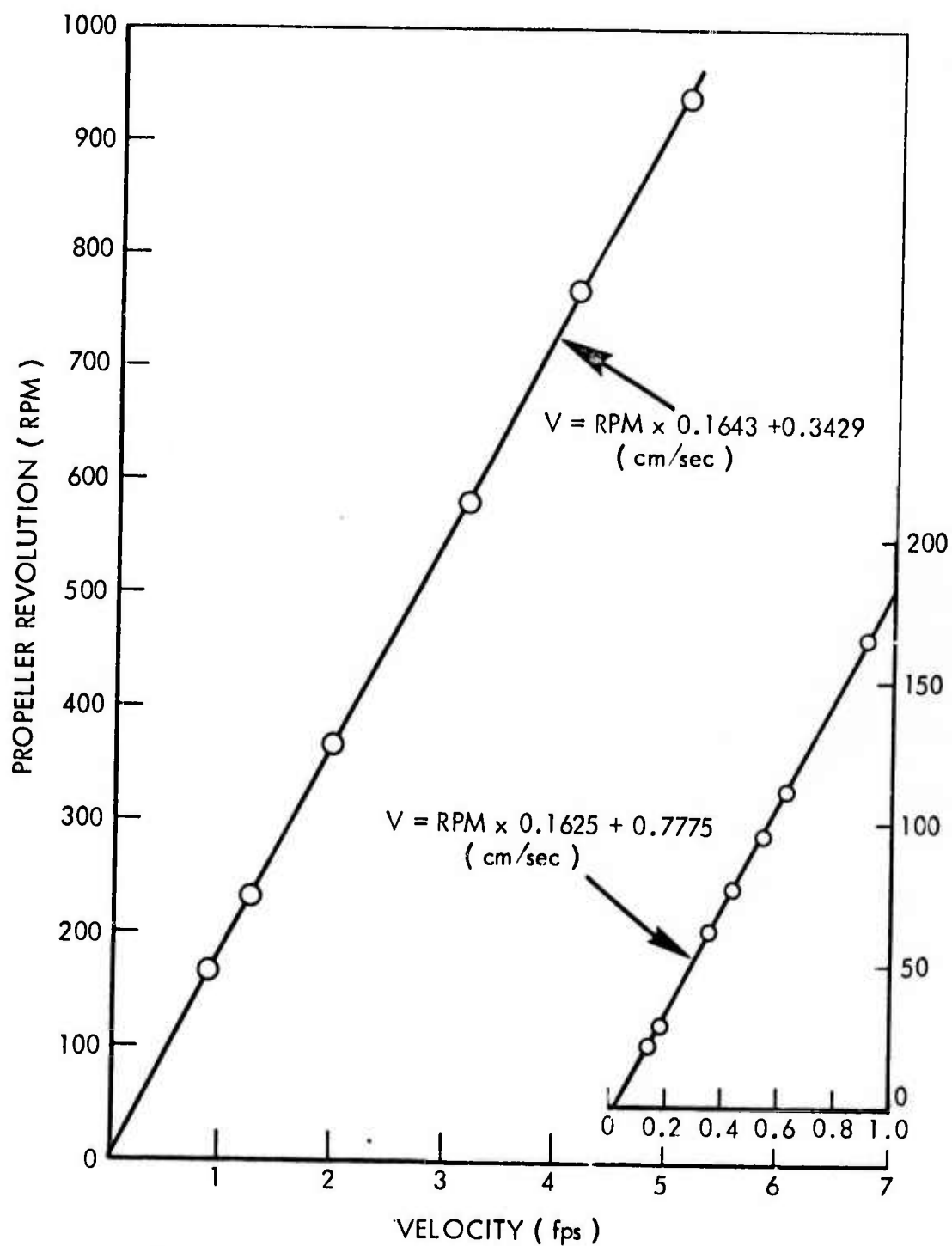


FIGURE 3 - CALIBRATION OF NYREPIC VELOCIMETER NO. 6272

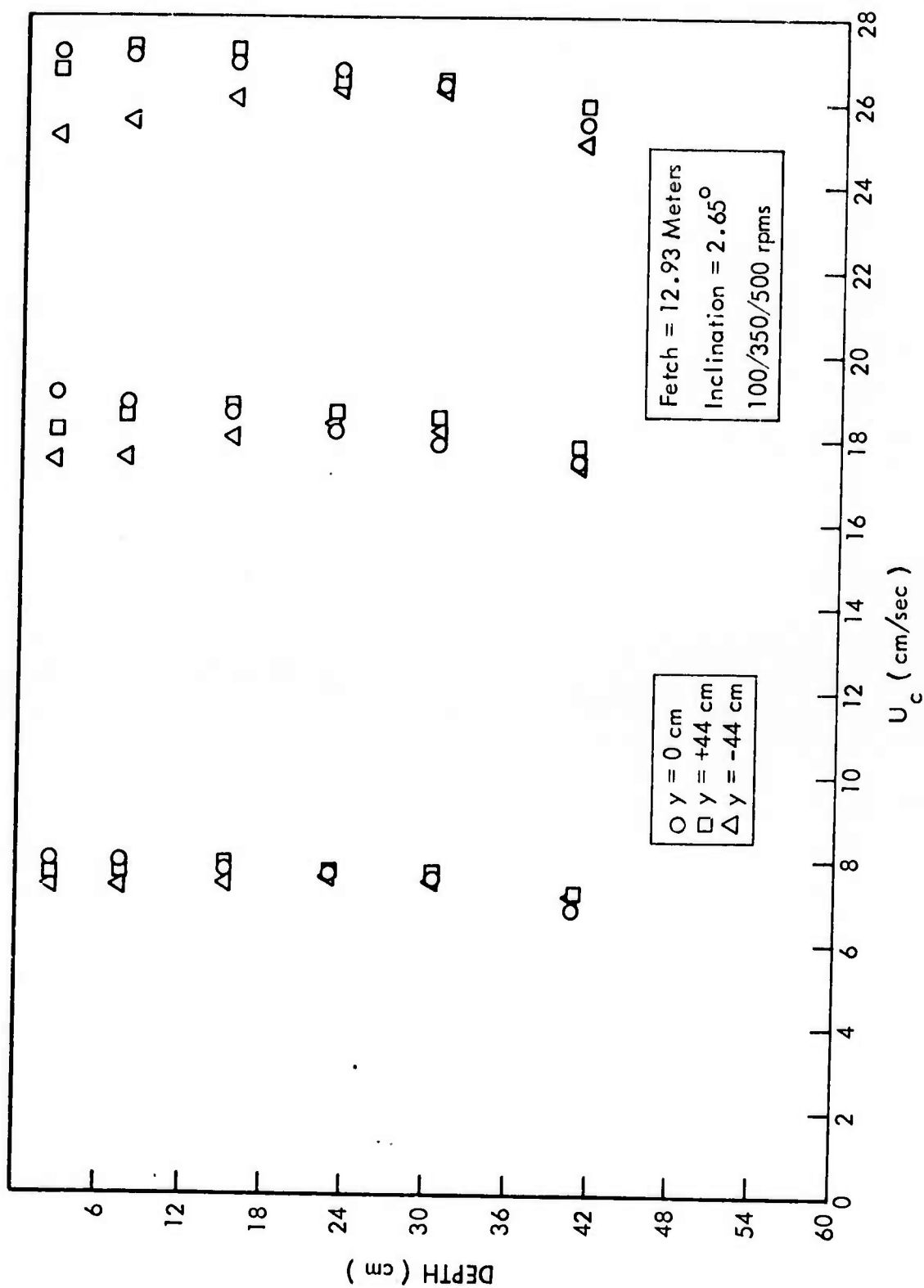


FIGURE 4 - CURRENT PROFILE - FAVORABLE FLOW

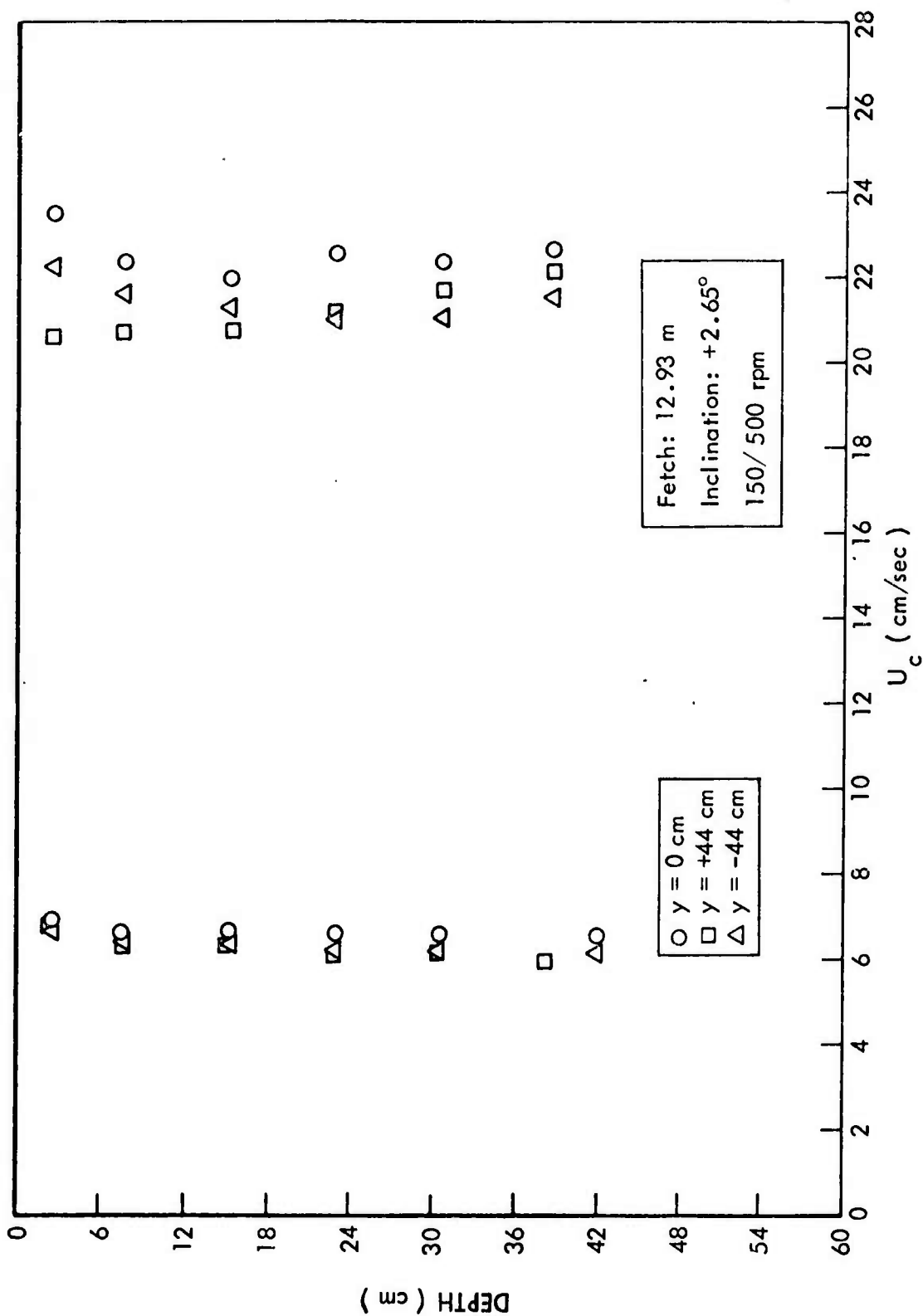
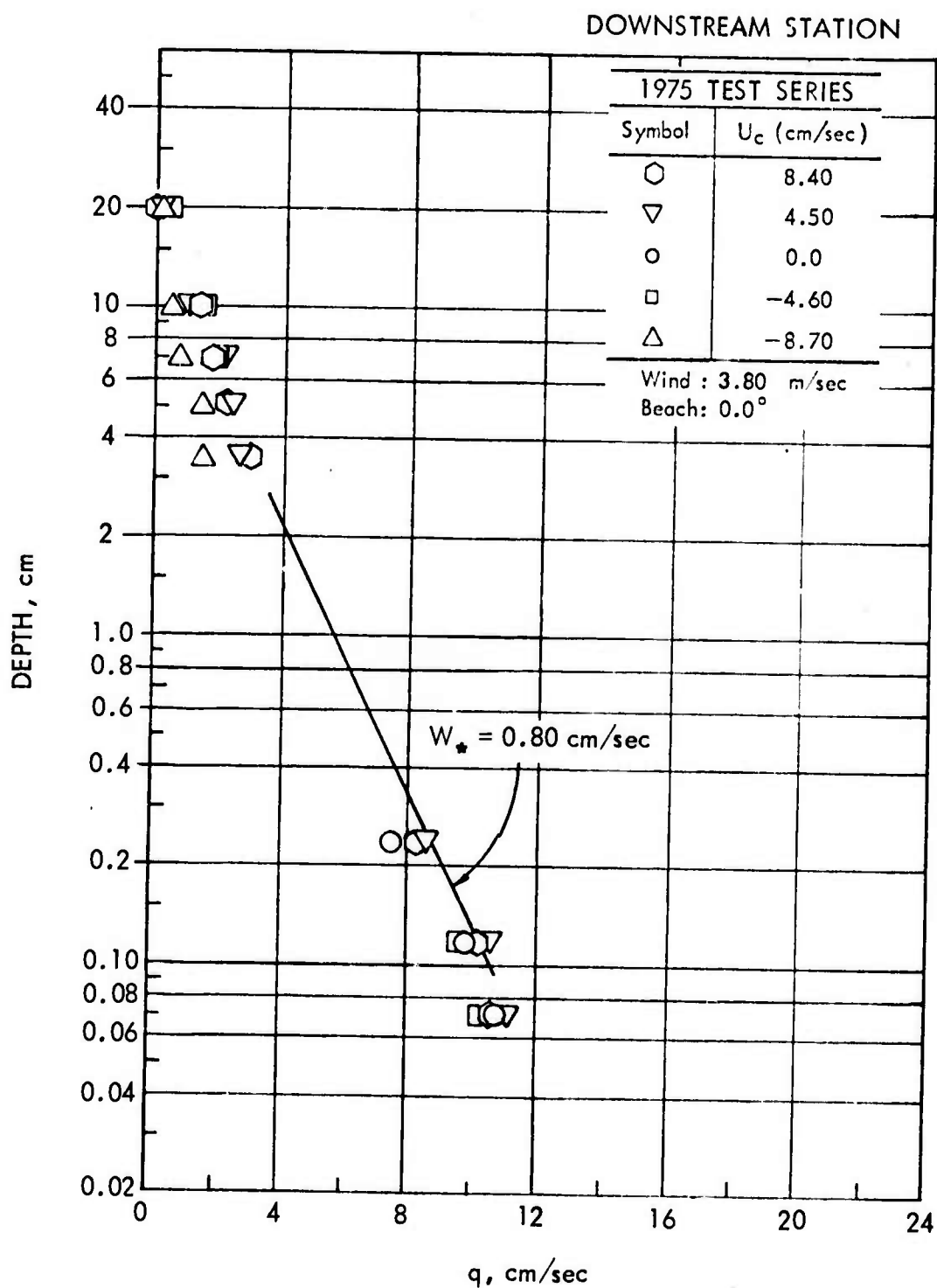


FIGURE 5 - CURRENT PROFILE - ADVERSE FLOW



Note: No "relaxation" apparent

FIGURE 6 - NEAR-SURFACE DRIFT MEASUREMENTS - SEMILOG PLOT

HYDRONAUTICS, INCORPORATED

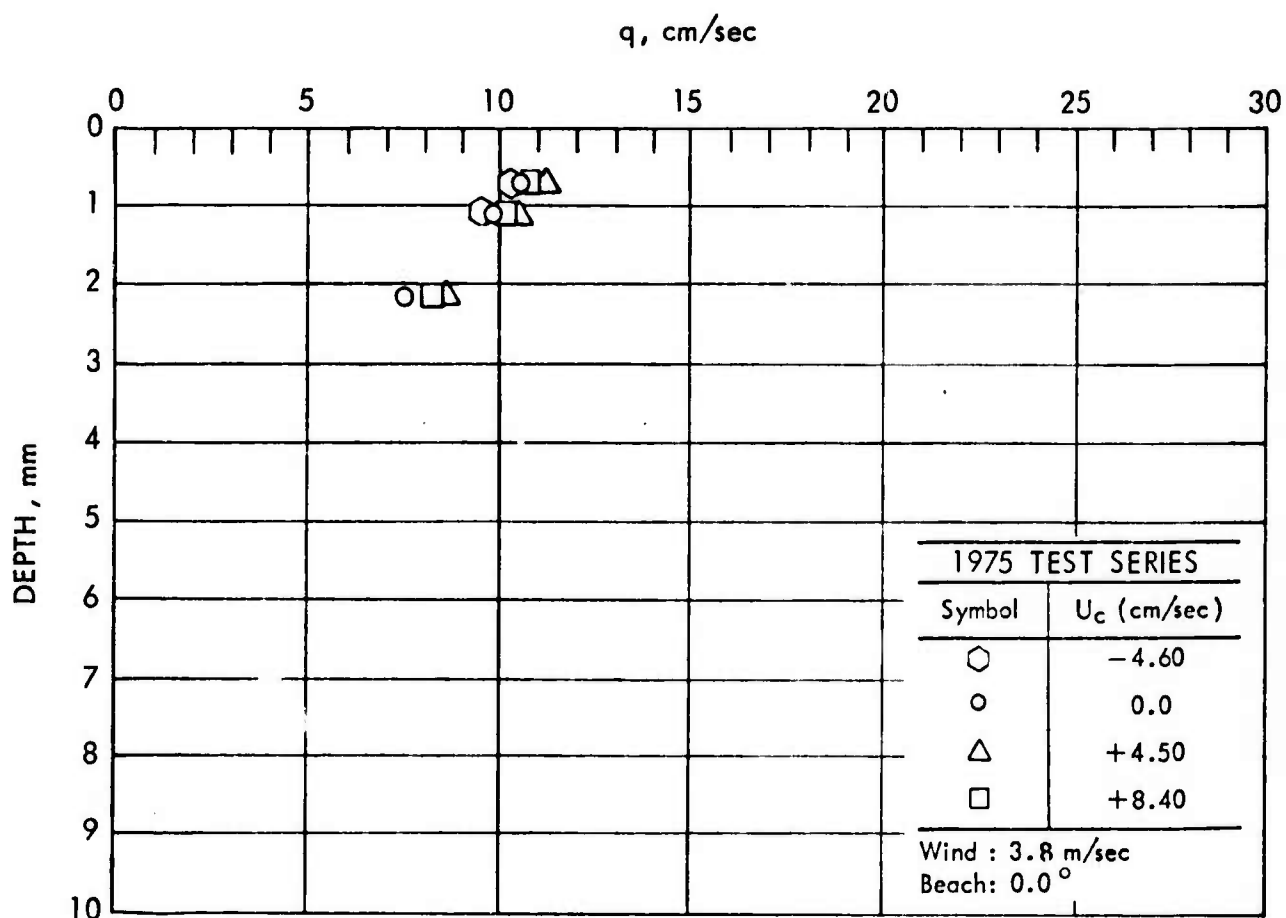


FIGURE 7 - NEAR-SURFACE DRIFT MEASUREMENTS

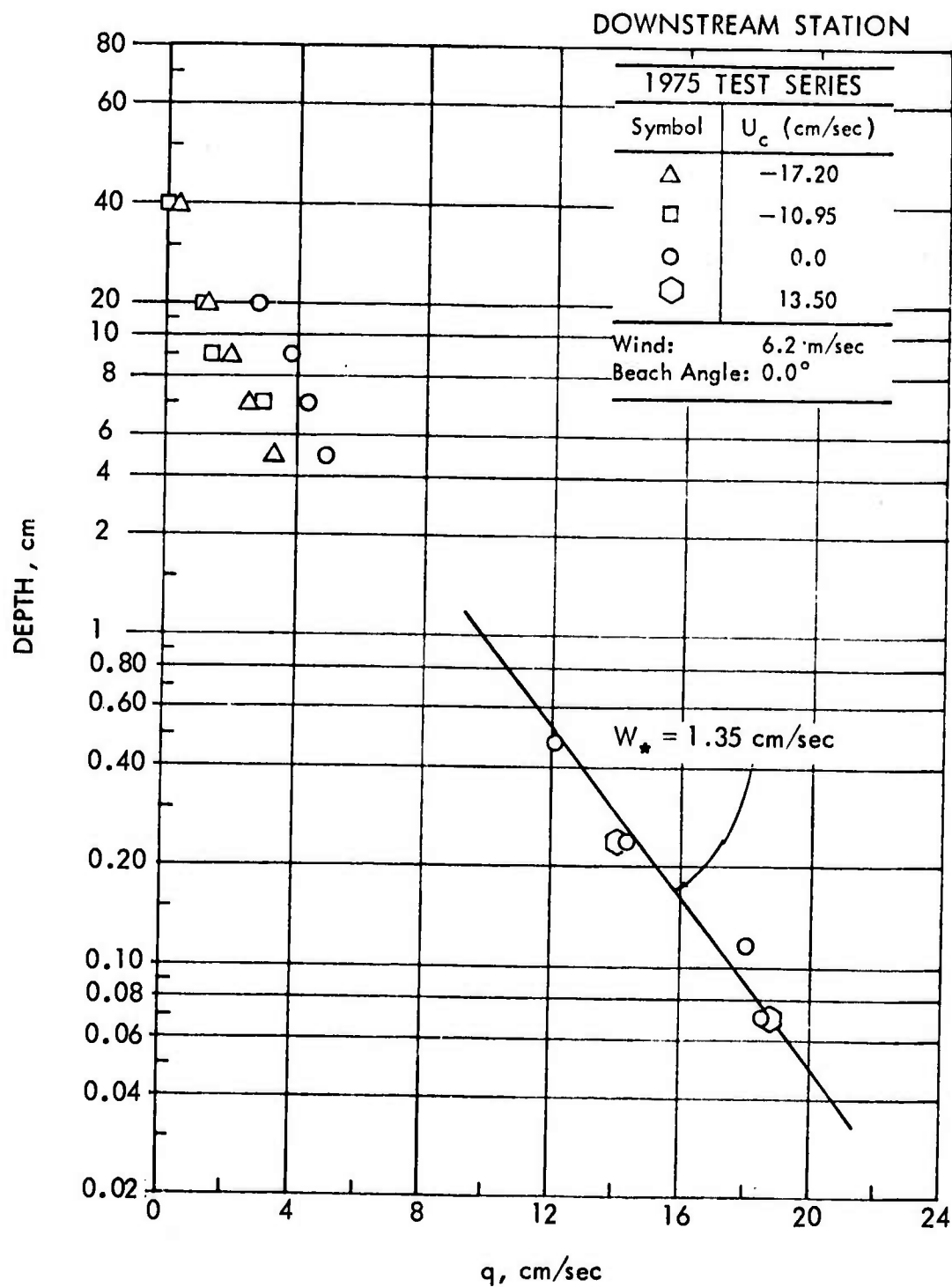


FIGURE 8 - NEAR-SURFACE DRIFT MEASUREMENTS - SEMILOG PLOT

HYDRONAUTICS, INCORPORATED

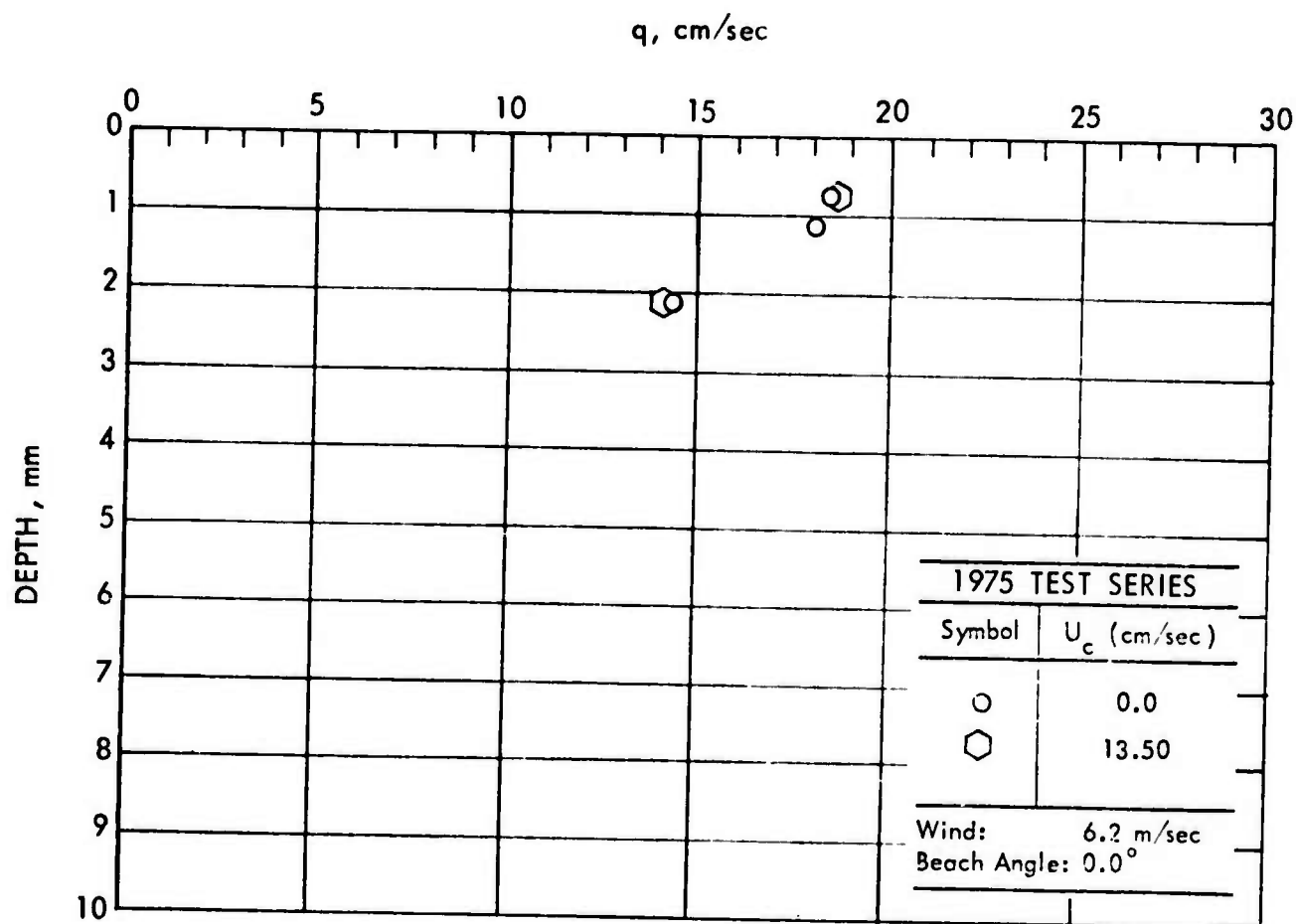


FIGURE 9 - NEAR-SURFACE DRIFT MEASUREMENTS

HYDRONAUTICS, INCORPORATED

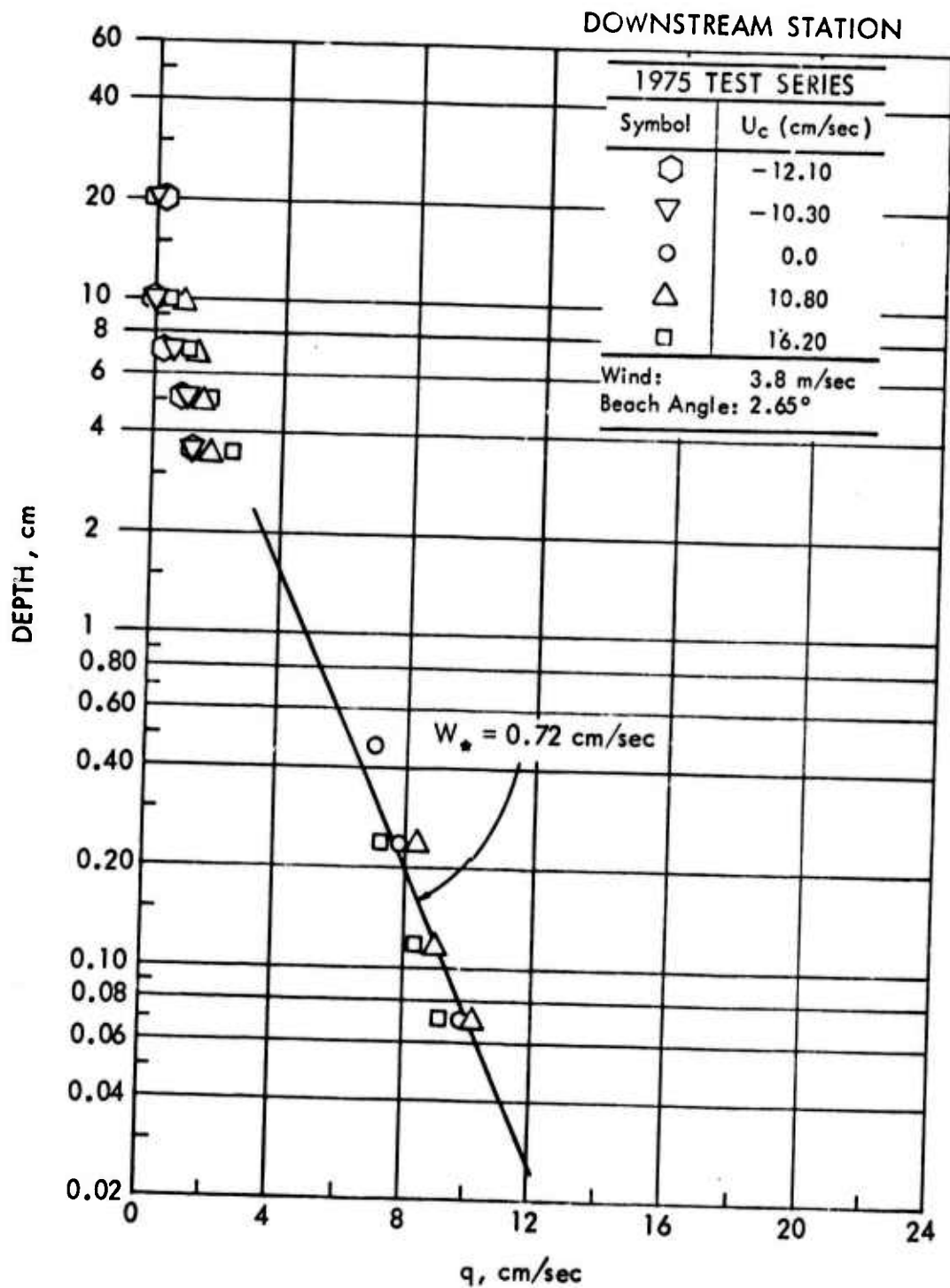


FIGURE 10 - NEAR-SURFACE DRIFT MEASUREMENTS - SEMILOG PLOT

HYDRONAUTICS, INCORPORATED

NEAR-SURFACE DRIFT MEASUREMENTS

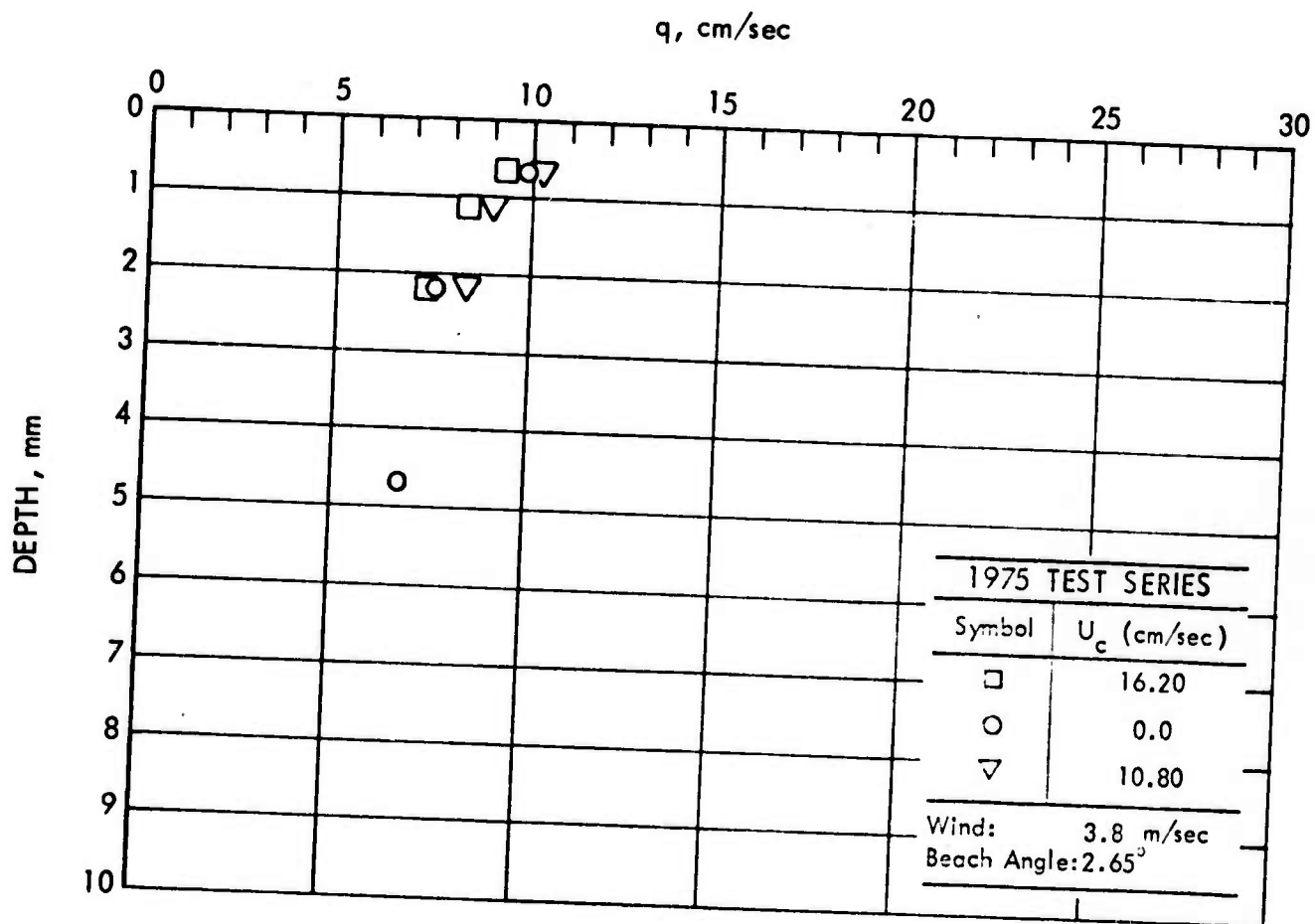


FIGURE 11 - NEAR-SURFACE DRIFT MEASUREMENTS

HYDRONAUTICS, INCORPORATED

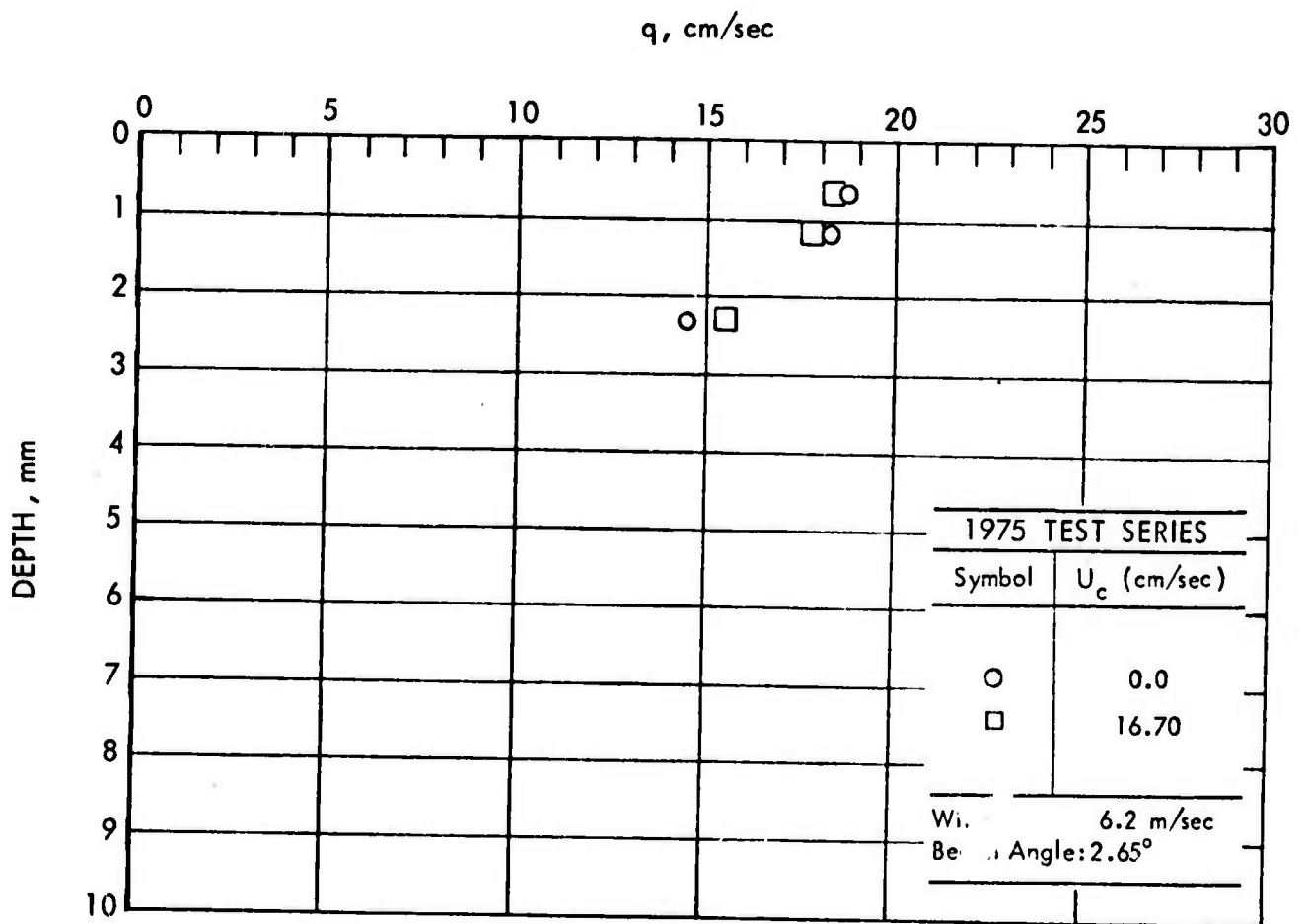


FIGURE 12 - NEAR-SURFACE DRIFT MEASUREMENTS

HYDRONAUTICS, INCORPORATED

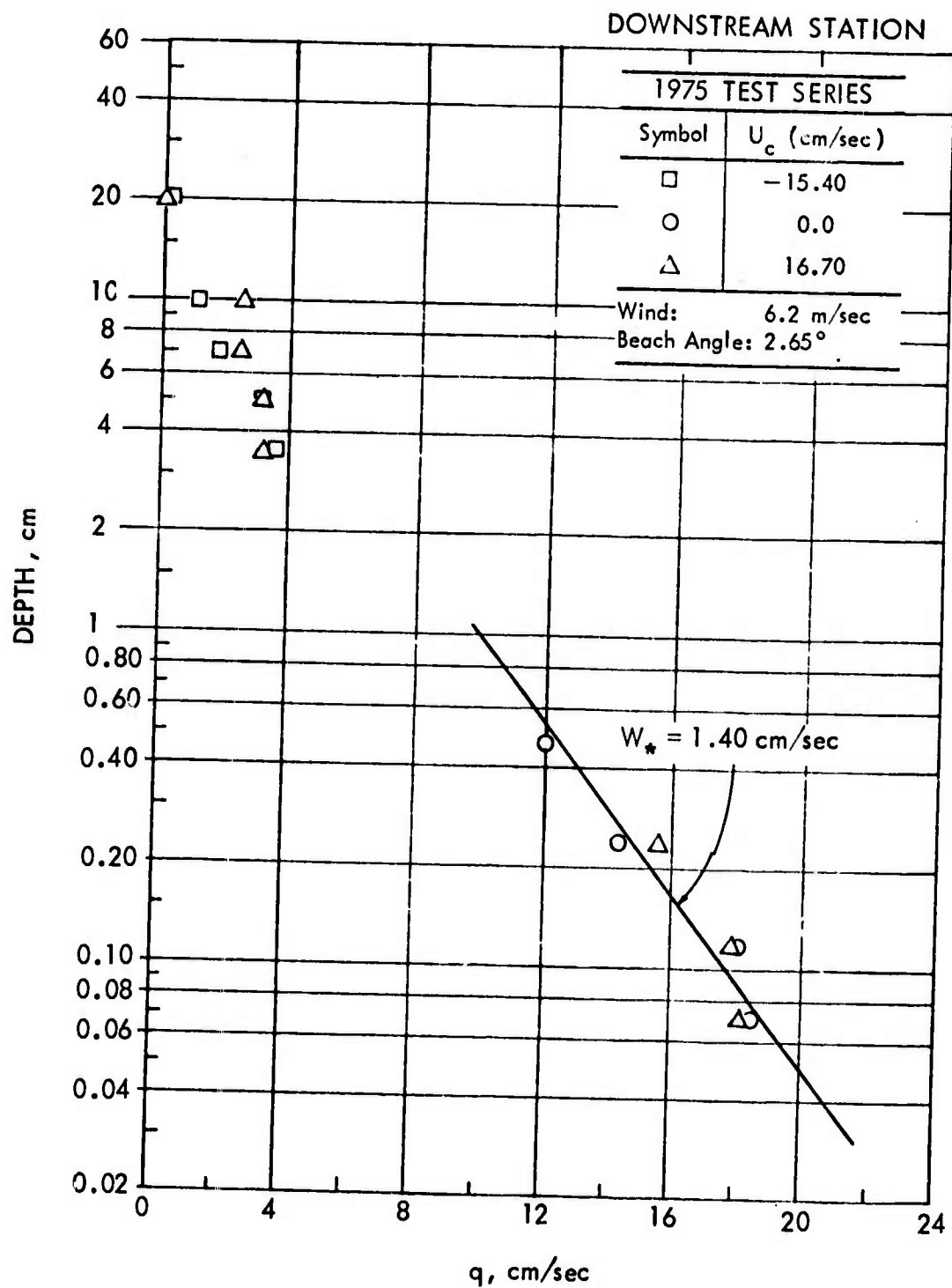


FIGURE 13

HYDRONAUTICS, INCORPORATED

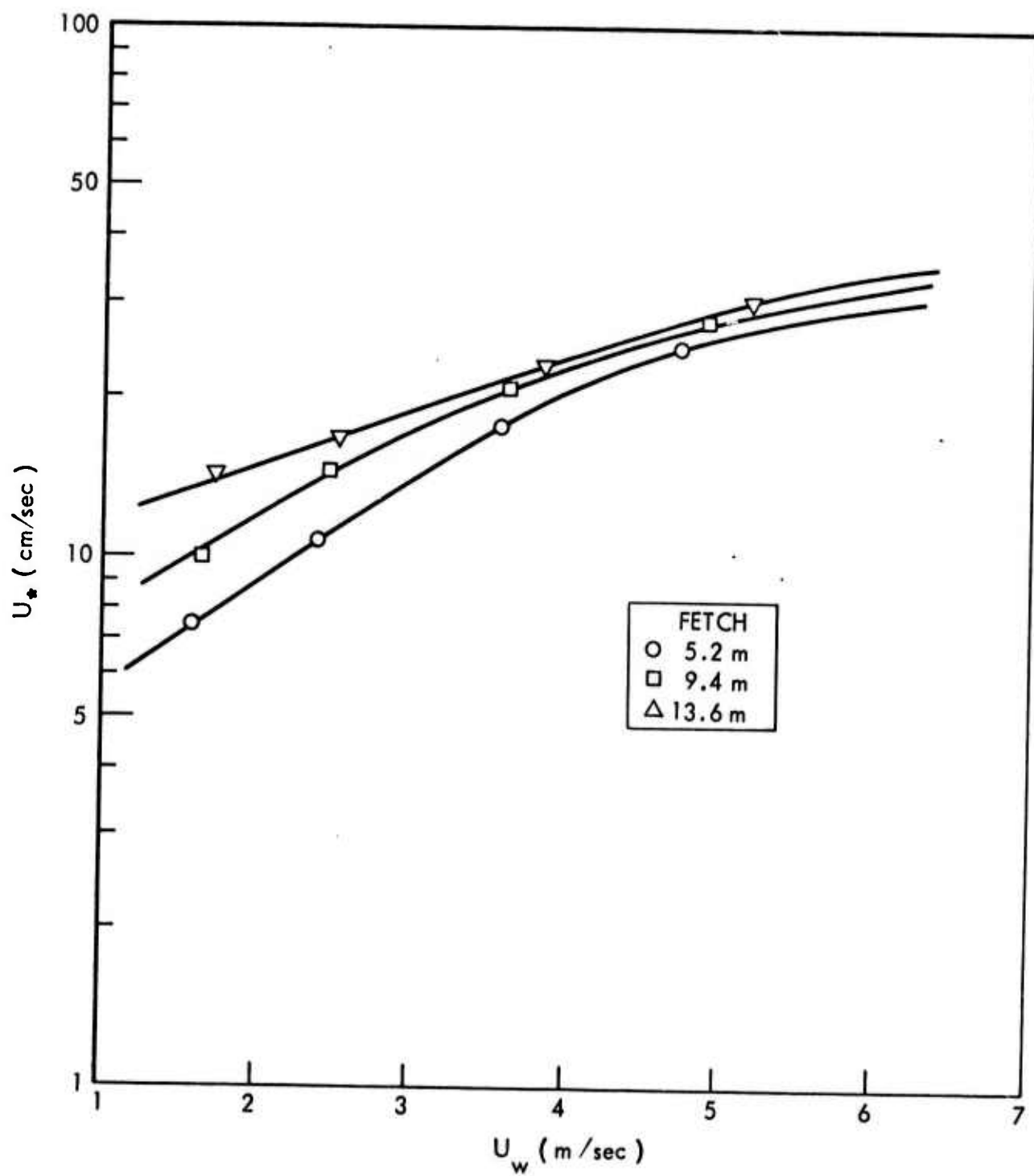


FIGURE 3 - U_* VS U_w

HYDRONAUTICS, INCORPORATED

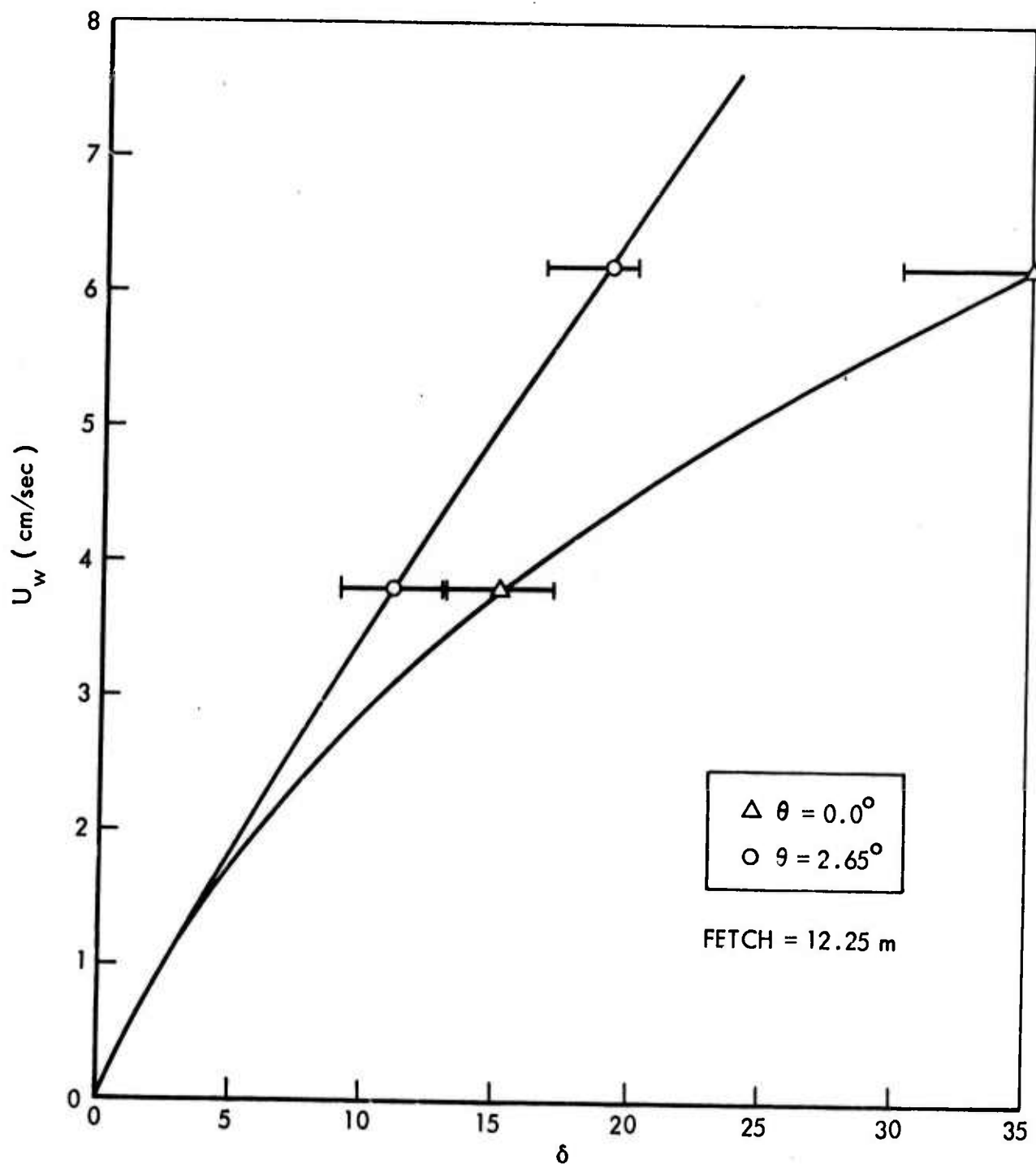


FIGURE 15 - WIND SPEED (U_w) VS DRIFT LAYER THICKNESS (δ) FOR TWO BEACH ANGLES (θ)

HYDRONAUTICS, INCORPORATED

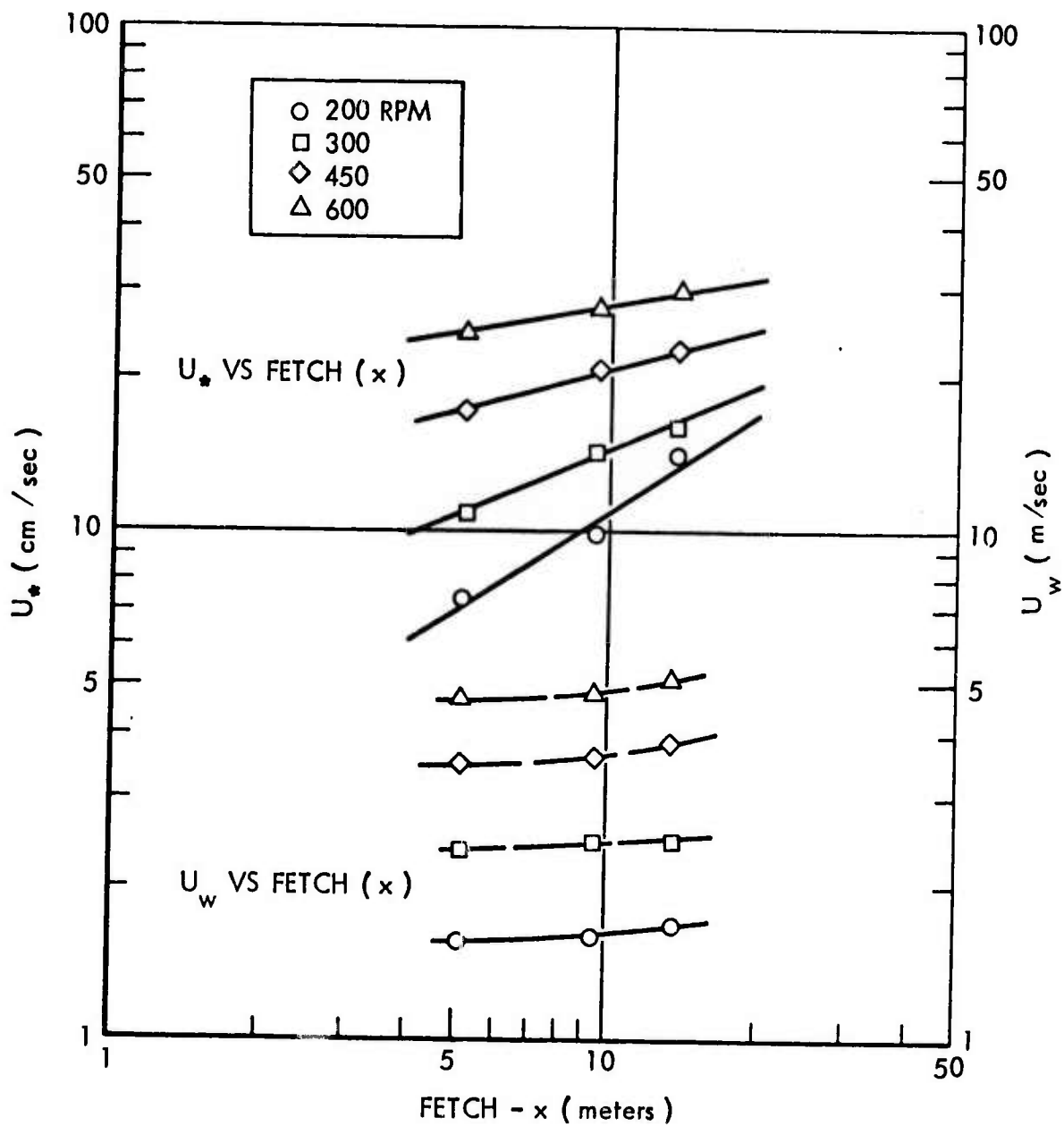


FIGURE 16 - FETCH EFFECTS

HYDRONAUTICS, INCORPORATED

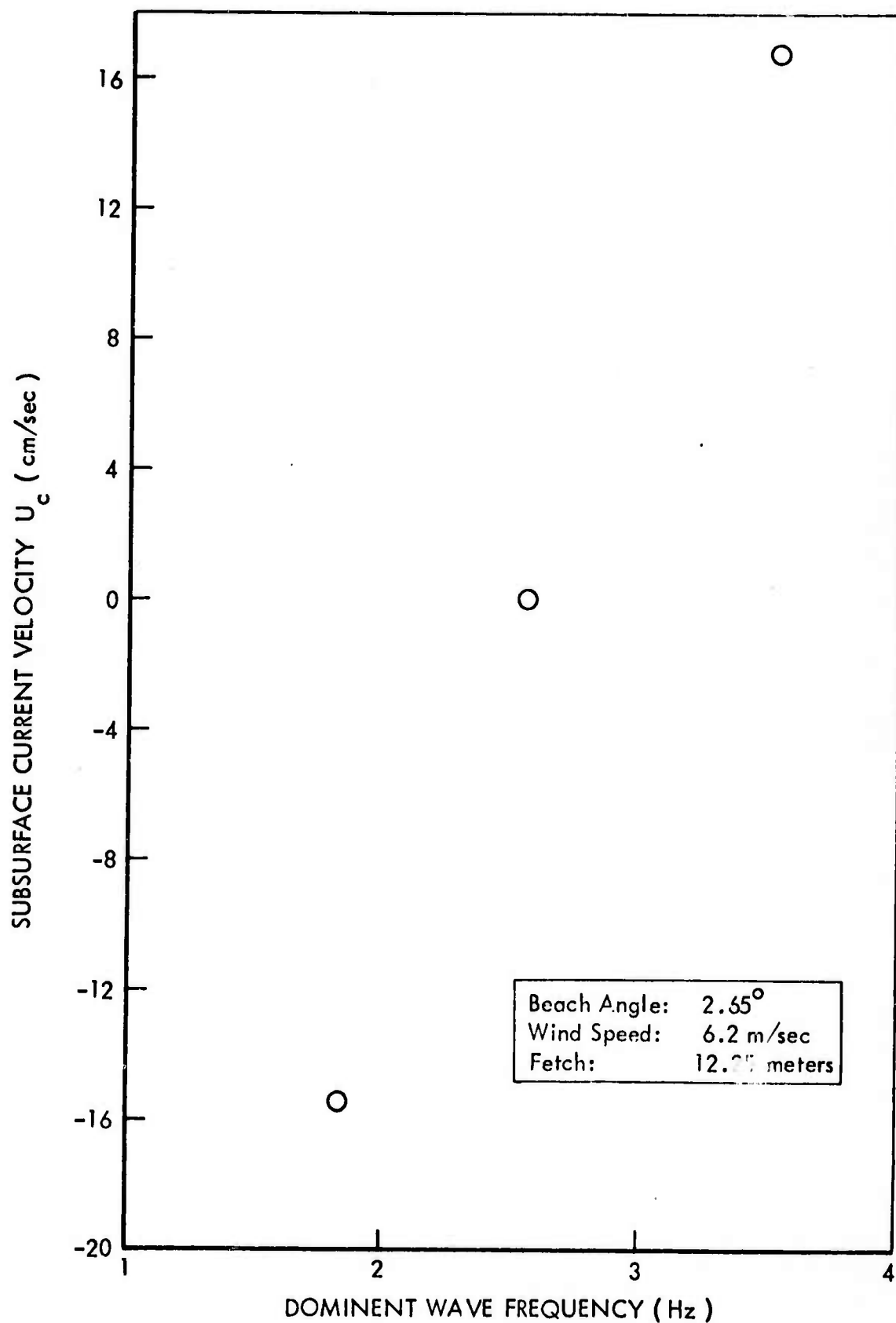


FIGURE 17 - SHIFT IN DOMINANT WIND WAVE FREQUENCY DUE TO SPATIAL VARYING SUBSURFACE CURRENTS

HYDRONAUTICS, INCORPORATED

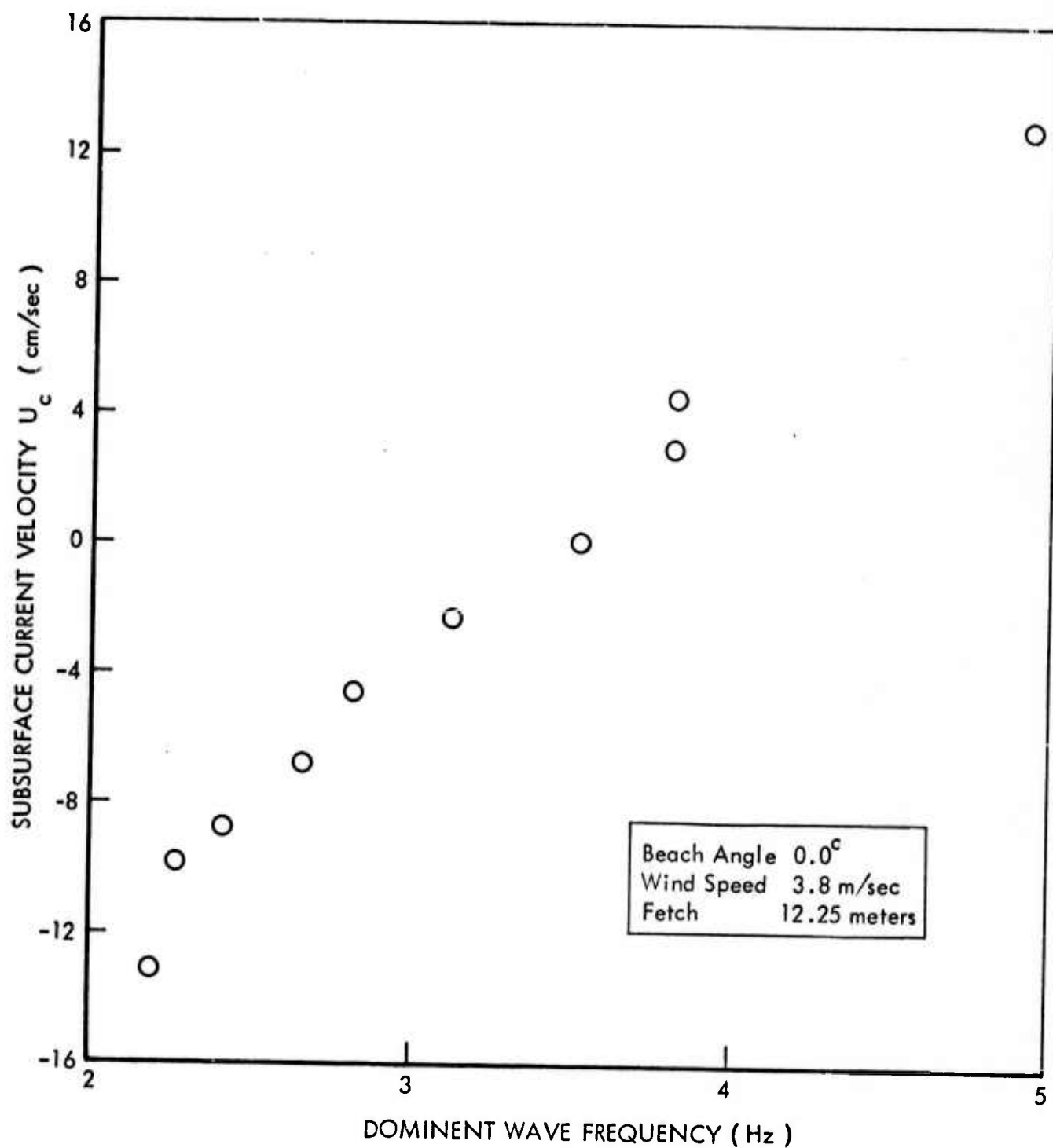


FIGURE 18 - SHIFT IN DOMINANT WIND-WAVE FREQUENCY DUE TO SPATIAL VARYING SUBSURFACE CURRENTS

HYDRONAUTICS, INCORPORATED

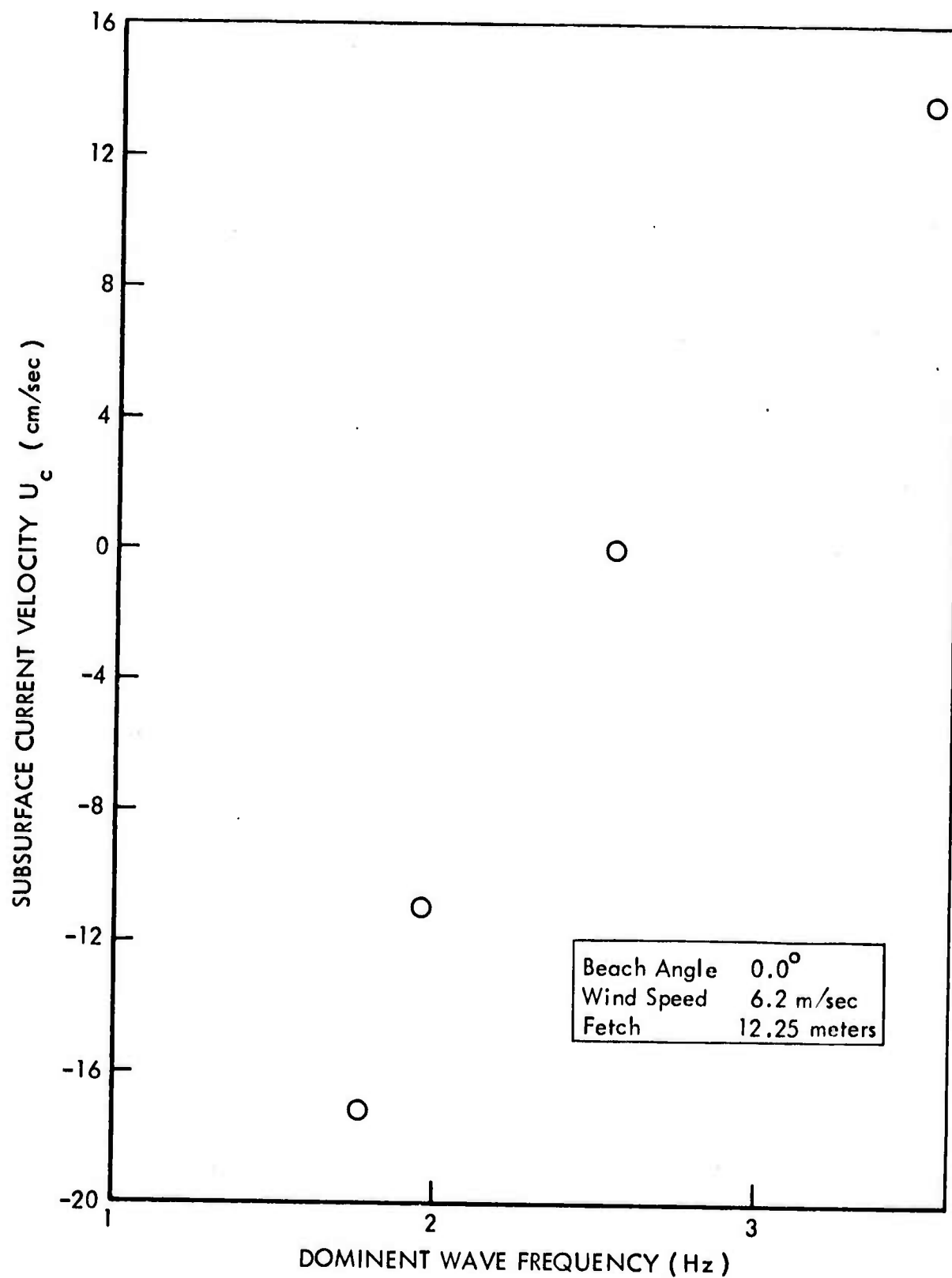


FIGURE 19 - SHIFT IN DOMINANT WIND WAVE FREQUENCY DUE TO SPATIAL VARYING SUBSURFACE CURRENTS

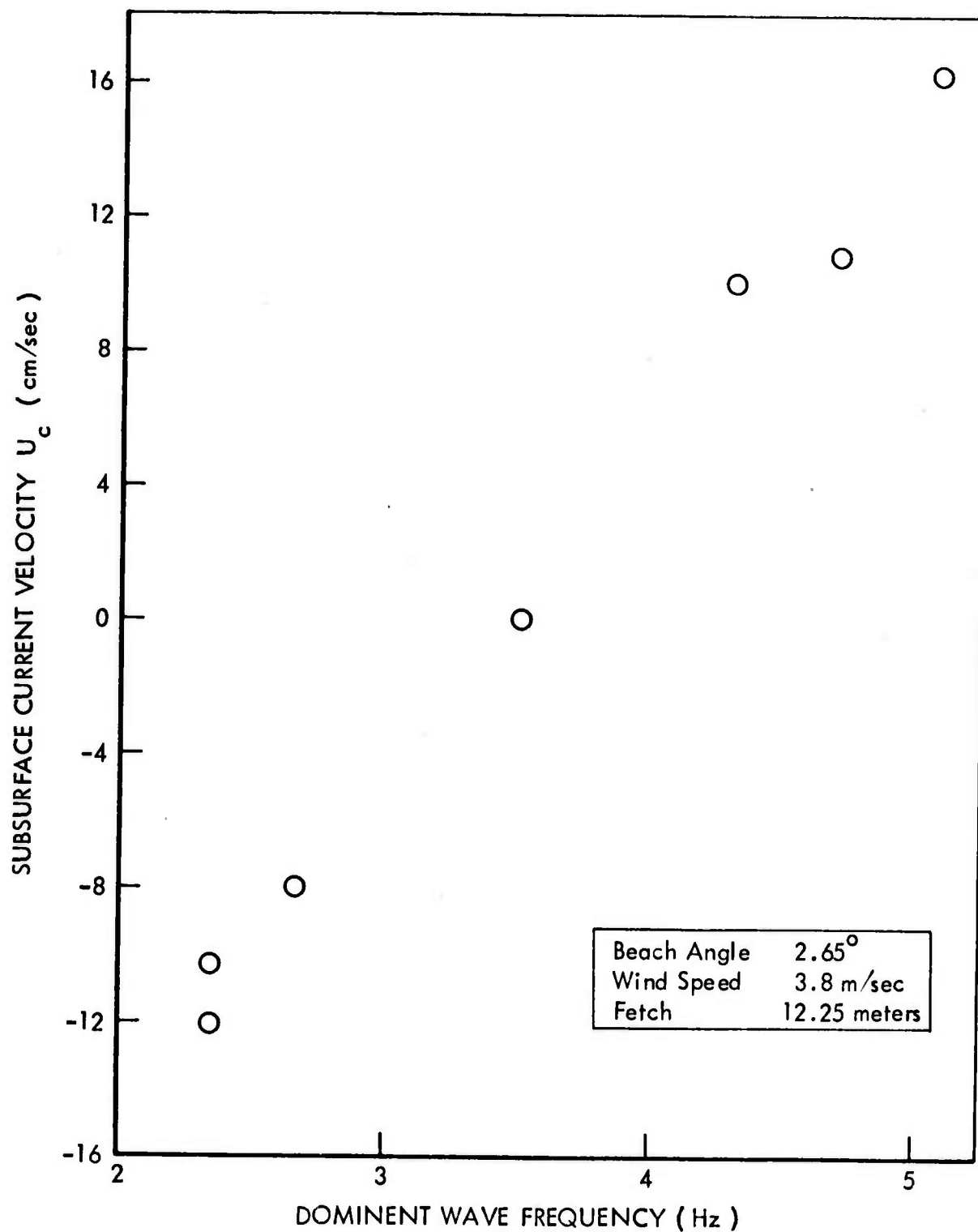


FIGURE 20 - SHIFT IN DOMINANT WIND WAVE FREQUENCY DUE TO SPATIAL VARYING SUBSURFACE CURRENTS

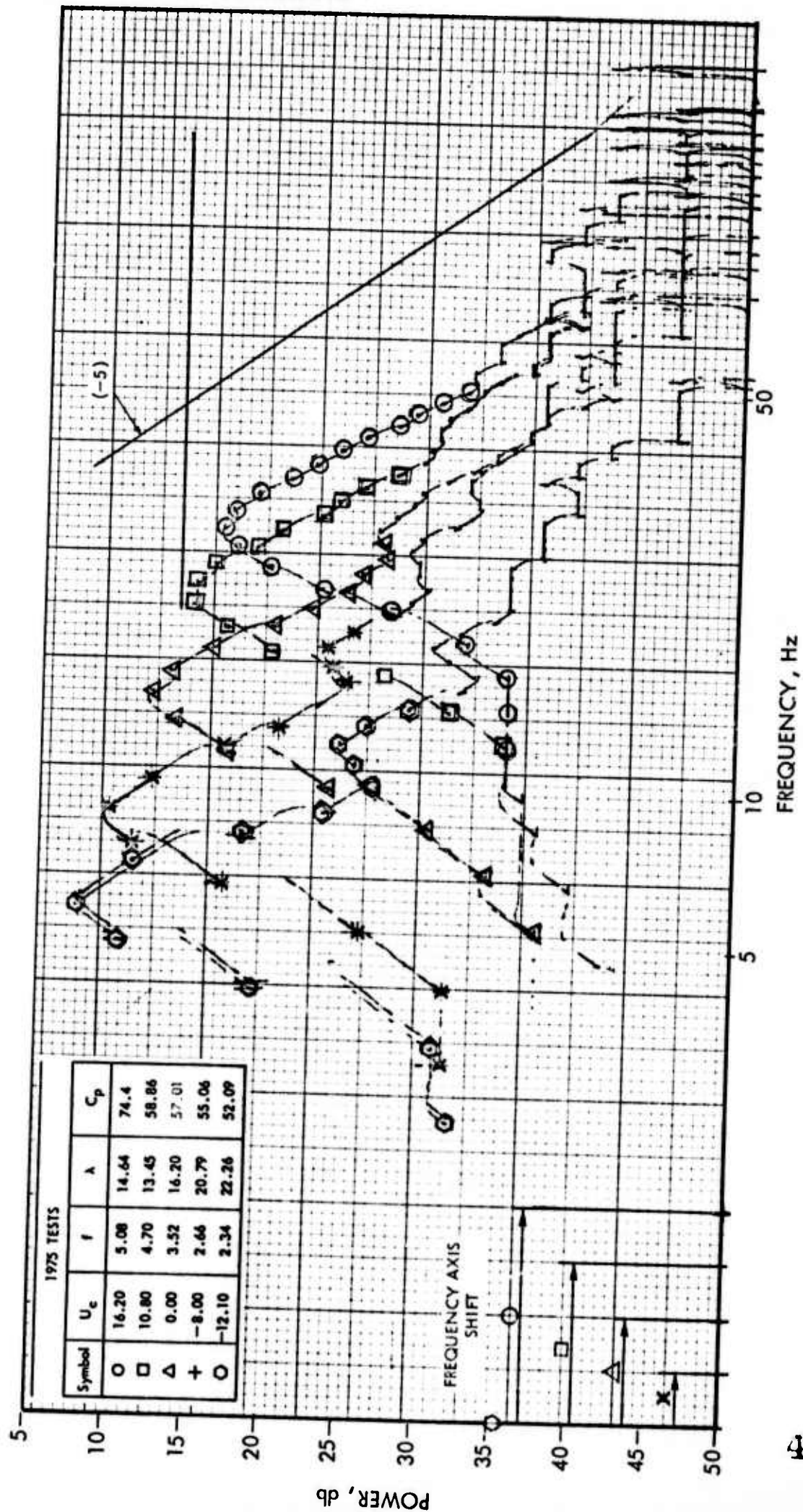


FIGURE 21 - SPECTRAL PLOT - EFFECT OF CURRENT ON DOMINANT WAVE FREQUENCY AND AMPLITUDE

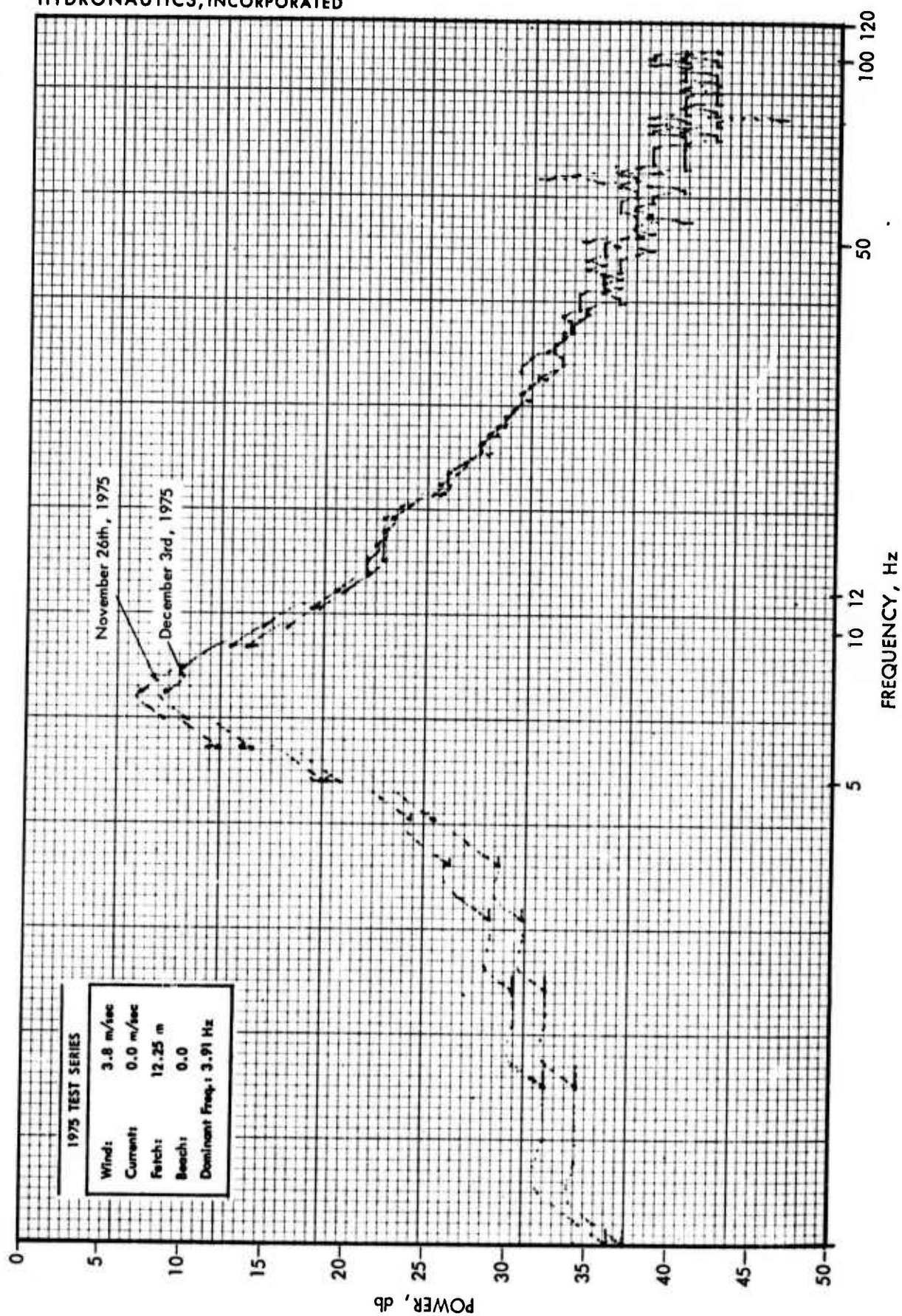


FIGURE 22 - POWER SPECTRA-REPEATABILITY TEST

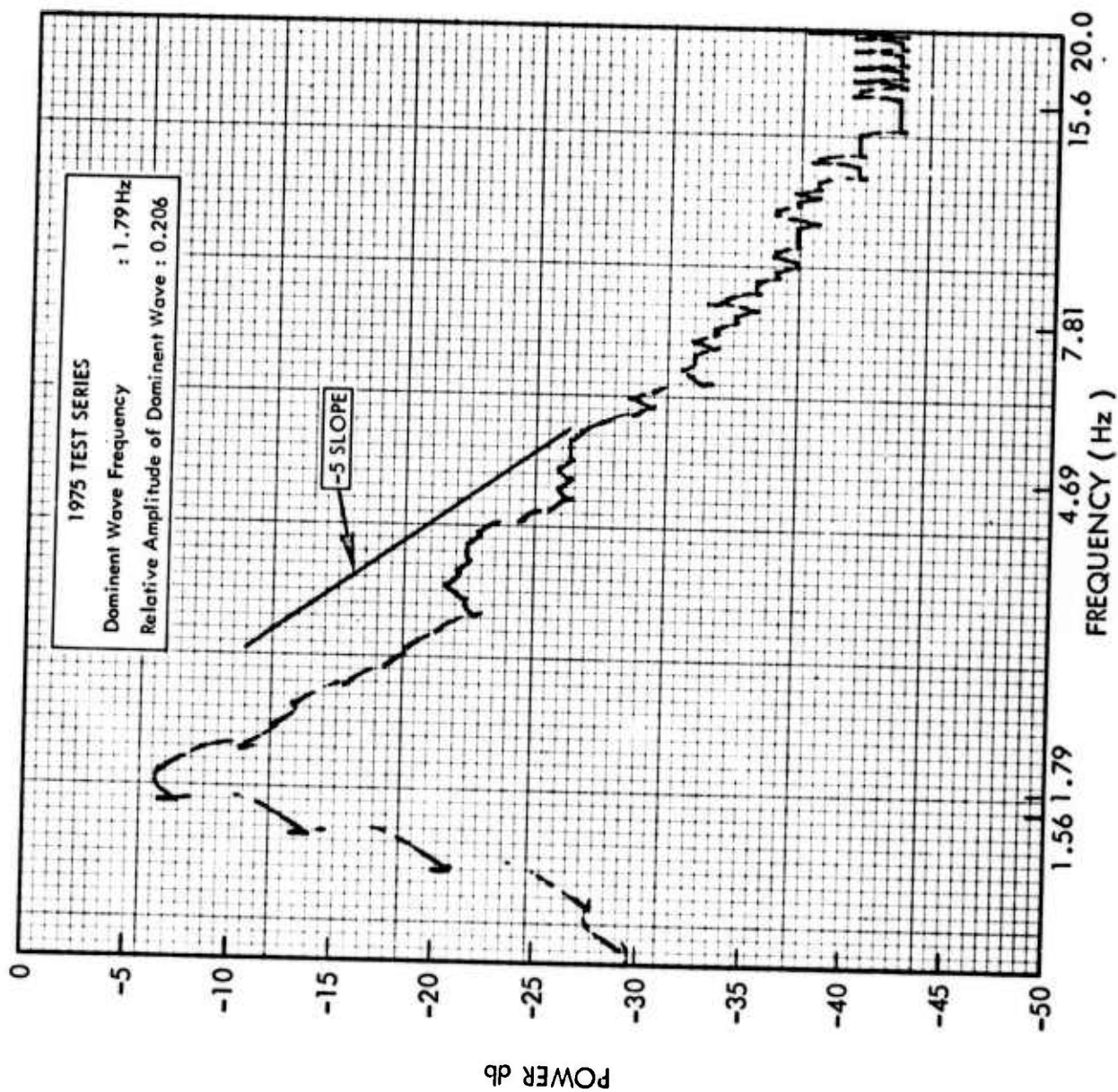


FIGURE 23 - CONDITION B1 C-600 W450 F1225 1124 POWER SPECTRUM

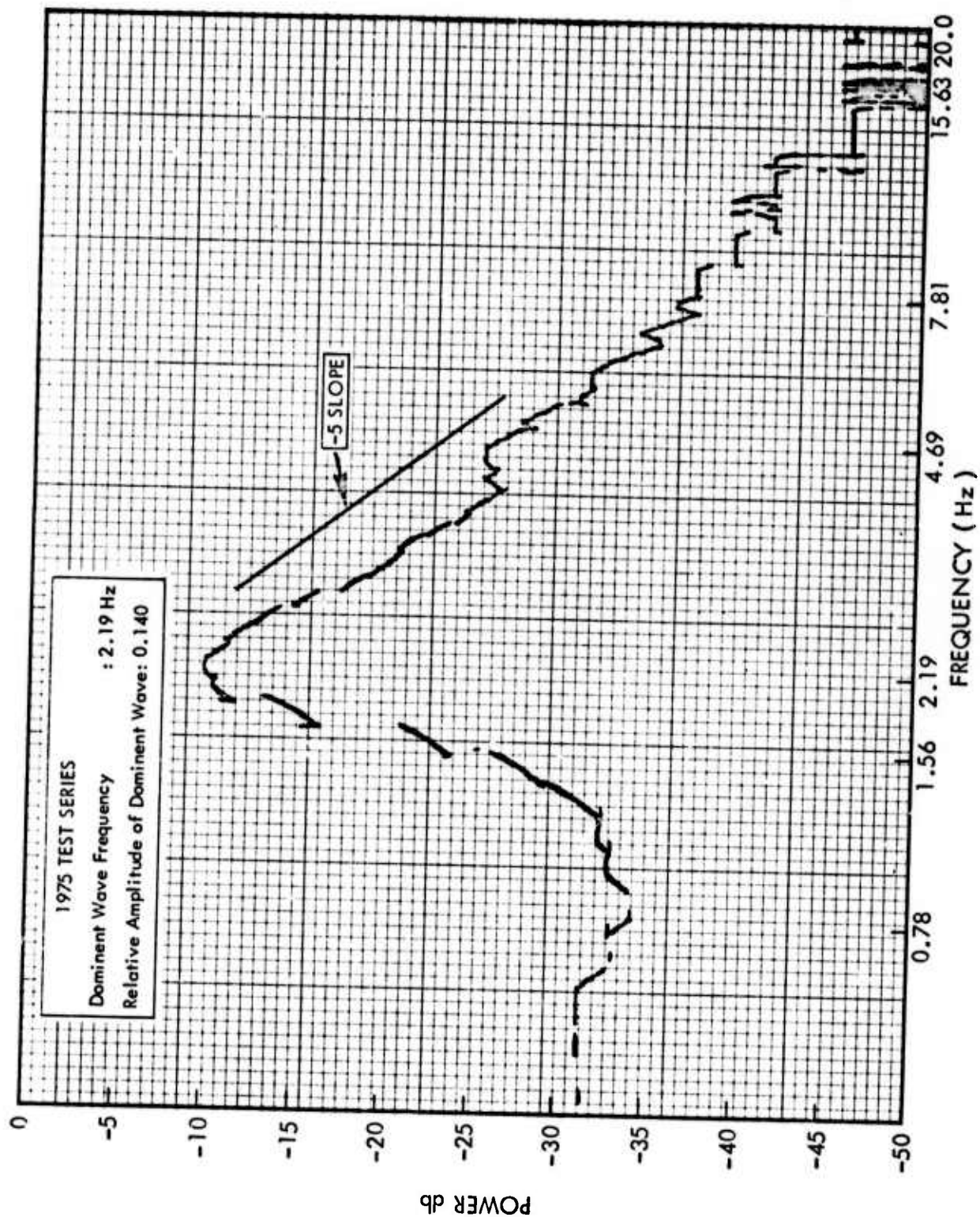


FIGURE 24 - CONDITION B1 C-424 W450 F1225 1209 POWER SPECTRUM

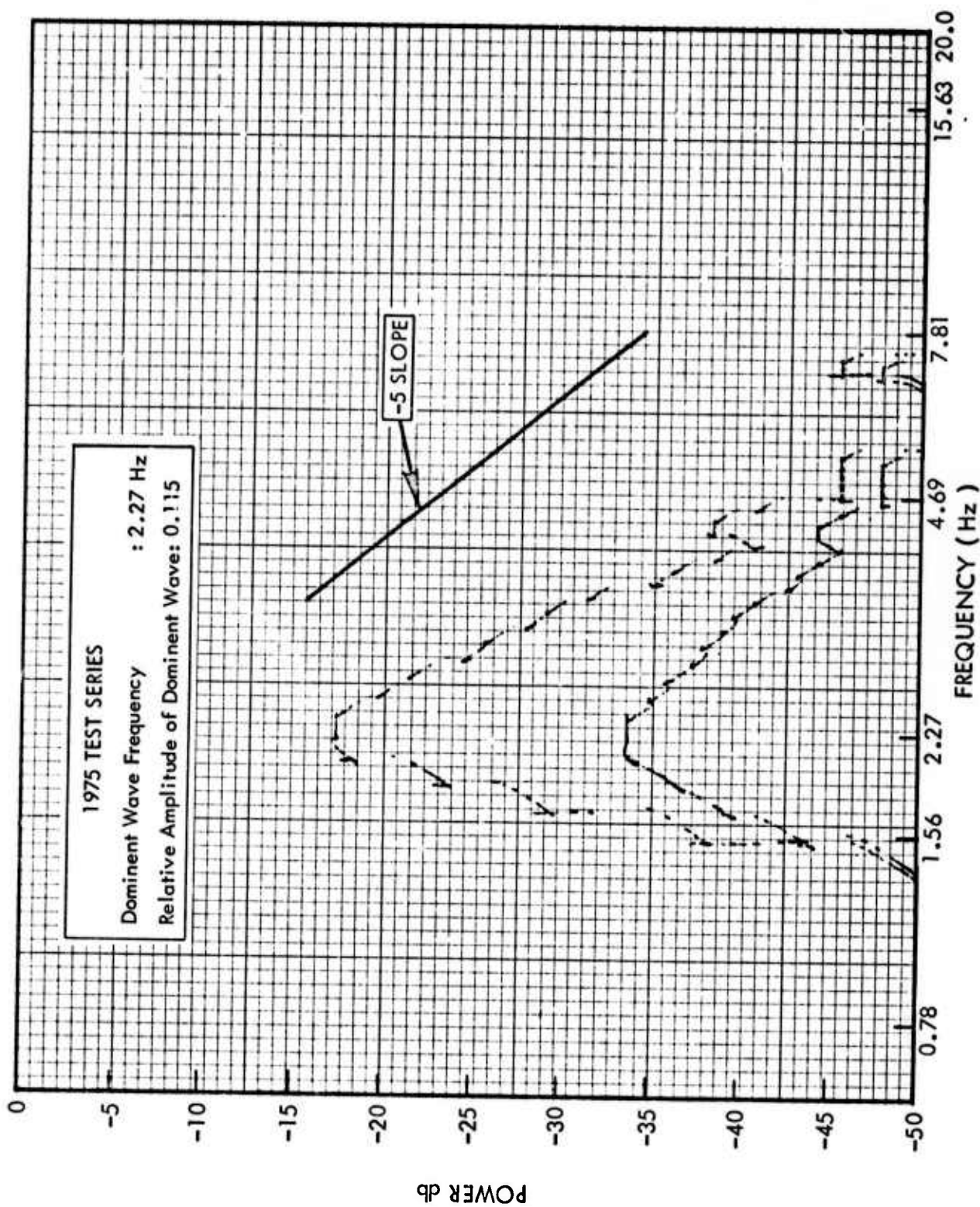


FIGURE 25 - CONDITION B1 C-315 W450 F1225 1201 POWER SPECTRUM

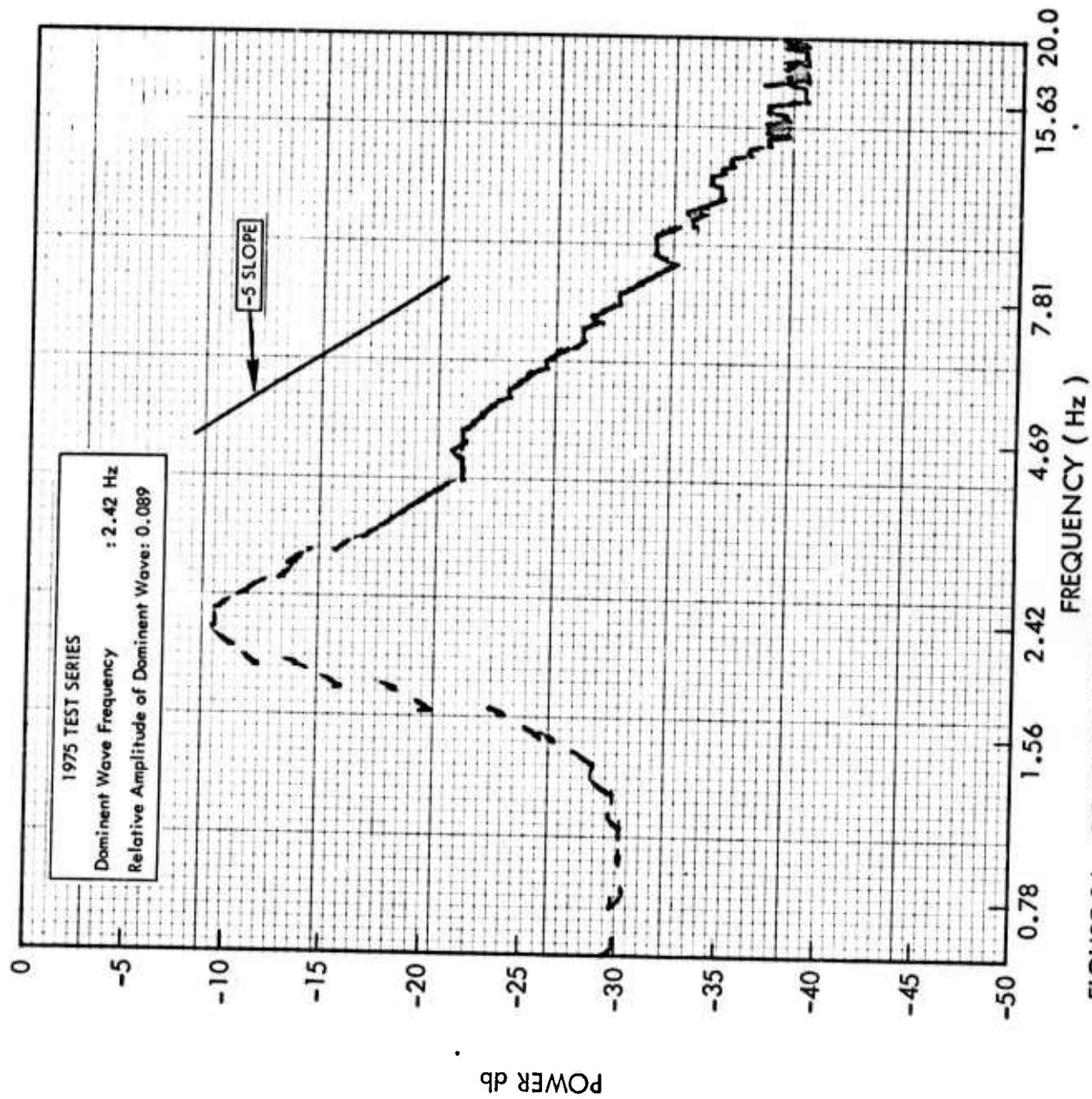


FIGURE 26 - CONDITION B1 C-284 W450 F1225 1209 POWER SPECTRUM

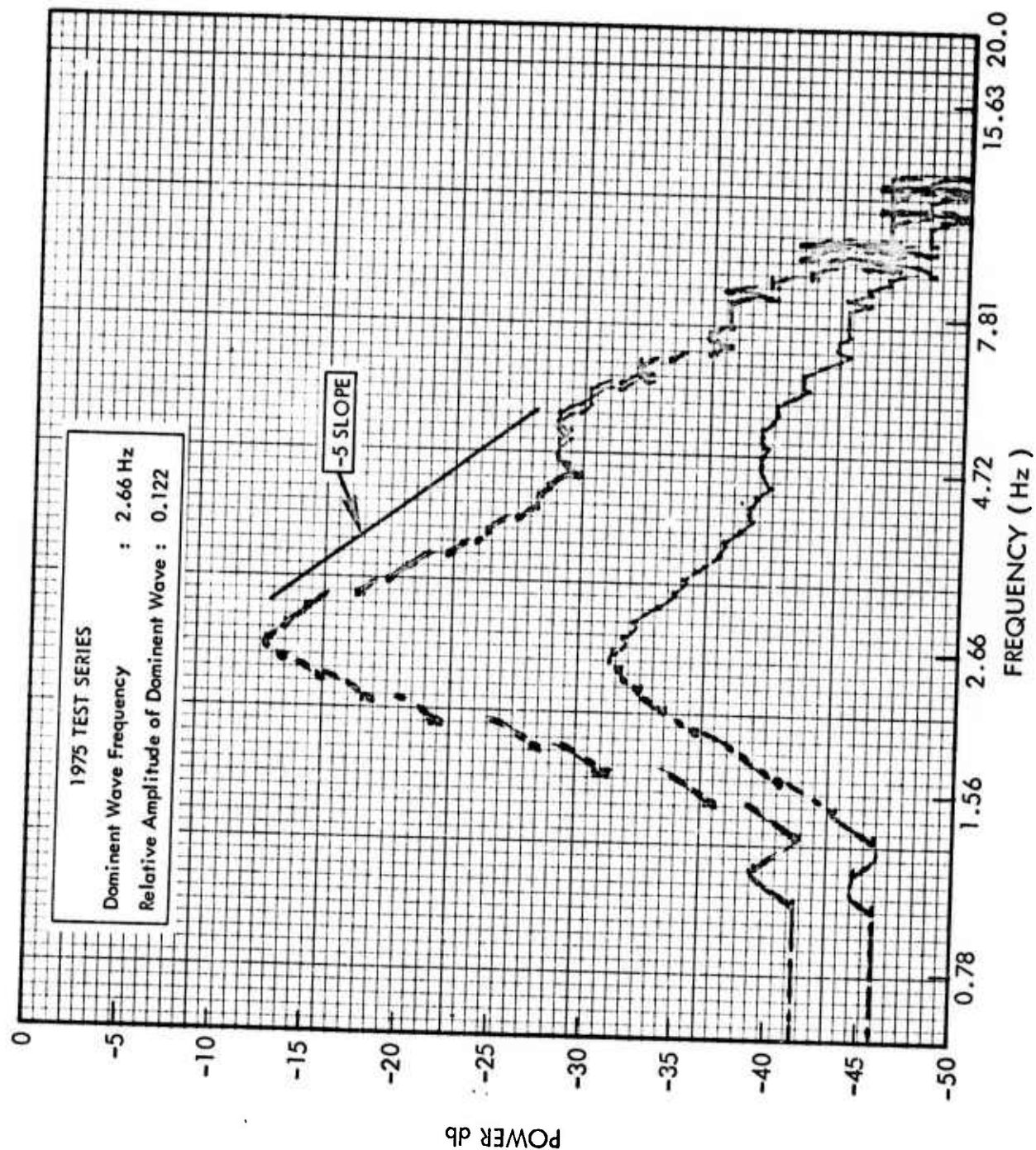


FIGURE 27 - CONDITION B1 C-219 W450 F1225 1205 POWER SPECTRUM

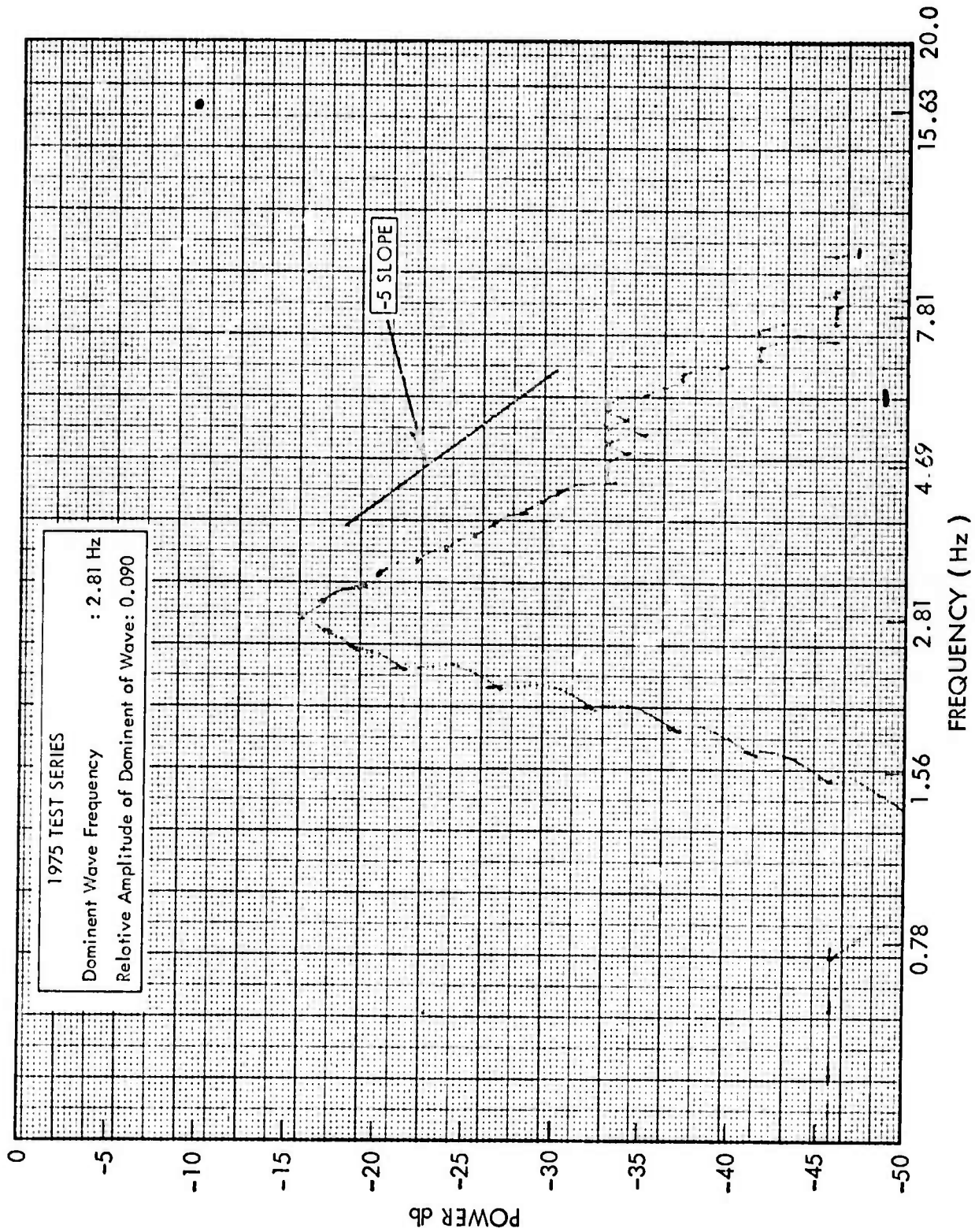


FIGURE 28 - CONDITION B1 C-145 W450 F1225 1204 POWER SPECTRUM

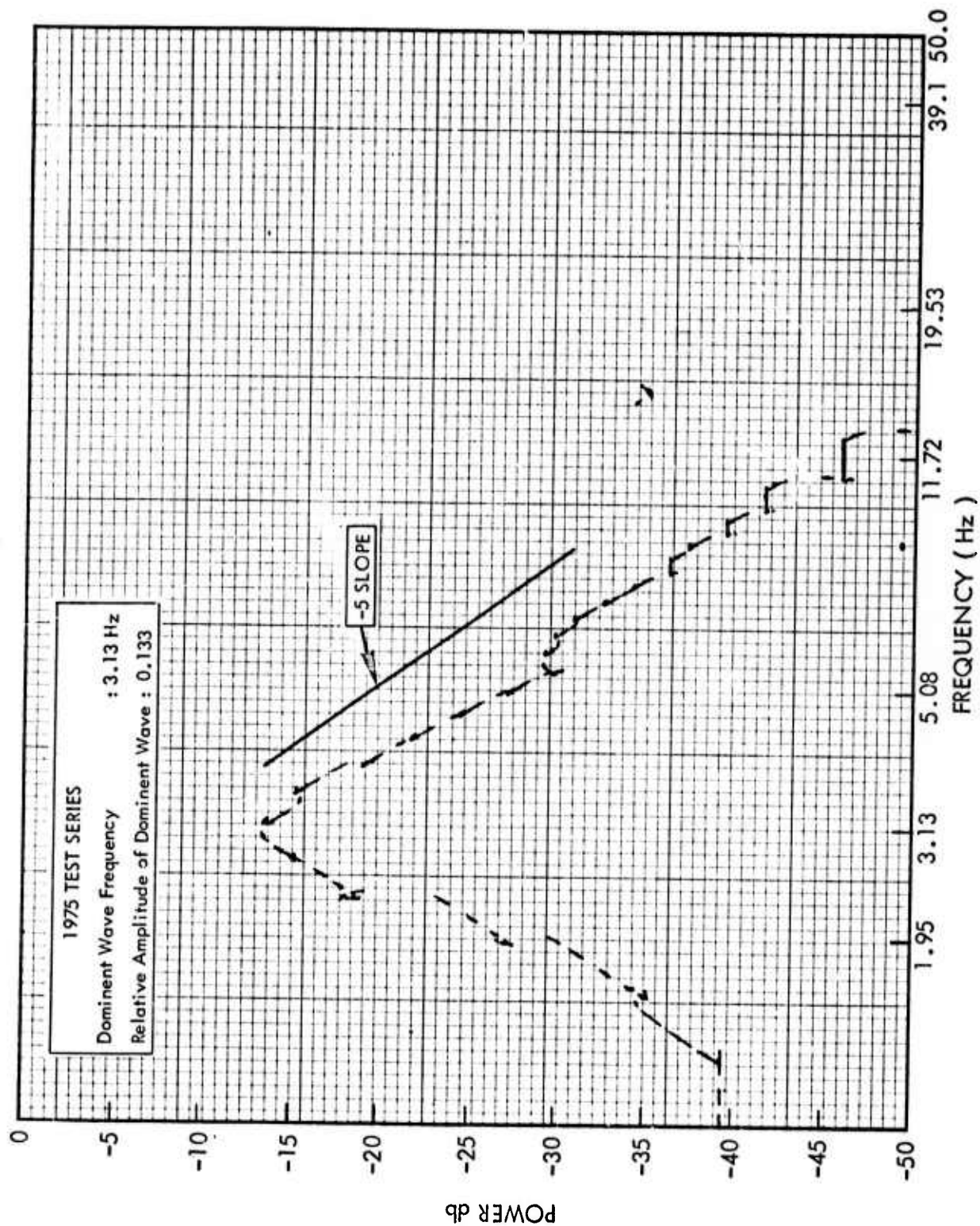


FIGURE 29 - CONDITION C-088 W450 F1225 1204 POWER SPECTRUM

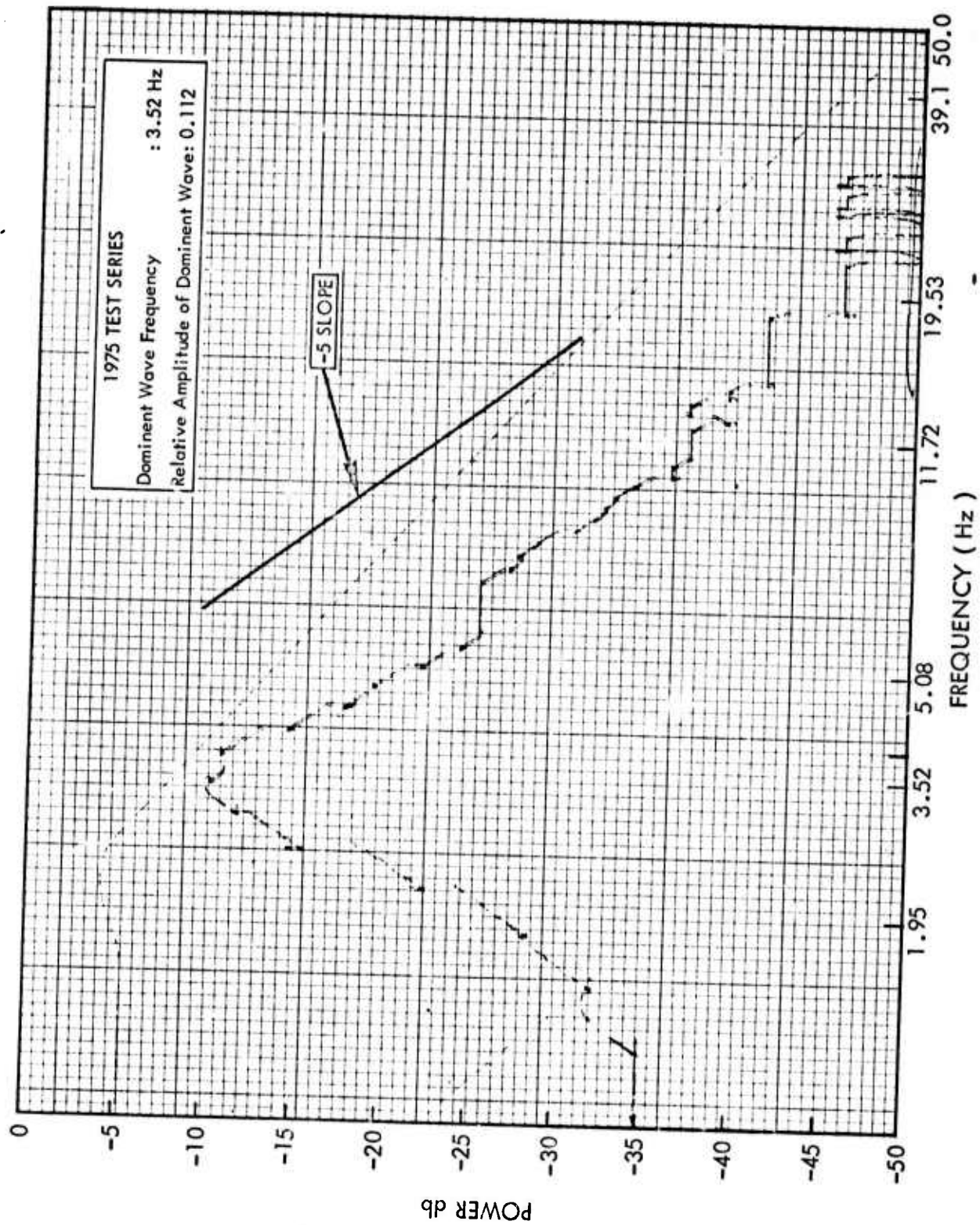


FIGURE 30 - CONDITION B1 C000 W450 F1225 1203 POWER SPECTRUM

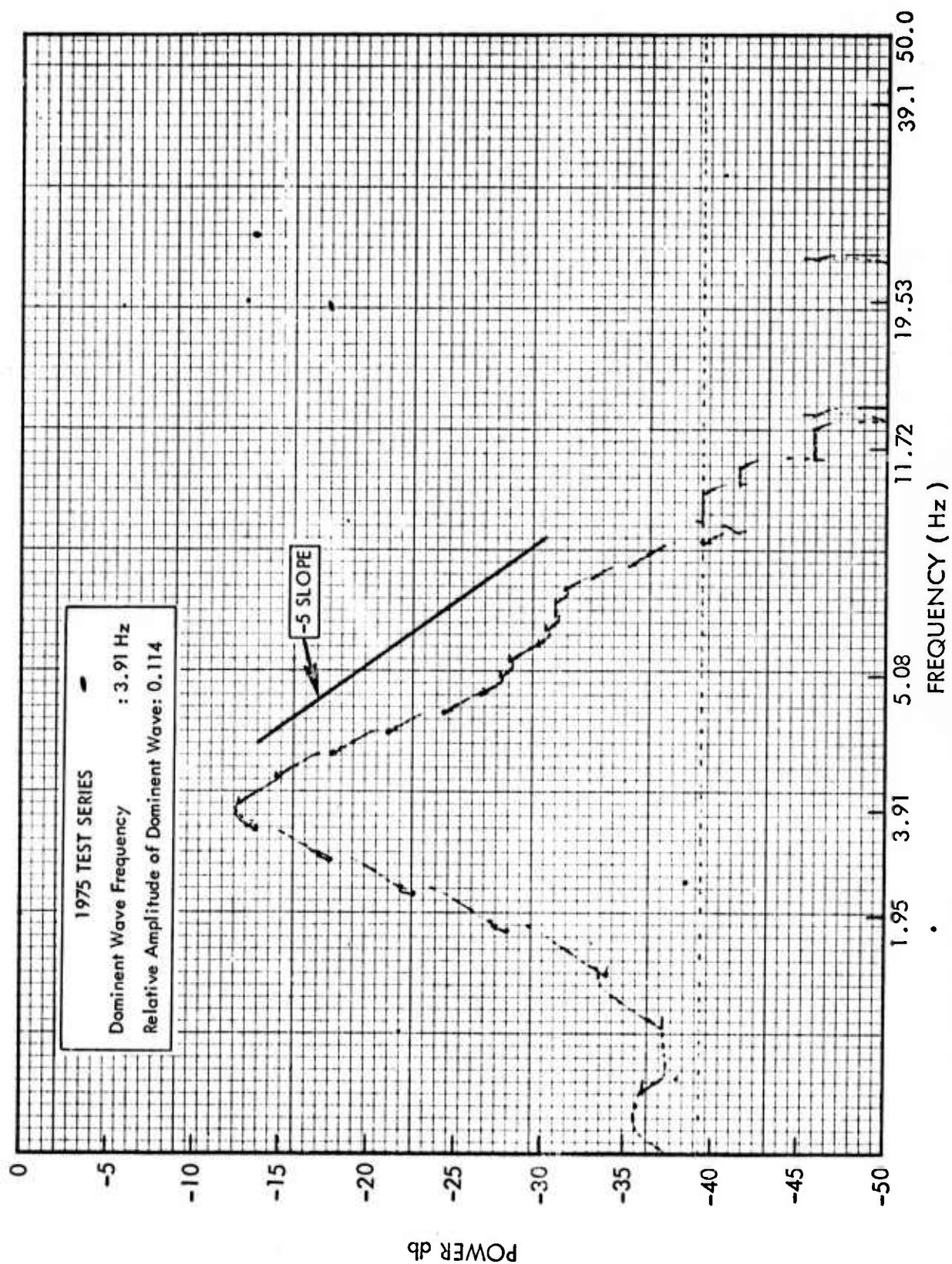


FIGURE 31 - CONDITION B1 C081 W450 F1225 1204 POWER SPECTRUM

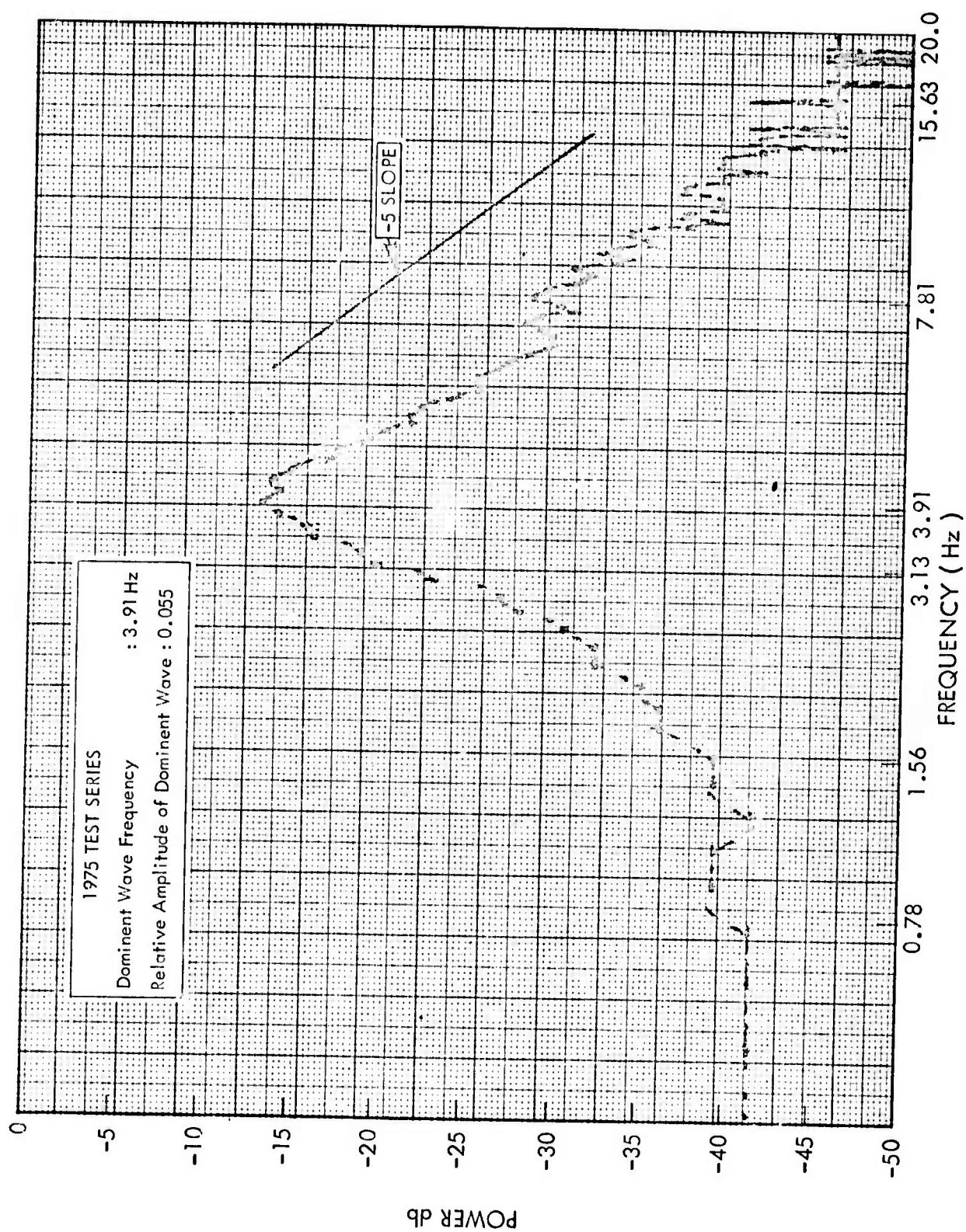


FIGURE 32 - CONDITION B1 C117 W450 F1225 1205 POWER SPECTRUM

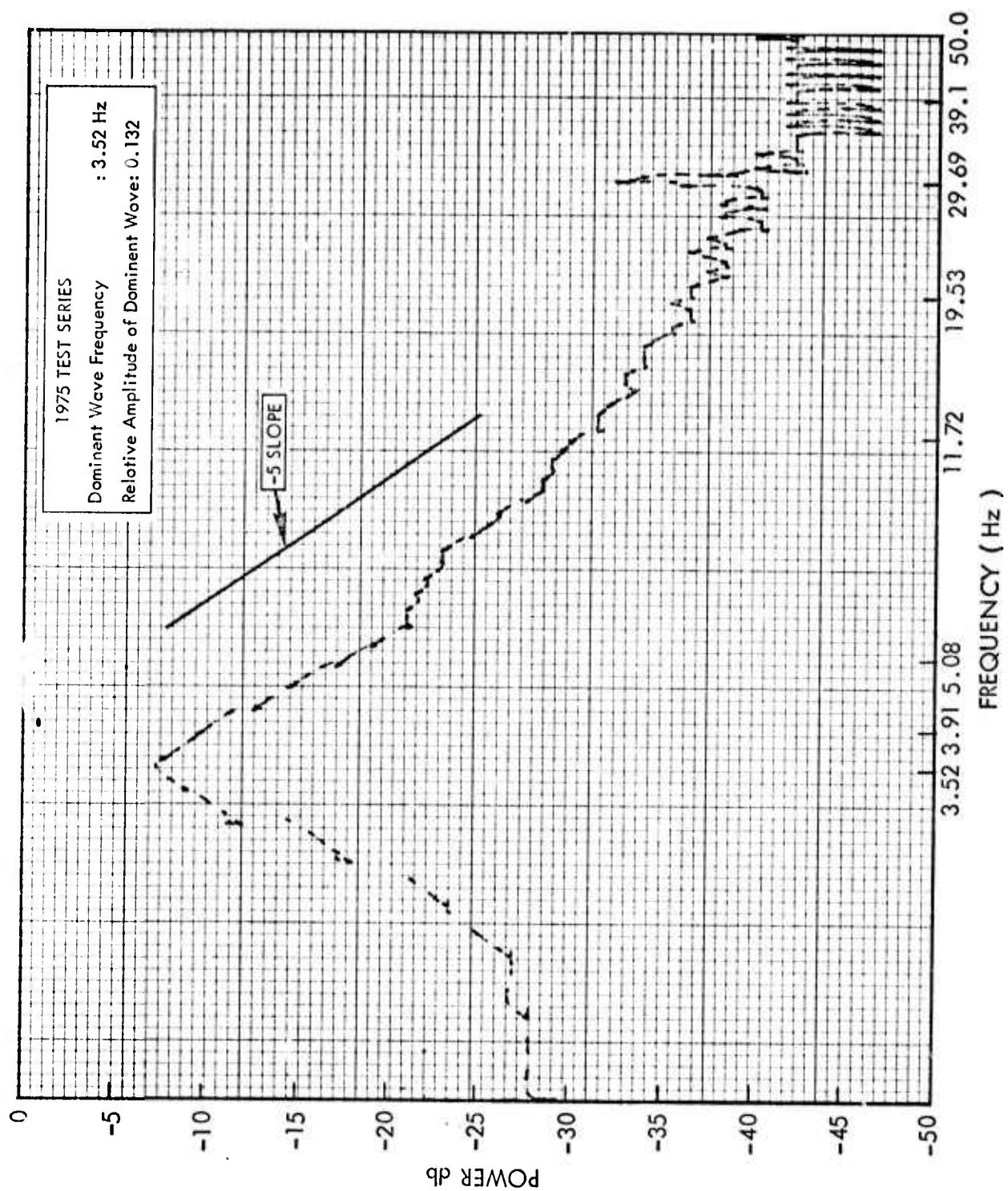


FIGURE 33 - CONDITION B1 C216 W450 F1225 1201 POWER SPECTRUM

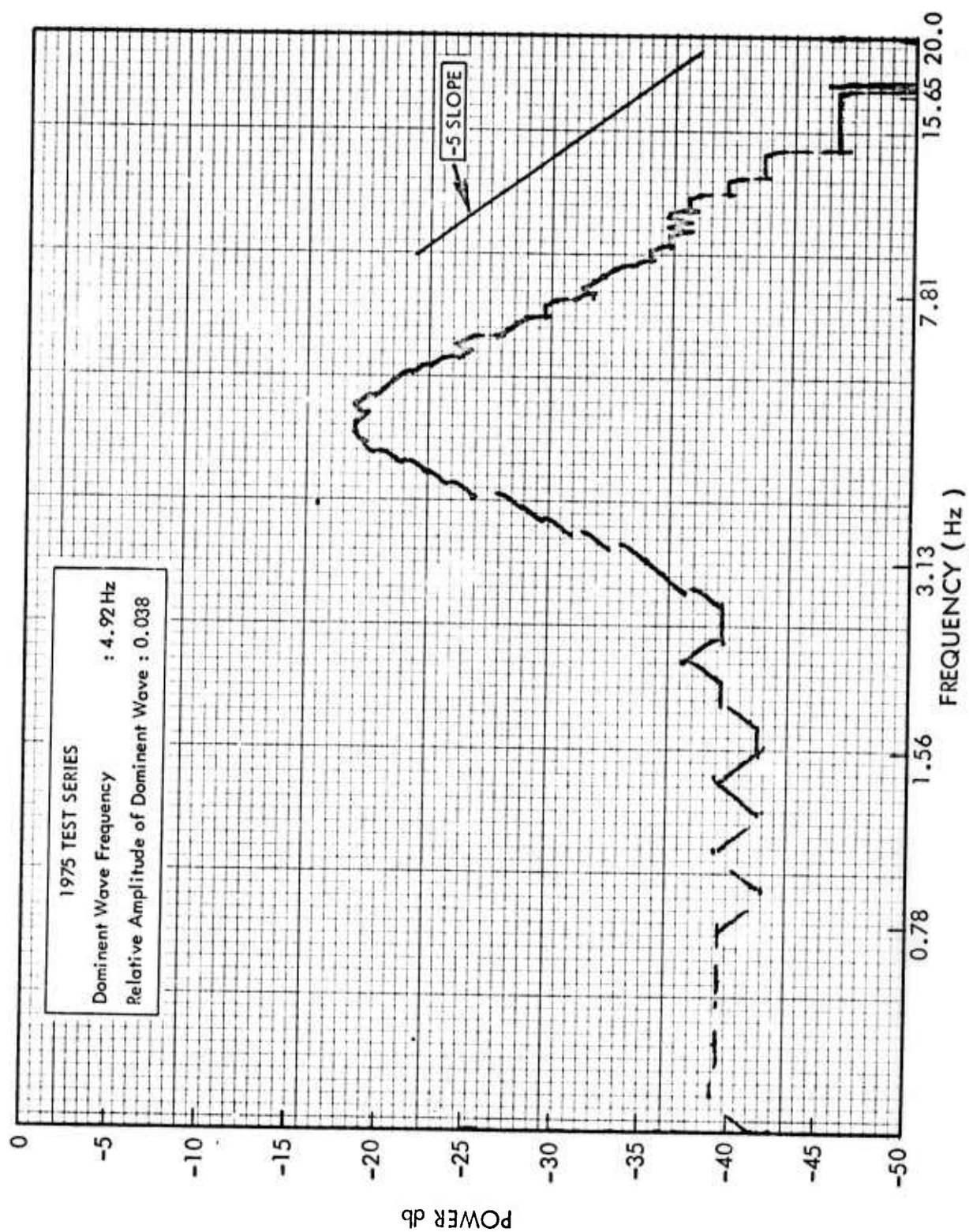


FIGURE 34 - CONDITION B1 C324 W450 F1225 1209 POWER SPECTRUM

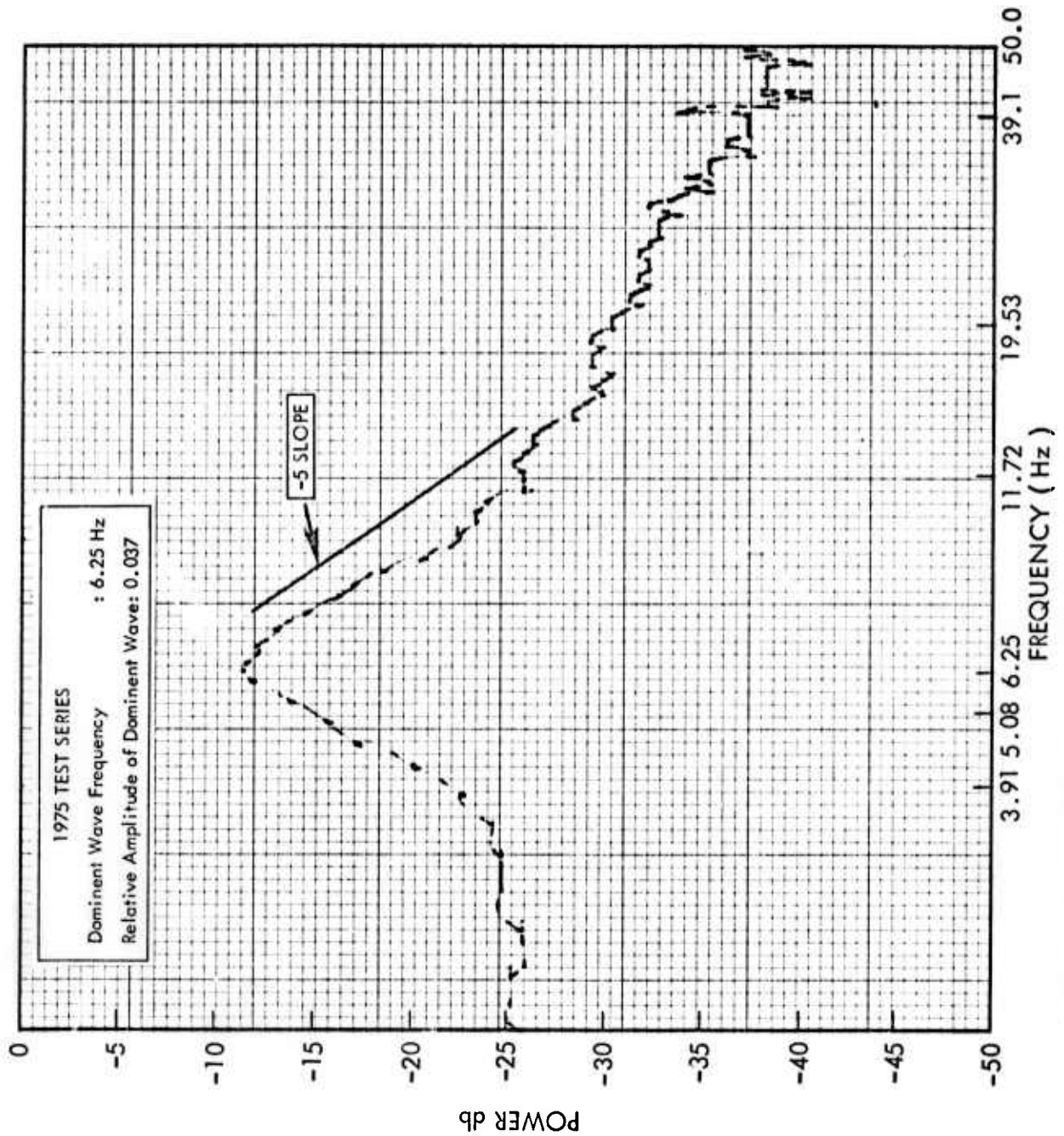


FIGURE 35 CONDITION B1 C446 W450 F1225 1125 POWER SPECTRUM

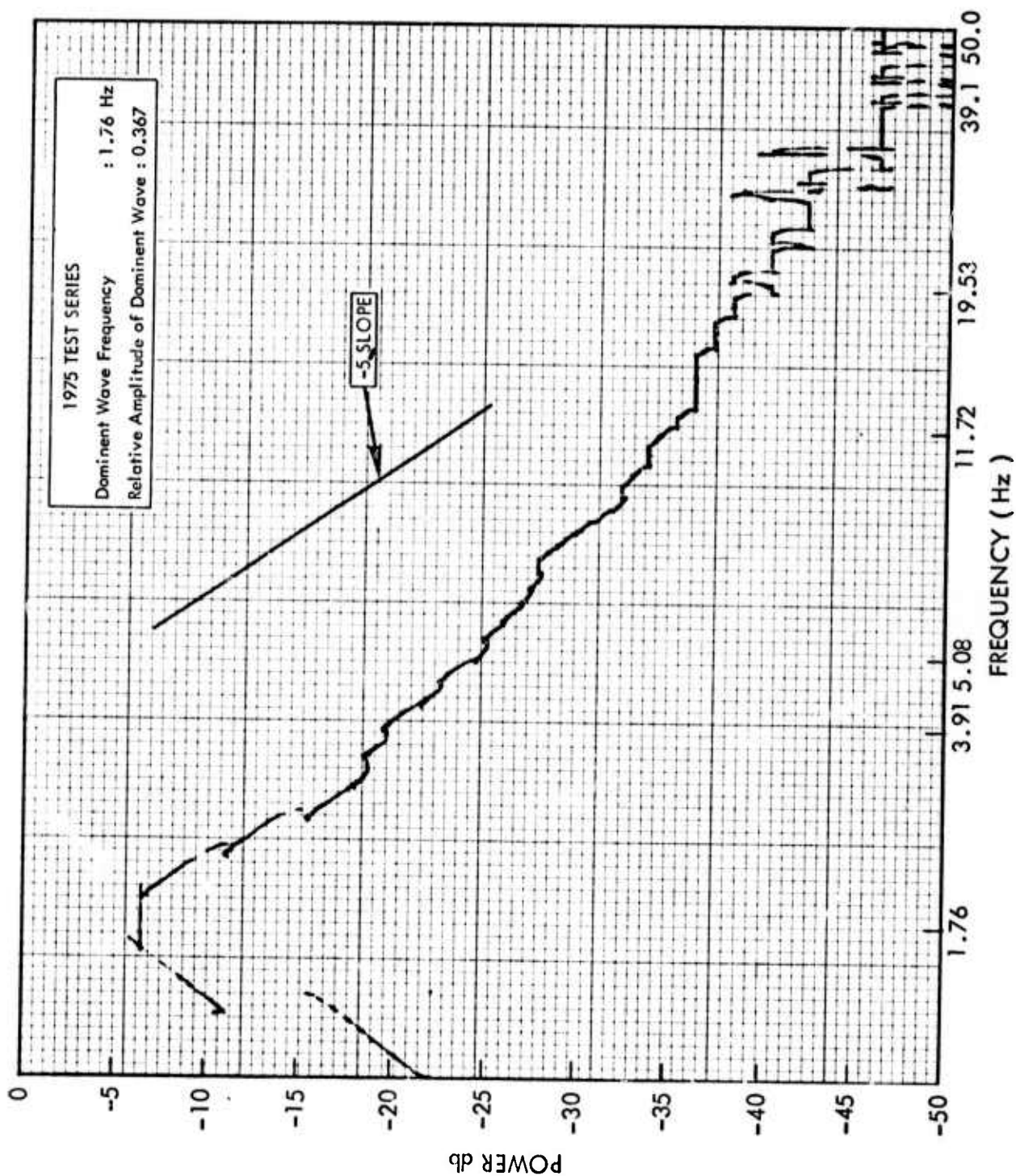


FIGURE 36 - CONDITION B1 C-550 W750 F1225 1210 POWER SPECTRUM

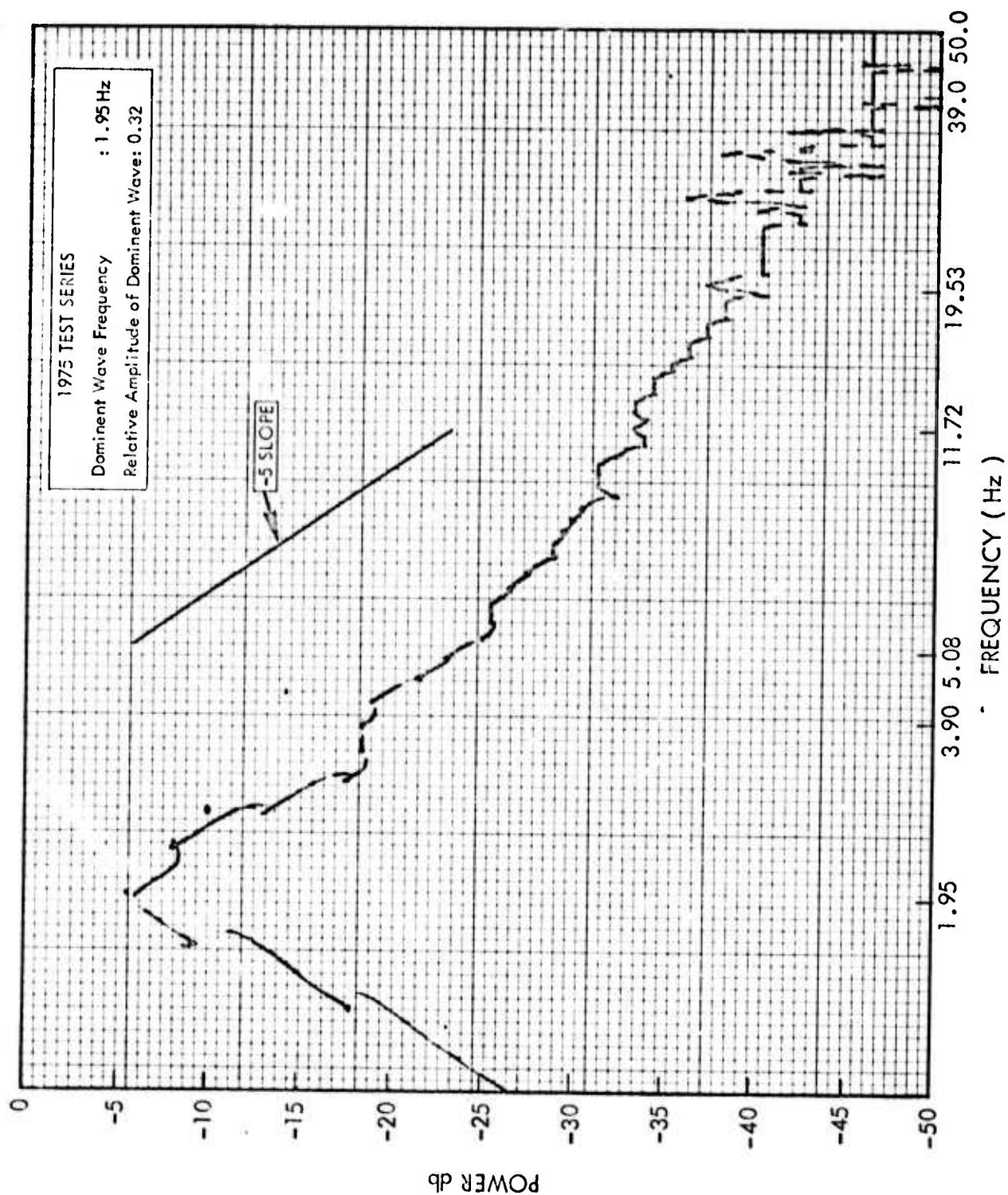


FIGURE 37 - CONDITION B1 C-355 W750 F1225 1210 POWER SPECTRUM

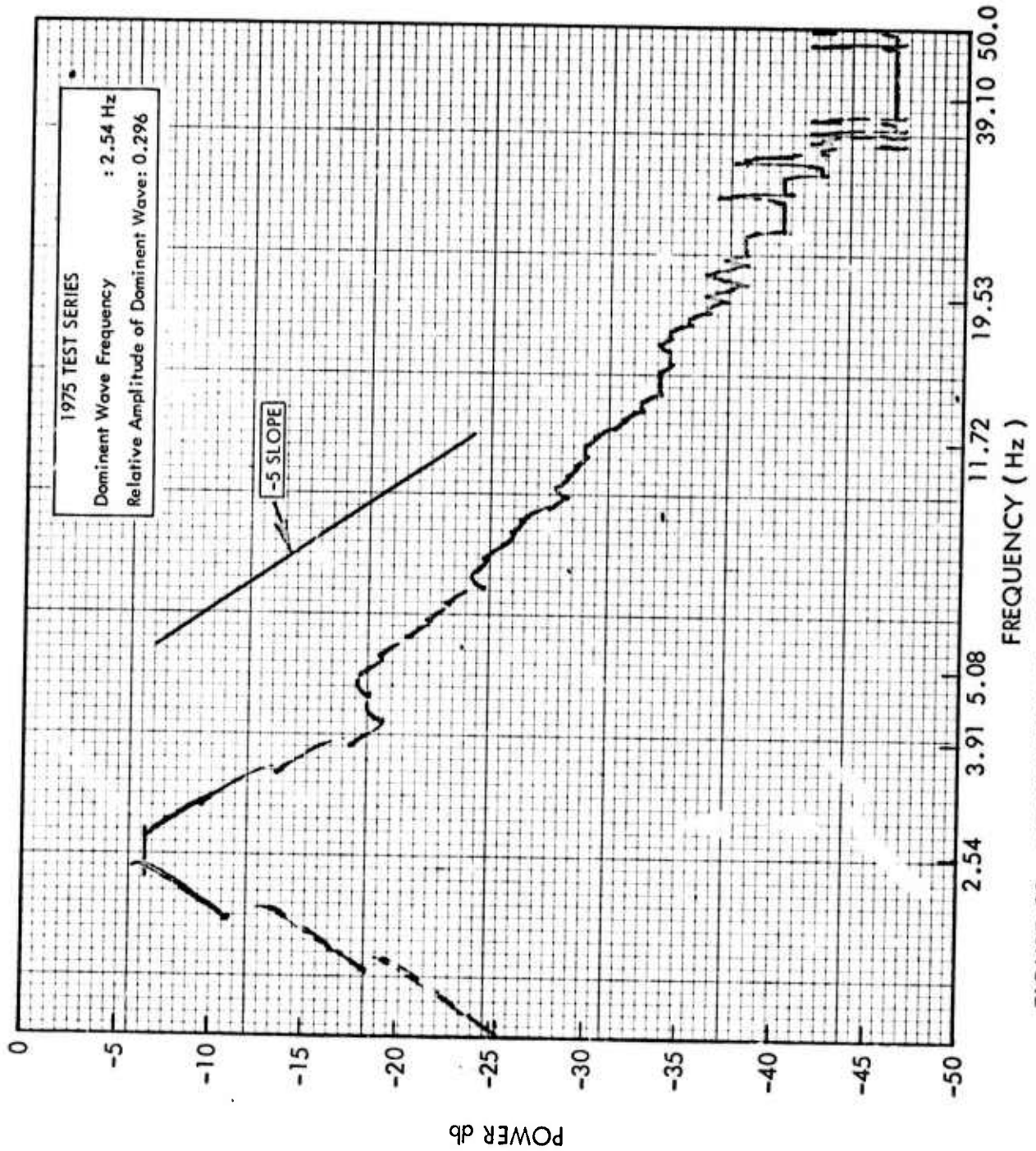


FIGURE 38 - CONDITION B1 C000 W750 F1225 1210 POWER SPECTRUM

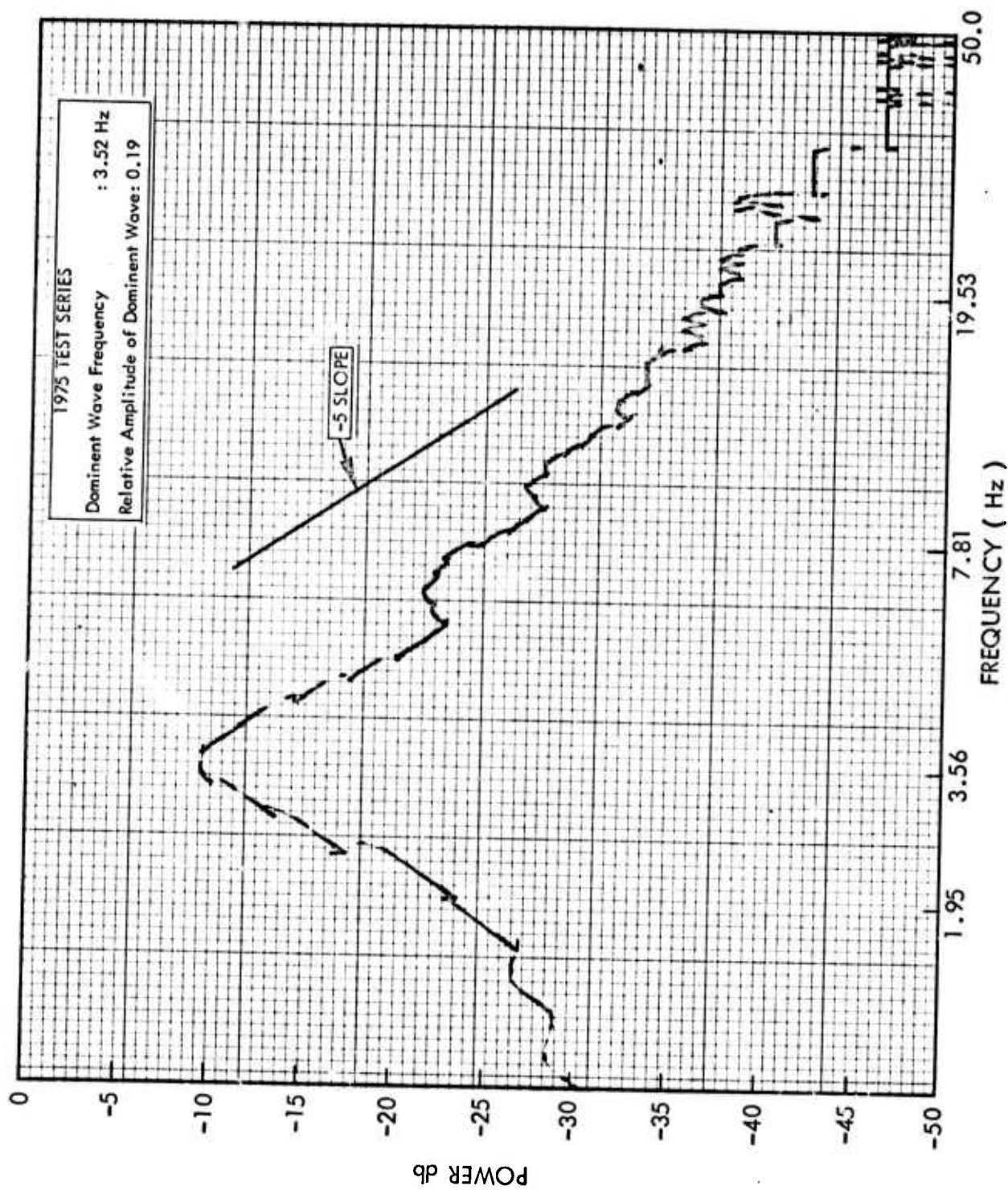


FIGURE 39 - CONDITION B1 C324 W750 F1225 1210 POWER SPECTRUM

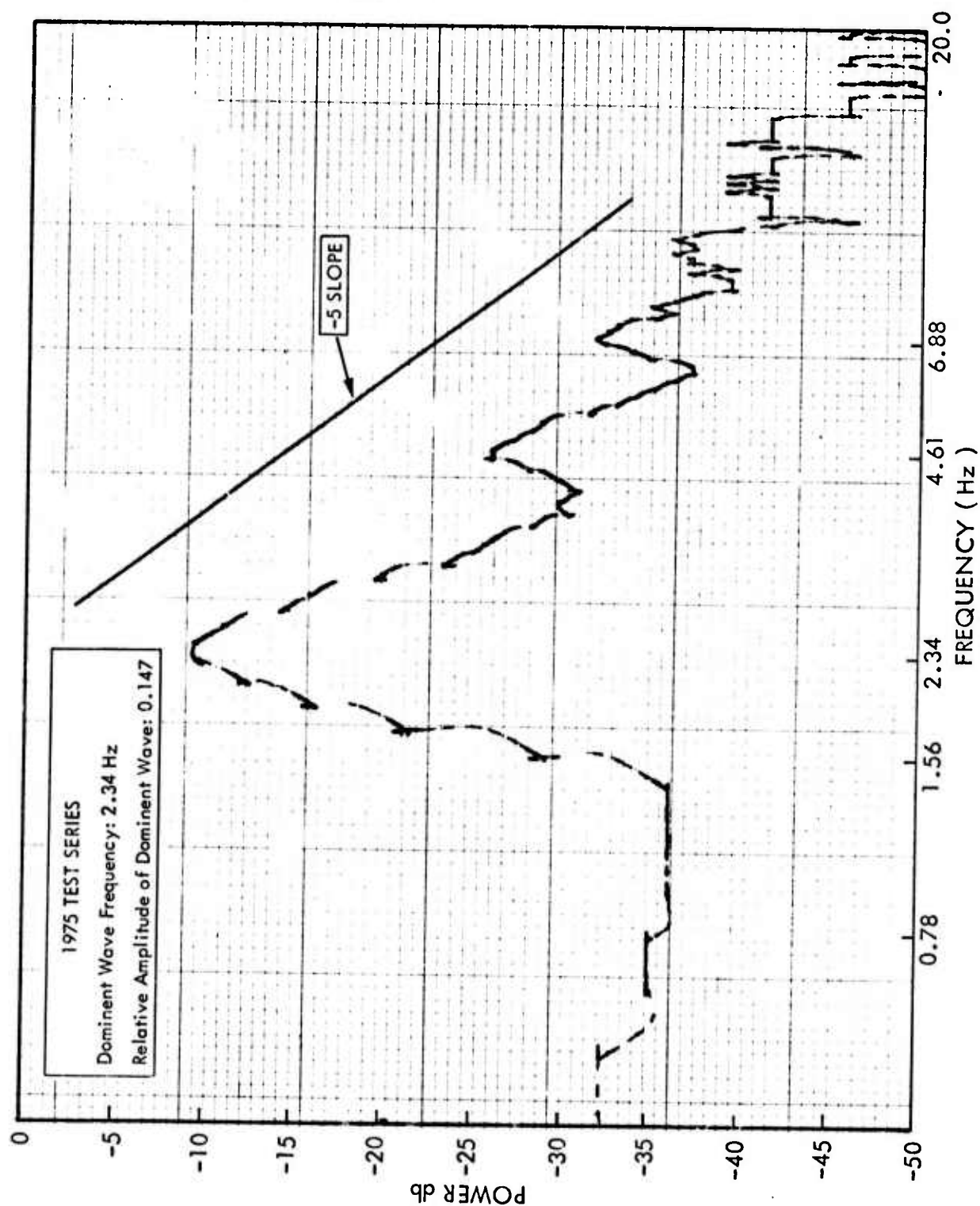


FIGURE 40 - CONDITION B4 C-262 W450 F1225 1221 POWER SPECTRUM

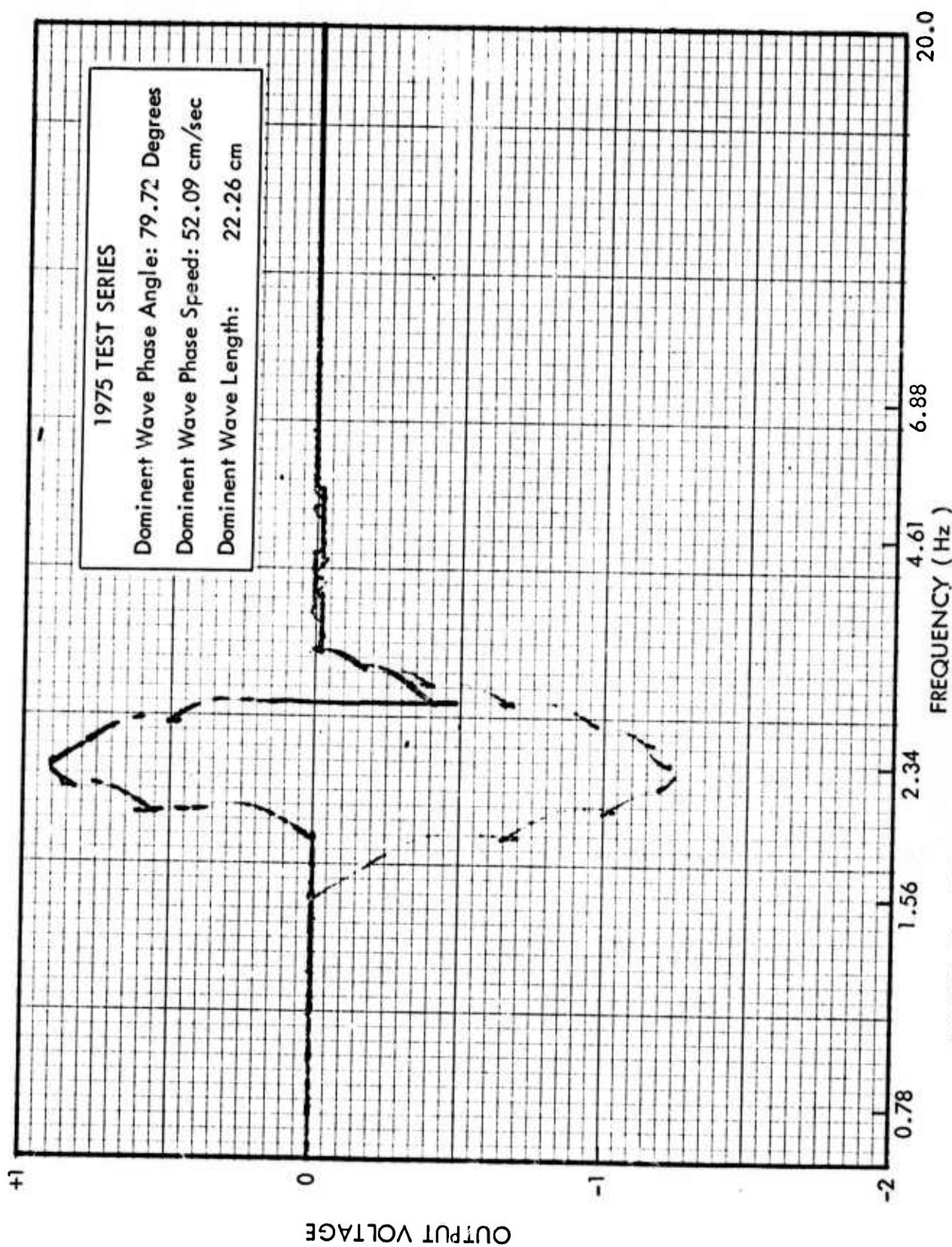


FIGURE 41 - CONDITION B4 C-262 W450 F1225 1211 CROSS SPECTRUM

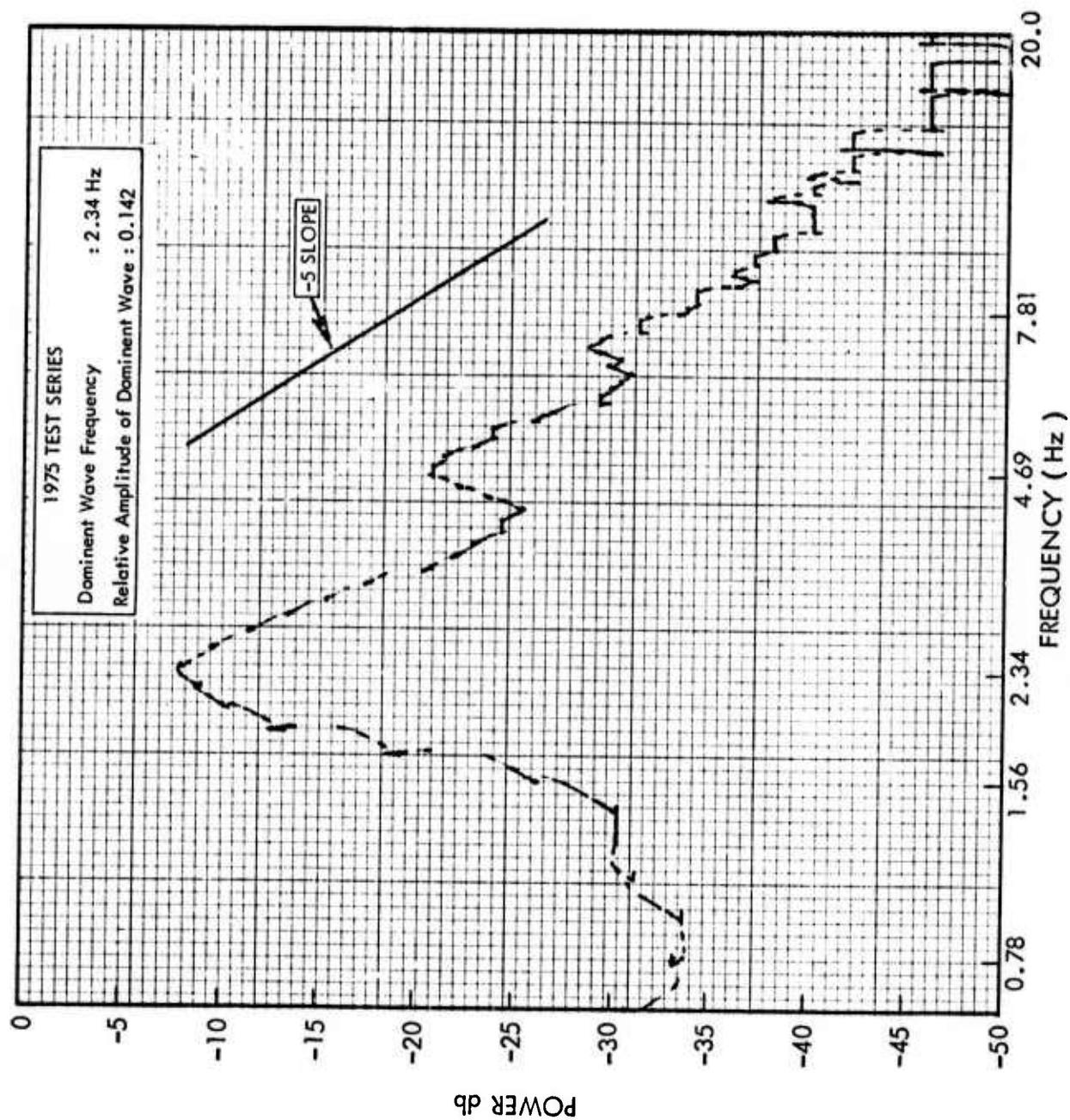


FIGURE 42 - CONDITION B4 C-261 W450 F1225 1211 POWER SPECTRUM

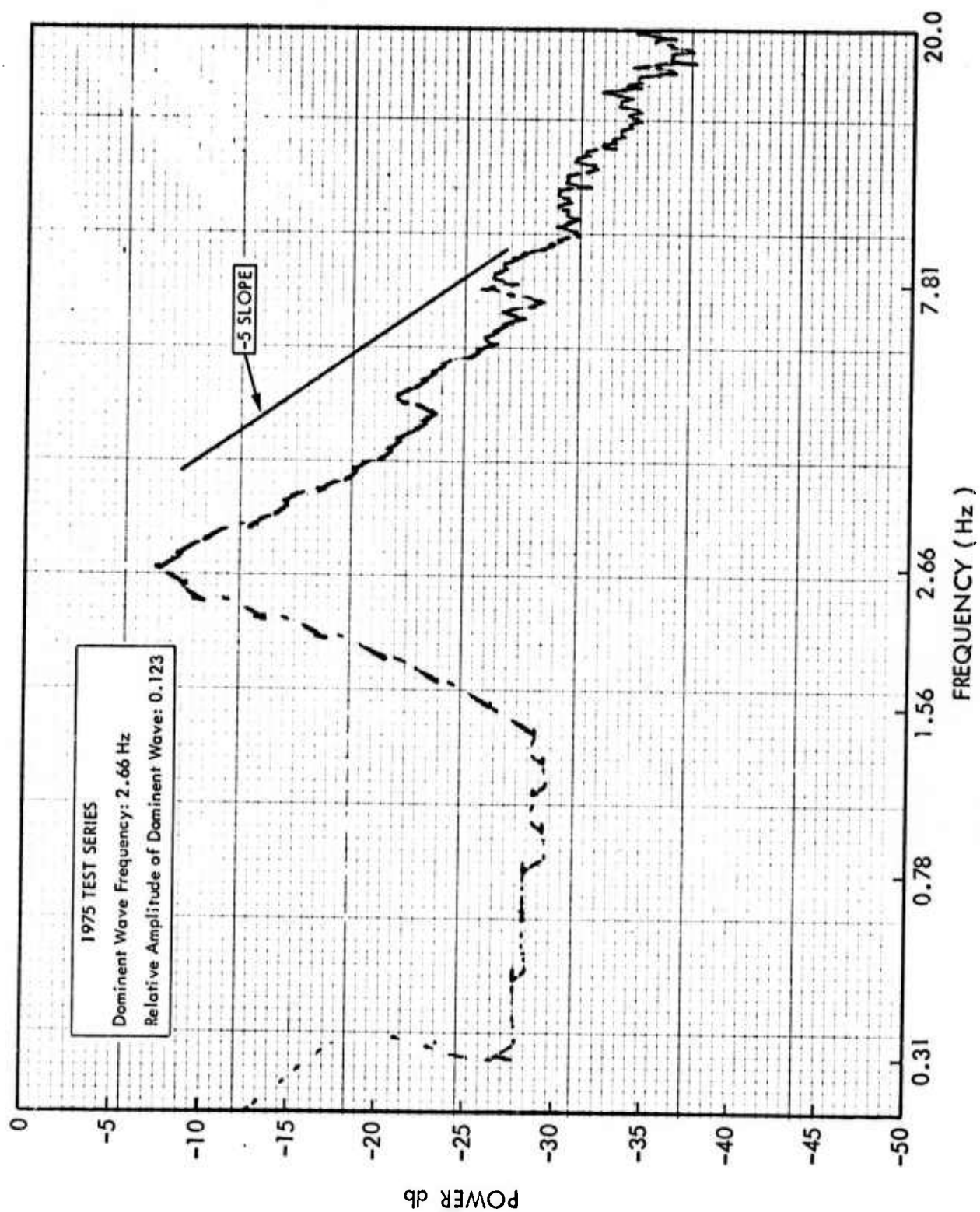


FIGURE 43 - CONDITION B4 C-174 W450 F1225 1211 POWER SPECTRUM

HYDRONAUTICS, INCORPORATED

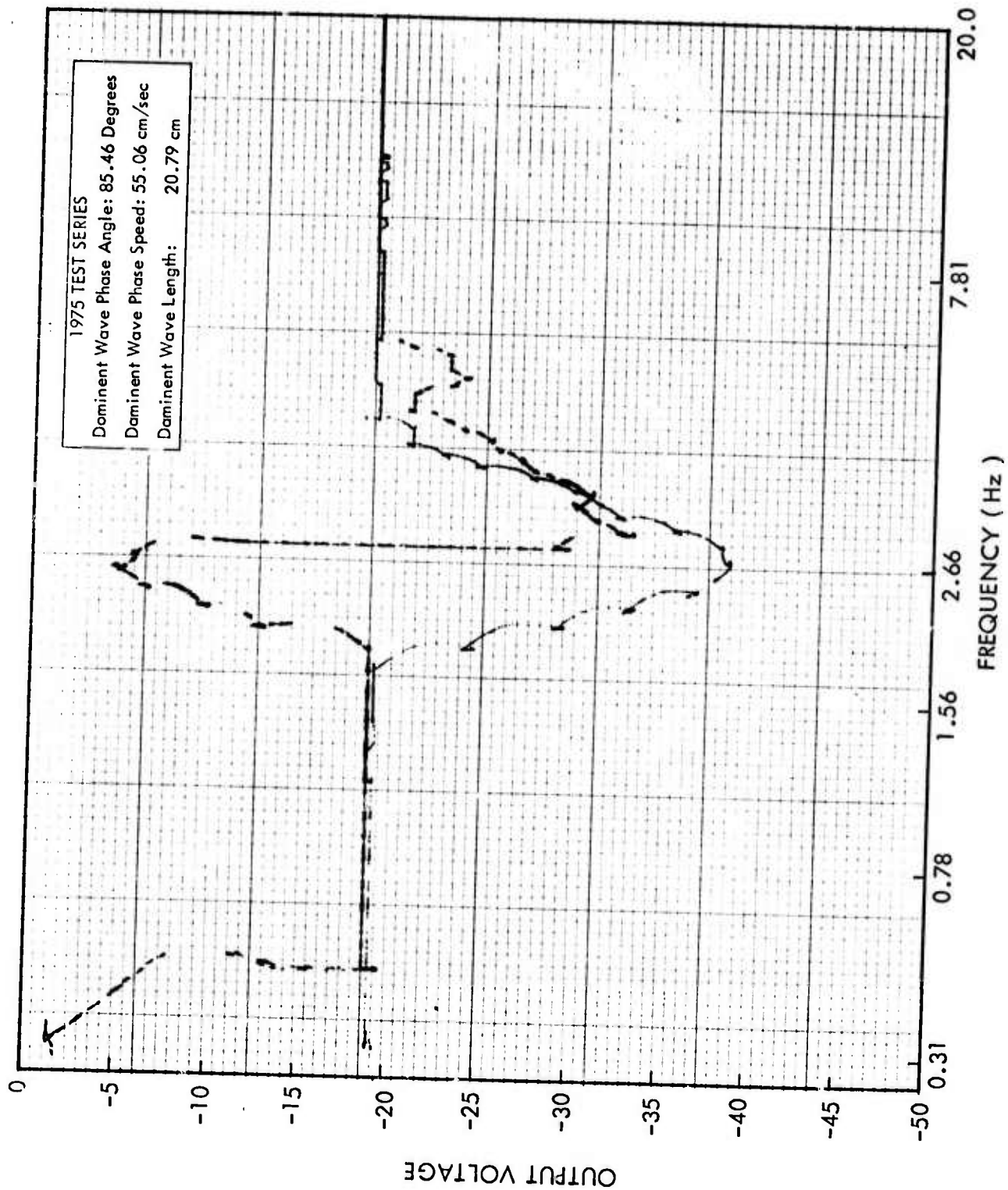


FIGURE 44 - CONDITION B4 C-174 W450 F1225 1211 CROSS SPECTRUM

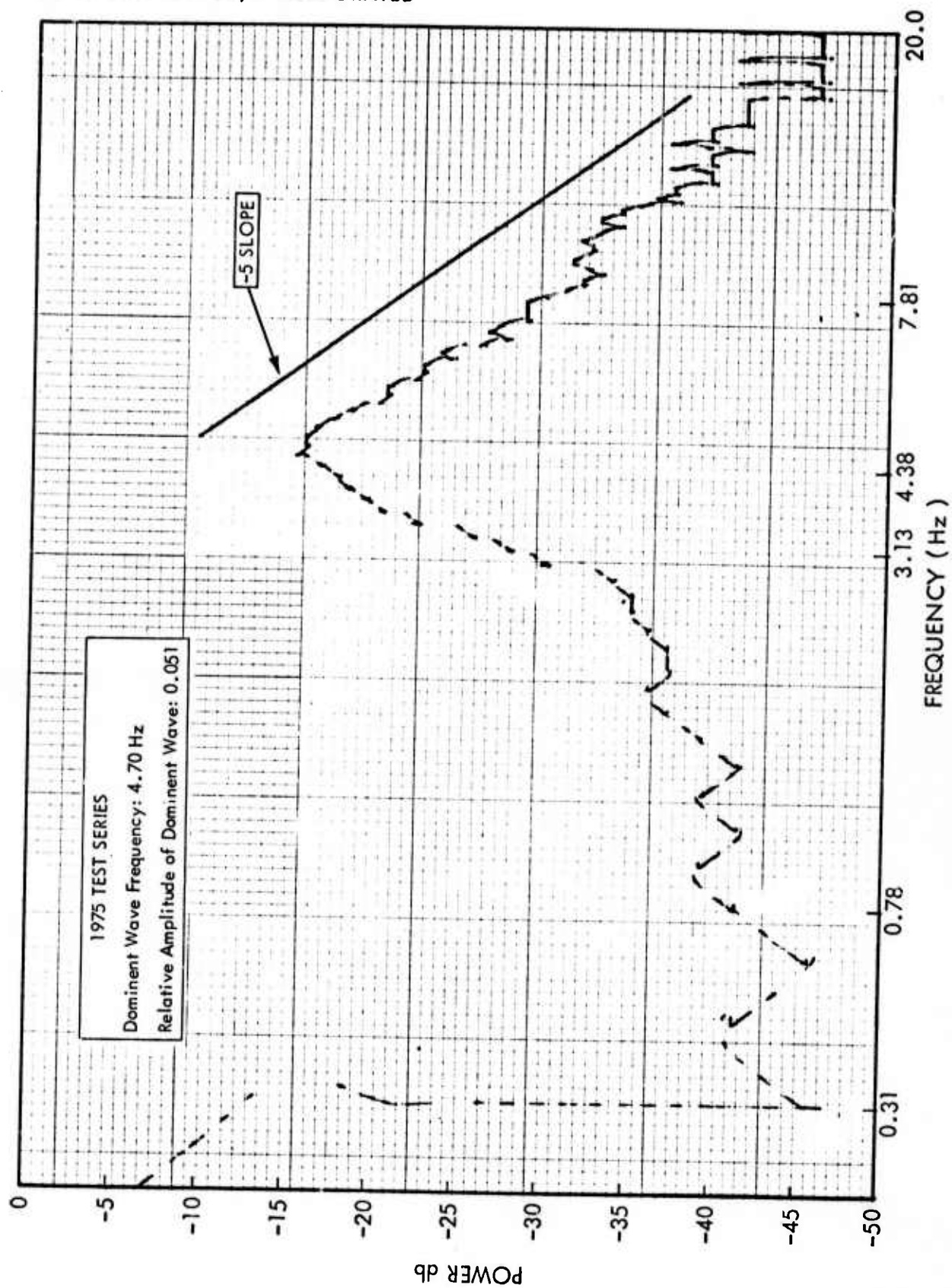


FIGURE 45 - CONDITION B4 C203 W450 F1225 1211 POWER SPECTRUM

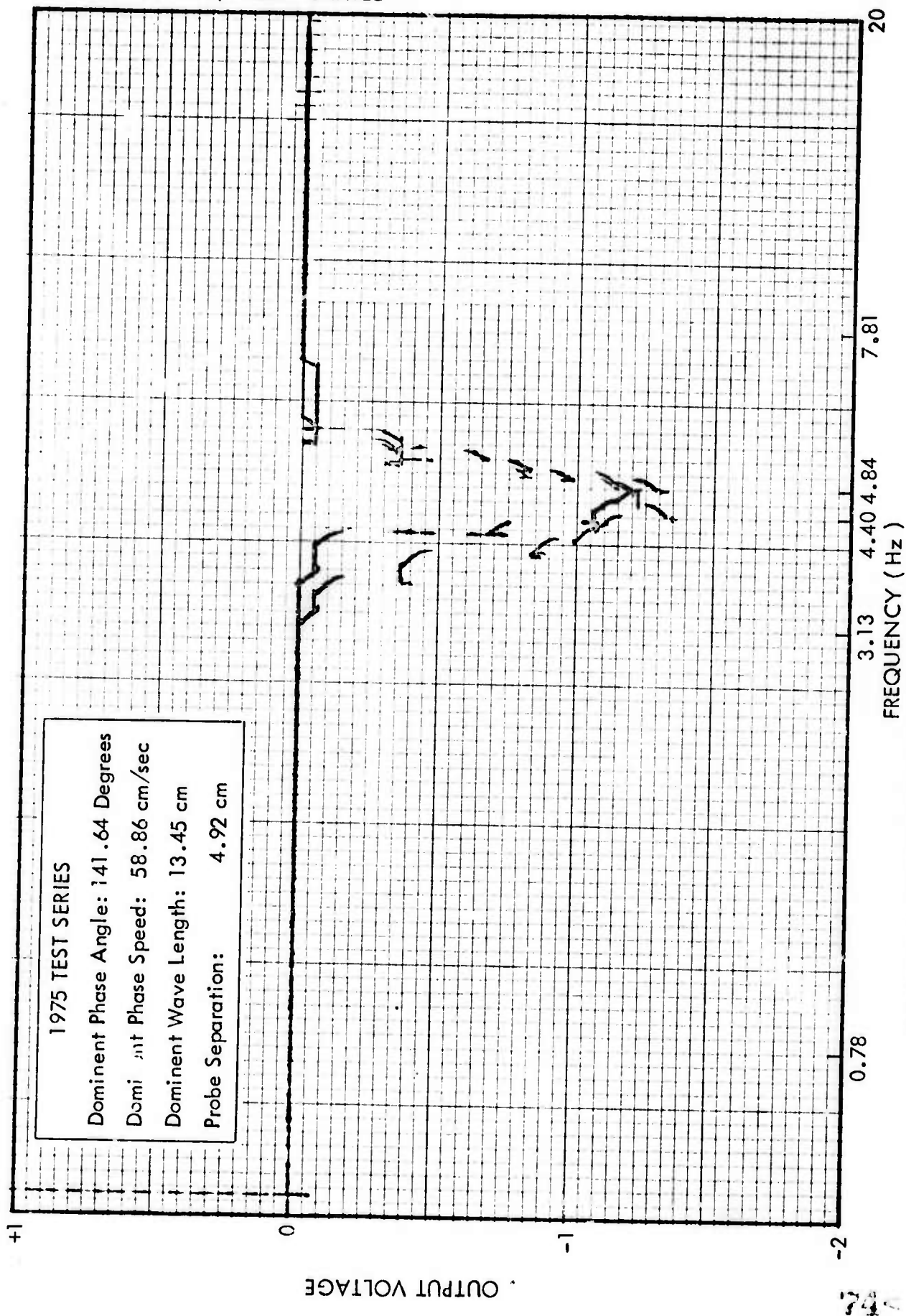


FIGURE 46 - CONDITION B4 C203 W450 F1225 1211 CROSS SPECTRUM

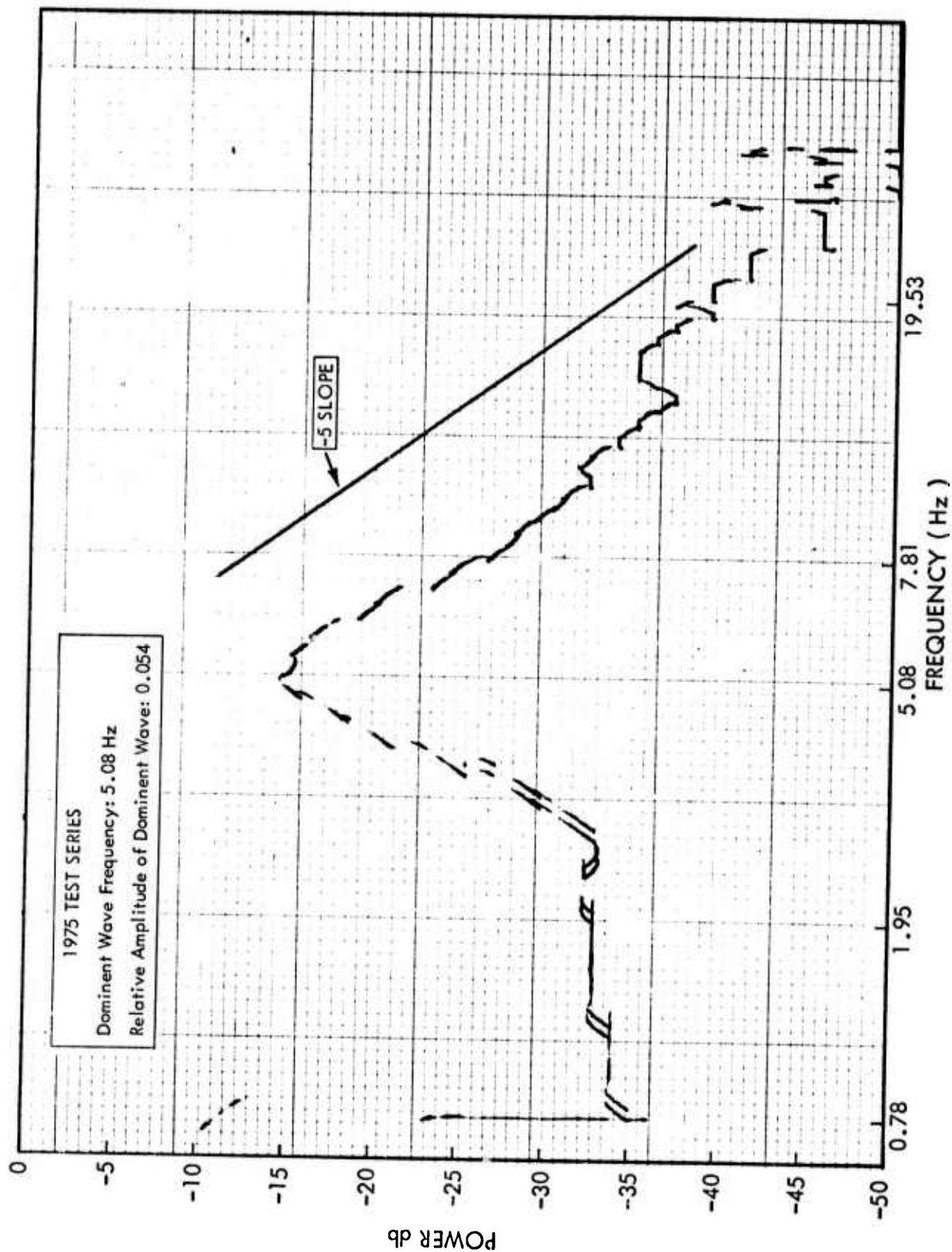


FIGURE 47 - CONDITION B4 C294 W450 F1225 1211 POWER SPECTRUM

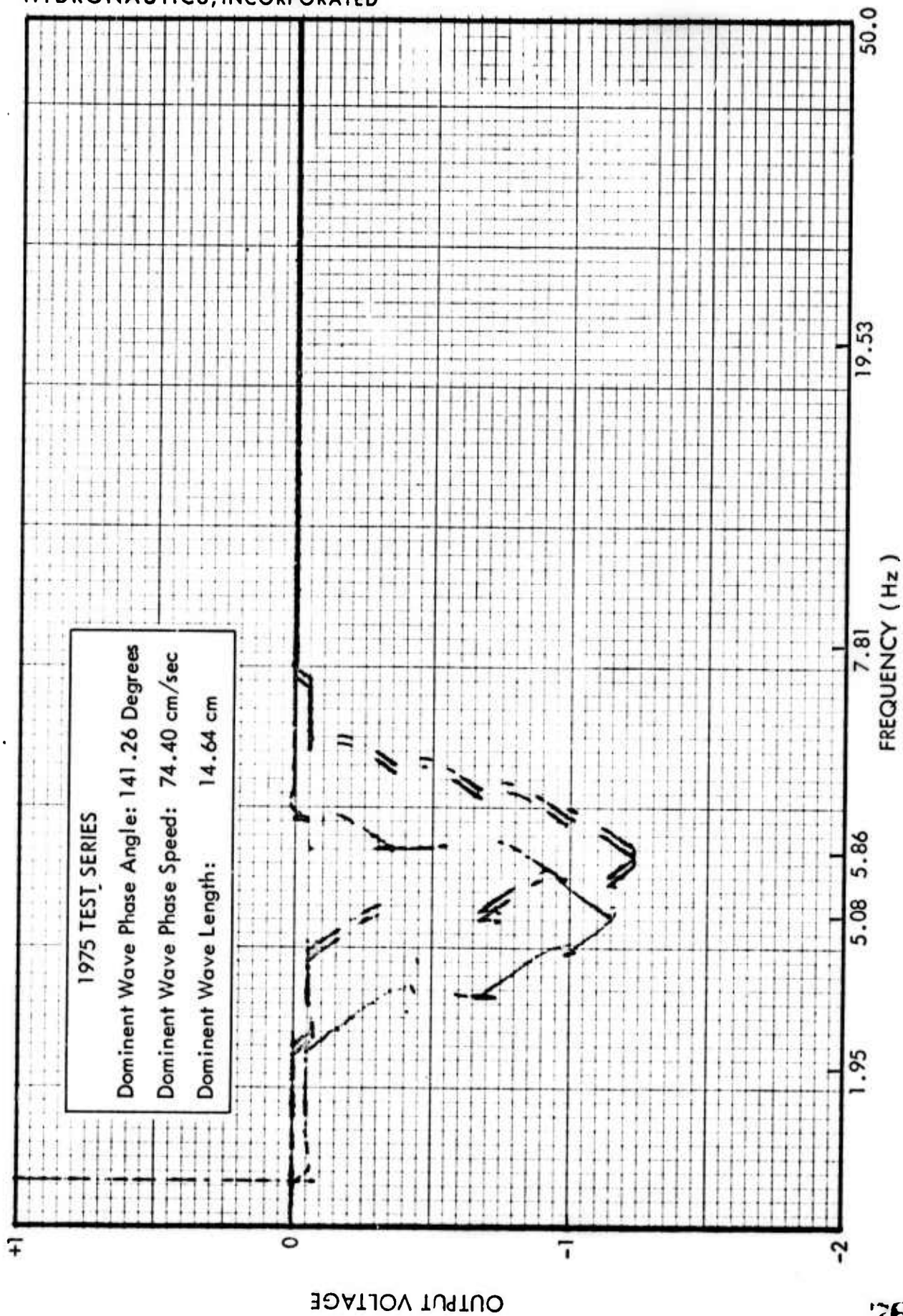


FIGURE 48 - CONDITION B4 C294 W450 F1225 1211 CROSS SPECTRUM

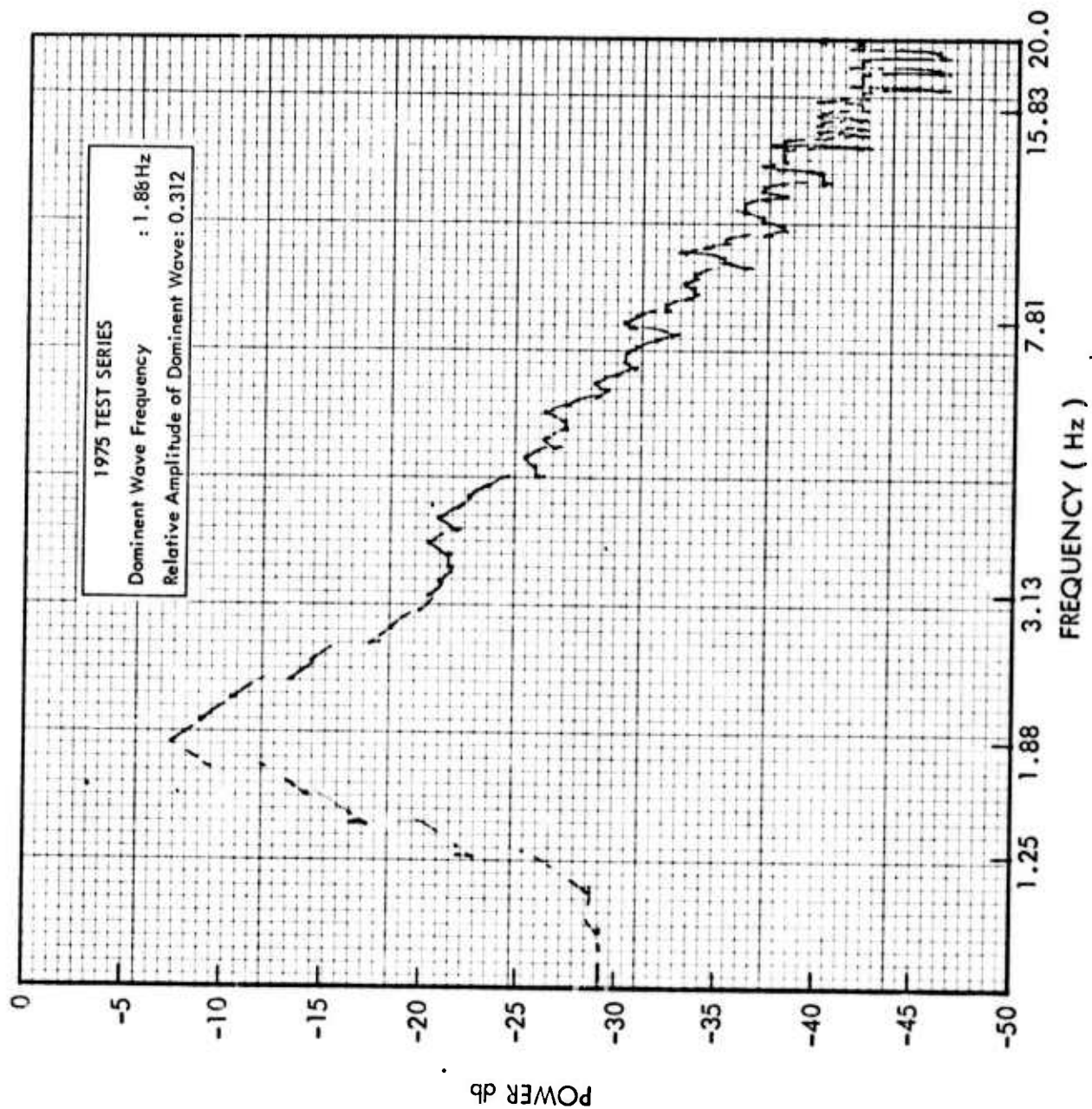


FIGURE 49 - CONDITION B4 C-324 W750 F1225 1211 POWER SPECTRUM

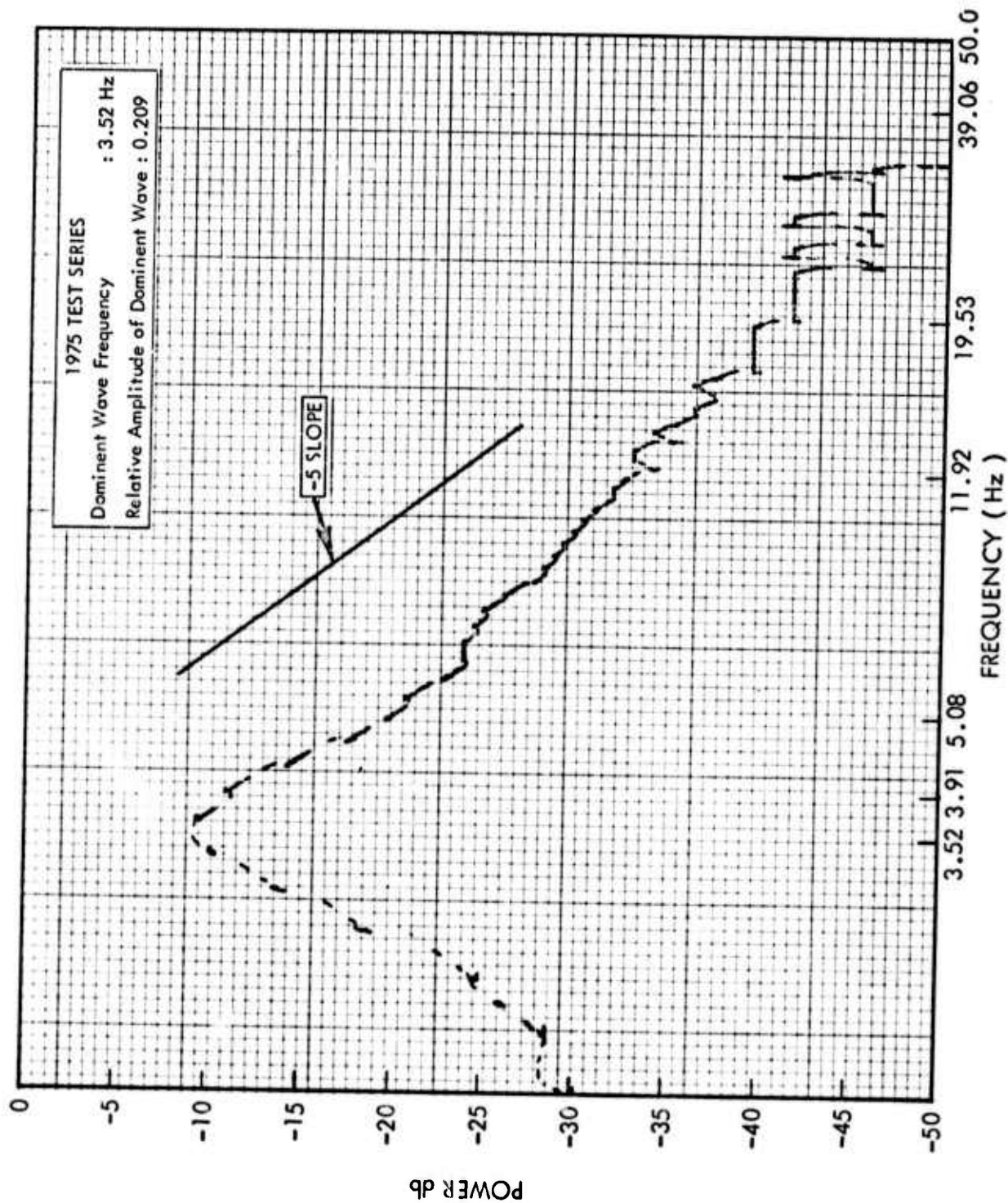


FIGURE 50 - CONDITION B4 C294 W750 F1225 1211 POWER SPECTRUM

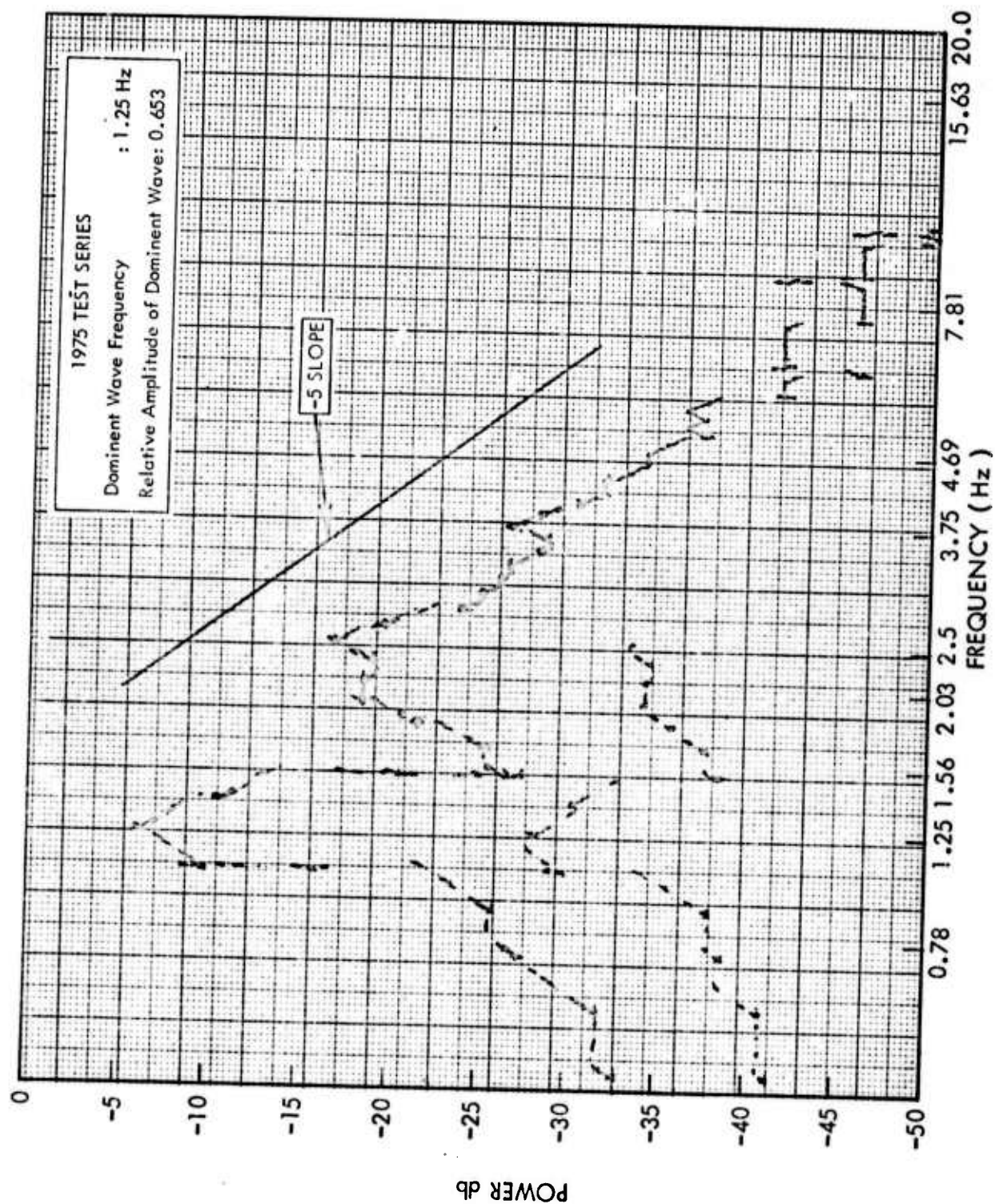


FIGURE 51 - CONDITION B1 C-145 W450 M75 F1225 1204 POWER SPECTRUM

HYDRONAUTICS, INCORPORATED

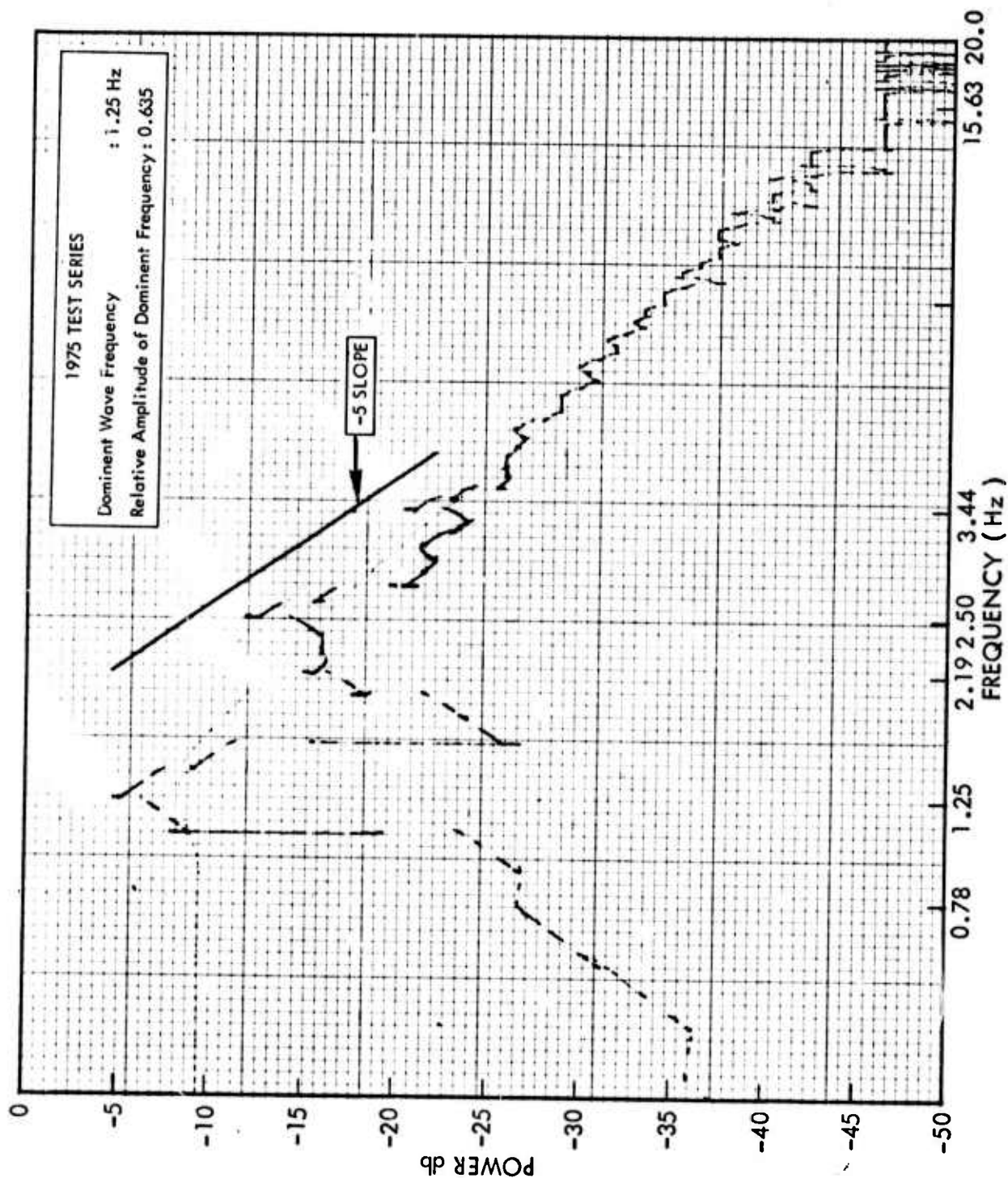


FIGURE 52 - CONDITION B1 C000 W450 M75 F1225 1203 POWER SPECTRUM

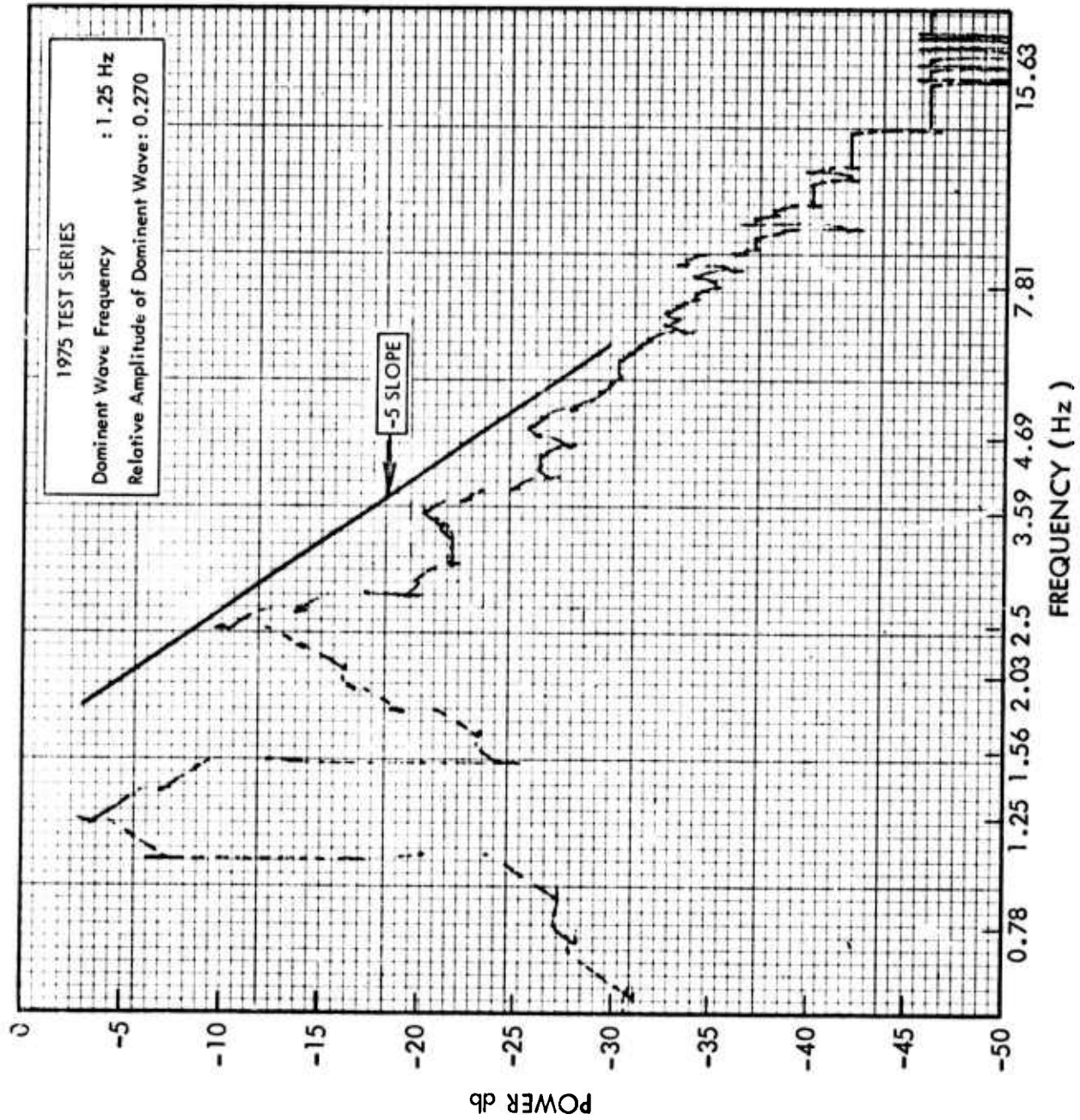


FIGURE 53 - CONDITION B1 C117 W450 M75 F1225 1205 POWER SPECTRUM